



UNIVERSITAT_{DE}
BARCELONA


Post-translational regulation of CPEB4 in cell cycle

Jordina Guillén Boixet

ADVERTIMENT. La consulta d'aquesta tesi queda condicionada a l'acceptació de les següents condicions d'ús: La difusió d'aquesta tesi per mitjà del servei TDX (www.tdx.cat) i a través del Dipòsit Digital de la UB (diposit.ub.edu) ha estat autoritzada pels titulars dels drets de propietat intel·lectual únicament per a usos privats emmarcats en activitats d'investigació i docència. No s'autoritza la seva reproducció amb finalitats de lucre ni la seva difusió i posada a disposició des d'un lloc aliè al servei TDX ni al Dipòsit Digital de la UB. No s'autoritza la presentació del seu contingut en una finestra o marc aliè a TDX o al Dipòsit Digital de la UB (framing). Aquesta reserva de drets afecta tant al resum de presentació de la tesi com als seus continguts. En la utilització o cita de parts de la tesi és obligat indicar el nom de la persona autora.

ADVERTENCIA. La consulta de esta tesis queda condicionada a la aceptación de las siguientes condiciones de uso: La difusión de esta tesis por medio del servicio TDR (www.tdx.cat) y a través del Repositorio Digital de la UB (diposit.ub.edu) ha sido autorizada por los titulares de los derechos de propiedad intelectual únicamente para usos privados enmarcados en actividades de investigación y docencia. No se autoriza su reproducción con finalidades de lucro ni su difusión y puesta a disposición desde un sitio ajeno al servicio TDR o al Repositorio Digital de la UB. No se autoriza la presentación de su contenido en una ventana o marco ajeno a TDR o al Repositorio Digital de la UB (framing). Esta reserva de derechos afecta tanto al resumen de presentación de la tesis como a sus contenidos. En la utilización o cita de partes de la tesis es obligado indicar el nombre de la persona autora.

WARNING. On having consulted this thesis you're accepting the following use conditions: Spreading this thesis by the TDX (www.tdx.cat) service and by the UB Digital Repository (diposit.ub.edu) has been authorized by the titular of the intellectual property rights only for private uses placed in investigation and teaching activities. Reproduction with lucrative aims is not authorized nor its spreading and availability from a site foreign to the TDX service or to the UB Digital Repository. Introducing its content in a window or frame foreign to the TDX service or to the UB Digital Repository is not authorized (framing). Those rights affect to the presentation summary of the thesis as well as to its contents. In the using or citation of parts of the thesis it's obliged to indicate the name of the author.



Post-translational regulation of CPEB4 in cell cycle

Jordina Guillén Boixet

PhD Thesis

Barcelona, 2015



UNIVERSITAT DE BARCELONA
FACULTAT DE FARMÀCIA
PROGRAMA DE DOCTORAT EN BIOMEDICINA

Post-translational regulation of CPEB4 in cell cycle

Memòria presentada per Jordina Guillén Boixet per optar al títol de doctor per la
Universitat de Barcelona.

Aquesta tesi ha estat realitzada sota la direcció del Dr. Raúl Méndez a l'Institut de
Recerca Biomèdica (IRB).

Dr. Raúl Méndez
Director de la tesi

Dra. Cristina Fillat
Tutora de la tesi

Jordina Guillén
Doctoranda

Barcelona, 2015

A la meva família,
i a tu.

“Ni tan alt, ni tan difícil”

Araceli Segarra

INDEX

| | |
|--|-----------|
| ABBREVIATIONS | 15 |
| KEY WORDS..... | 21 |
| ABSTRACT | 25 |
| INTRODUCTION | 29 |
| 1. An overview of gene expression | 31 |
| 2. mRNA structure..... | 31 |
| 2.1. The cap structure and the poly(A) tail..... | 32 |
| 2.2. The coding sequence and the untranslated regions..... | 33 |
| 3. mRNA translation: from mRNAs to proteins..... | 35 |
| 3.1. Translation initiation..... | 35 |
| 3.2. Translation elongation | 37 |
| 3.3. Translation termination and ribosome recycling | 37 |
| 3.4. The closed-loop model | 38 |
| 4. Translational control of gene expression..... | 39 |
| 4.1. Global versus specific control of mRNA translation..... | 39 |
| 4.2. Translational control by poly(A) tail length: cytoplasmic polyadenylation and deadenylation | 41 |
| 4.3. mRNPs and mRNP granules | 43 |
| 5. Intrinsically disordered proteins..... | 46 |
| 5.1. Intrinsically disordered regions in RNA-binding proteins | 47 |
| 5.2. Intrinsically disordered regions in the formation of membraneless organelles | 47 |
| 6. Protein phosphorylation and hyperphosphorylation | 50 |
| 7. Cytoplasmic polyadenylation element binding proteins | 53 |
| 7.1. The CPEB family of RNA-binding proteins: C-terminal and N-terminal domains | 53 |
| 7.2. CPEB mediated translational repression | 58 |
| 7.3. CPEB mediated translational activation..... | 61 |
| 7.4. CPEBs in meiotic progression of <i>Xenopus</i> oocytes..... | 63 |

| | |
|---|----|
| 7.4.1. A combinatorial code of <i>cis</i> -acting elements defines the time and extent of translational control during meiosis..... | 66 |
| 7.4.2. Sequential waves of polyadenylation and deadenylation drive meiosis . | 69 |
| 7.4.3. Why two different CPEBs are required for meiotic progression? | 71 |
| 7.5. CPEBs beyond meiosis | 74 |
| 7.5.1. CPEBs and multimer formation..... | 76 |

OBJECTIVES 79

RESULTS 83

| | |
|--|-----|
| 1. Functional validation of CPEB1 and CPEB4 tandem RRM structures | 85 |
| 2. CPEB4 is highly phosphorylated in the N-terminal domain during meiosis | 97 |
| 3. p42MAPK and Cdc2 kinases drive xCPEB4 phosphorylation..... | 101 |
| 4. Identification of xCPEB4 phosphorylation sites by mass spectrometry | 104 |
| 5. xCPEB4 hyperphosphorylation is essential for xCPEB4 function in meiosis | 108 |
| 5.1. Analysis of xCPEB4 functional phosphorylation sites by MS2-tethering experiments | 108 |
| 5.2. Analysis of xCPEB4 functional phosphorylation sites by competition experiments | 109 |
| 5.2.1. xCPEB4 hyperphosphorylation in the N-terminal domain is required for cytoplasmic polyadenylation | 109 |
| 5.2.2. Non-phosphorylated xCPEB4 has the ability to repress mRNA translation | 114 |
| 5.2.3. xCPEB4 RRM2 phosphorylation does not affect xCPEB4 function | 115 |
| 5.3. xCPEB4 hyperphosphorylation is required for meiotic progression | 116 |
| 6. xCPEB4 hyperphosphorylation does not regulate the interaction with cofactors | 119 |
| 7. xCPEB4 hyperphosphorylation modulates its aggregation properties | 121 |
| 7.1. xCPEB4 aggregation properties could not be adequately evaluated in <i>Xenopus laevis</i> oocytes | 121 |
| 7.2. Non-phosphorylated xCPEB4 distributes in cytoplasmic granules in U2OS cells..... | 124 |
| 7.3 Purified xCPEB4 N-terminal domain forms aggregates <i>in vitro</i> that are regulated by p42MAPK and Cdc2 phosphorylation..... | 126 |
| 8. xCPEB4 aggregates recruit CPE-containing mRNAs | 131 |

DISCUSSION 135

| | |
|--|-----|
| 1. CPEB1 and CPEB4 RNA-binding domain structures reveal similitudes and differences between CPEB paralogs..... | 137 |
| 2. CPEB4 activity is regulated by Cdc2- and p42MAPK-mediated hyperphosphorylation | 141 |
| 3. xCPEB4 hyperphosphorylation as a mechanism to generate ultrasensitivity and switch-like responses | 143 |
| 4. xCPEB4 hyperphosphorylation regulates the assembly of membraneless organelles through bulk electrostatics | 144 |
| 5. CPEBs are differentially regulated at a post-translational level | 146 |
| 6. CPEB1 and CPEB4 activities are coordinated in meiosis | 148 |
| 7. CPEB4 regulation beyond meiosis..... | 150 |

CONCLUSIONS 153

MATERIALS AND METHODS 157

REFERENCES 179

APPENDIX 195

| | |
|--|-----|
| Appendix 1. xCPEB4 12A- and 12D-interacting proteins | 197 |
| Appendix 2. GFP-xCPEB4 live cell imaging..... | 201 |
| Appendix 3. Publications | 203 |

ACKNOWLEDGEMENTS 205

ABBREVIATIONS

A site: acceptor site

APA: alternative polyadenylation

APC/C: anaphase promoting complex or cyclosome

ARE: AU-rich element

Cdc2: cell division cycle 2 (synonym of Cdk1)

Cdk: cyclin-dependent kinase

CDS: coding sequence

CPE: cytoplasmic polyadenylation element

CPEB: cytoplasmic polyadenylation element binding protein

CPSF: cleavage and polyadenylation specificity factor

CSF: cytostatic factor

CstF: cleavage stimulation factor

DSE: downstream sequence element

E site: exit site

EDEN: embryonic deadenylation element

eEF: eukaryotic elongation factor

eIF: eukaryotic initiation factor

ePAB: embryonic poly(A)-binding protein

4E-BP: eIF4E-binding protein

FUS: fused in sarcoma

Gld-2: defective in germline development factor 2

Hex: hexanucleotide (synonym of PAS)

IDP: intrinsically disordered protein

IDR: intrinsically disordered region

IRES: internal ribosome entry site

MI: metaphase I

MII: metaphase II

MAPK: mitogen activated protein kinase

MBE: Musashi-binding element

miRNA: microRNA

miRISC: miRNA-induced silencing complex

MPF: maturation promoting factor

mRNA: messenger RNA

mRNP: messenger ribonucleoprotein particle

NMR: nuclear magnetic resonance

NTD: N-terminal domain

P site: peptidyl site

PI: prophase I

PAP: poly(A) polymerase

PAPB: poly(A) binding protein

PARN: poly(A)-specific ribonuclease

PAS: poly(A) signal

PBE: Pumilio-binding element

P-bodies: processing bodies

Poly(A): polyadenosine

RBD: RNA-binding domain

RBP: RNA-binding protein

RNAP II: RNA polymerase II

RRM: RNA recognition motif

TTP: tristetraprolin

uORF: upstream open reading frame

UTR: untranslated region

ZZ domain: zinc-binding domain

KEY WORDS

3' UTR

Cdc2

CPEB4

Cytoplasmic polyadenylation

Hydrogel

Hyperphosphorylation

Intrinsically disordered protein

Maternal mRNAs

Meiosis

Membraneless organelles

Metaphase

Oocyte maturation

p42MAPK

Poly(A)

RRM

Translational control

Xenopus laevis

ABSTRACT

Cytoplasmic polyadenylation element binding proteins (CPEBs) are a family of RNA-binding proteins essential for the translational regulation of mRNAs in various biological contexts. CPEBs recognize CPE elements in the 3' untranslated region of target mRNAs and regulate their translational fate through cytoplasmic polyadenylation. This process is especially important during meiosis, since its progression relies on the translational activation of stored maternal mRNAs. CPEB1 and CPEB4 are the two members of the family required for meiotic progression. While CPEB1 mediates the translational activation of mRNAs until metaphase I (MI), CPEB4 activates mRNAs from interkinesis to metaphase II (MII). CPEBs share a conserved RNA-binding domain and regulate overlapping mRNA subpopulations. Hence, the requirement of two distinct CPEBs to complete meiosis leans on their differential post-translational regulation. In fact, the N-terminal domain of the CPEBs is highly variable and harbours different regulatory motifs. While CPEB1 is activated by Aurora A kinase and is targeted for degradation by Cdc2 and Plk1-mediated phosphorylation, CPEB3 is controlled by monoubiquitination and SUMOylation, which regulate the transition from an inactive monomeric CPEB3 form to an active beta-amyloid-like aggregate. How the other CPEBs are post-translationally regulated is unknown. Nevertheless, unveiling how the different CPEBs are differentially regulated is crucial for understanding how they respond to different stimuli and how they are interconnected in particular scenarios of co-existence. We found that CPEB4 activity is regulated by hyperphosphorylation during the meiotic cell cycle. Specifically, CPEB4 is phosphorylated in twelve residues by two different kinases and in a phase-specific manner. All phosphorylated residues are located in the intrinsically disordered N-terminal half of CPEB4 and are required for cytoplasmic polyadenylation of target mRNAs. Accordingly, these twelve phosphorylation sites are essential for meiotic progression. Furthermore, we have shown that hyperphosphorylation of CPEB4 disordered domain modulates its aggregation properties. Hence, non-phosphorylated CPEB4 forms non-amyloid aggregates that specifically recruit and repress CPE-containing mRNAs, whereas hyperphosphorylated CPEB4 remains monomeric and is active in cytoplasmic polyadenylation. Importantly, CPEB4 aggregates are dynamic and reversible upon phosphorylation on the identified phosphosites. These results contribute greatly to the understanding of how the CPEBs are differentially regulated and how they would differentially respond in a given cellular environment.

INTRODUCTION

1. An overview of gene expression

Eukaryotic gene expression is a complex stepwise process subjected to a high degree of regulation. Every step in gene expression, from transcription to translation, is tightly regulated and the different processes are interconnected. Protein-coding genes are transcribed by RNA polymerase II (RNAP II). During transcription, the nascent pre-mRNA undergoes 5'-end capping, splicing and 3'-end cleavage and polyadenylation. These processes are coupled in part by the C-terminal domain of the largest subunit of RNAP II, which acts as a loading platform for transcription and mRNA processing factors (Aguilera, 2005; Shukla and Oberdoerffer, 2012). Then, the mature mRNA molecule, coated with multiple RNA-binding proteins (RBPs), is released from the site of transcription and exported to the cytoplasm (Schmid and Jensen, 2008). Once in the cytoplasm, mRNAs can be translated, stored and localized at specific subcellular compartments or degraded. The fate of an mRNA in the cytoplasm is determined by the subset of RBPs associated to it, which in turn depends on the *cis*-acting regulatory elements present in each mRNA.

In this introduction, the structure of the mRNA molecule will be dissected, emphasizing the role of the untranslated regions (UTRs), and the RBPs bound to them, in the translational control of gene expression.

2. mRNA structure

The mature mRNA molecule consists of an RNA body flanked by two modifications not coded in the DNA, the 5' cap and the 3' polyadenosine tail (poly(A) tail). The mRNA body contains the coding sequence (CDS) surrounded by the 5' and the 3' UTRs. While the CDS codifies for the coded-protein and is translated by ribosomes, the UTRs are regulatory sequences involved in the control of mRNA translation, storage, transport and decay.

2.1. The cap structure and the poly(A) tail

5'-end capping is the first processing event that a pre-mRNA undergoes. It occurs co-transcriptionally as soon as RNAP II transcribes the first 25-30 nucleotides. mRNA capping requires three enzymatic reactions: first, the 5'-end-triphosphorylated RNA (pppN) is converted to diphosphorylated RNA (ppN); then, a guanine monophosphate is coupled to the 5' end via an unusual 5' to 5' triphosphate linkage, which results in a capped mRNA (GpppN); and finally, the cap is methylated to generate the 7-methylguanosine cap (m⁷GpppN). The mature methylated cap is critical to protect the nascent mRNA from 5' → 3' exonucleases, as well as being essential for cap-dependent mRNA translation. Capping has also been linked to mRNA splicing, 3'-end processing of pre-mRNAs and export of mature mRNAs to the cytoplasm (Hocine et al., 2010; Jurado et al., 2014; Shatkin and Manley, 2000).

The 3'-end processing of pre-mRNAs occurs in a coupled, two-step reaction before the transcripts are released and exported to the cytoplasm. First, an endonucleolytic cleavage of the nascent RNA takes place. Then, a polyadenosine tract is added at the 3' end, with the exception of canonical histone mRNAs that are not polyadenylated. Key sequence elements in the 3' UTR of pre-mRNAs are recognized by specific protein complexes to mediate the 3'-end cleavage and polyadenylation. The major sequence elements include the poly(A) signal (PAS), which consists in the hexanucleotide 5'-AAUAAA-3' and is located 10-30 nucleotides upstream of the cleavage site; the cleavage site itself that is often after a CA dinucleotide; and the U- or G/U-rich downstream sequence element (DSE). The protein complexes required for 3'-end cleavage and polyadenylation are the cleavage and polyadenylation specificity factor (CPSF), which binds to the PAS; the cleavage stimulation factor (CstF) that recognizes the DSE; and the cleavage factors I and II. Together, these factors specify the cleavage site, which is specifically cleaved by the CPSF-73 subunit. After the cleavage event, the poly(A) polymerase (PAP), recruited by CPSF, adds a poly(A) tail of approximately 250 adenosines. The poly(A) tail is coated by poly(A) binding proteins (PABP) that protect mRNAs from degradation. PABPs are also involved in nuclear export and, importantly, promote mRNA translation (Jurado et al., 2014; Proudfoot, 2011).

All mRNAs, except canonical histone mRNAs, receive a tail of approximately 250 adenines by default. However, once the tail has been synthesized, the length of the

poly(A) tail is subsequently modulated in a highly regulated manner (Zhang et al., 2010). Therefore, in the cytoplasm, mRNAs are heterogeneous in poly(A) tail length, ranging from 30 to 250 nucleotides, which influences mRNA translation.

2.2. The coding sequence and the untranslated regions

The CDS constitutes the translated region of the mRNA, which starts with the AUG initiation codon and ends with one of the three stop codons UAA, UAG or UGA.

The CDS is flanked by the 3' and the 5' UTRs, which are encoded by exons but do not codify for proteins. The UTRs contain structural features and regulatory *cis*-acting elements that specifically control the translational fate of mRNAs, as well as their stability and subcellular localization (Figure 1).

The 5' UTR regulatory motifs that influence mRNA translation include secondary structures, which can repress cap-dependent translation by inhibiting the binding or the scanning of the pre-initiation complex; upstream open reading frames (uORF), which normally inhibit translation by limiting the access of ribosomes to the main start codon, although under conditions where eIF2 is phosphorylated the translation of the main ORF is favoured; internal ribosome entry sites (IRES) that recruit ribosomes and initiate translation independently of the cap structure; and specific binding sites for regulatory proteins (Gray and Wickens, 1998; Somers et al., 2013).

The 3' UTR also contains specific binding sites for regulatory proteins, which may affect the stability, the localization or the translation efficiency of target mRNAs. Moreover, it can harbour binding sites for microRNA (miRNA) that can repress mRNA translation as well as destabilize mRNAs (Gebauer and Hentze, 2004; Gray and Wickens, 1998). At this point it is worthy to emphasize the role of cytoplasmic polyadenylation elements (CPEs) in the 3' UTR of specific mRNAs, which, together with the PAS, regulate the cytoplasmic polyadenylation of CPE-containing mRNAs.

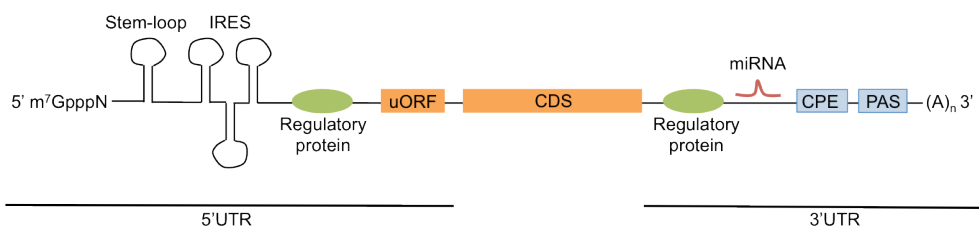


Figure 1. Regulatory elements in the 5' and 3' UTRs. The major elements that affect mRNA translation, transport and stability are depicted. In the 5' UTR, the cap structure (m⁷GpppN) is shown, followed by a stem-loop that can negatively affect translation. Internal ribosome entry sites (IRES) mediate cap-independent translation, while upstream open reading frames (uORF) normally reduce translation from the main coding sequence (CDS). The 5' UTR and 3' UTR contain *cis*-acting elements bound by RNA-binding proteins that regulate mRNA fate (shown in green). The 3' UTR can be targeted by microRNAs (miRNAs) that repress translation and destabilize mRNAs. Cytoplasmic polyadenylation elements (CPEs), together with the poly(A) signal (PAS), regulate the cytoplasmic polyadenylation of mRNAs. Finally, the poly(A) tail is shown as (A)_n.

Importantly, different 3' UTRs can be generated by alternative polyadenylation (APA). As a consequence, mRNAs codifying for the same protein but harbouring different 3' UTRs can present diverse behaviours in mRNA stability, localization and translation. Longer 3' UTRs contain more regulatory motifs and, stochastically, are more prone to negative regulation by miRNAs, while shorter 3' UTRs tend to produce higher levels of protein. The mechanisms leading to the usage of upstream or downstream PAS encompass variations in the level or activity of core polyadenylation factors, as well as the action of specific RNA-binding proteins that influence the PAS choice (Bava et al., 2013; Di Giammartino et al., 2011; Jenal et al., 2012). APA is a widespread mechanism of regulation. Accordingly, 70% of human genes encode multiple transcripts derived from APA (Derti et al., 2012). Differential APA occurs during development and the PAS choice changes depending on the proliferation rate of the tissue. In particular, highly proliferating cells tend to use proximal PAS, whereas differentiated cells in later developmental stages tend to use more distal PAS that generate long 3' UTRs subjected to fine regulation (Sandberg et al., 2008; Ulitsky et al., 2012). Correspondingly, cancer cells that have a high proliferation rate also present changes in APA towards the use of proximal PAS (Mayr and Bartel, 2009).

3. mRNA translation: from mRNAs to proteins

mRNA translation into proteins is the final step of gene expression. It is a complex process subjected to tight regulation in order to modulate protein levels in a wide range of biological situations. Translation of mRNAs occurs in four phases: initiation, elongation, termination and ribosome recycling.

In this section, the molecular mechanisms behind cap-dependent translation are described.

3.1. Translation initiation

Translation initiation represents the most complex and rate-limiting step in translation, involving more than 25 proteins in eukaryotes.

Cap-dependent translation initiation (Figure 2) starts with the binding of the ternary complex to the small ribosomal subunit 40S. This results in the formation of the 43S pre-initiation complex that binds the mRNA near the 5' cap. The ternary complex is composed by the methionine-charged initiator tRNA and the GTP-bound form of the eukaryotic initiation factor 2 (eIF2). The binding of the ternary complex to the 40S subunit is supported by several initiation factors (eIFs), comprising eIF1, eIF1A, eIF5 and eIF3. The binding of the 43S pre-initiation complex to the mRNA occurs via interaction between eIF3 and the eIF4F protein complex already bound to the 5'-end of the mRNA. The eIF4F complex is composed by eIF4E, which binds the cap structure, eIF4A, an RNA helicase that unwinds secondary structures in the 5' UTR to help 43S binding and scanning, and eIF4G, which acts as a scaffold protein interacting with eIF4E, eIF4A and eIF3. eIF4G also interacts with PABP and brings both ends of the mRNA together in a closed-loop conformation (discussed in section 3.4). Once the 43S pre-initiation complex binds the mRNA, it scans along the 5' UTR until it recognizes the initiation codon AUG in an appropriate sequence context (Kozak, 2002). Binding of the 43S to the AUG initiation codon through base pairing with the initiator tRNA results in the formation of the 48S initiation complex. Following AUG recognition, eIF5 triggers the hydrolysis of the GTP bound to eIF2

and most of the initiation factors are released. Subsequently, the large 60S ribosomal subunit joins in a process that requires GTP hydrolysis on eIF5B, and elongation starts (Gebauer and Hentze, 2004; Hinnebusch and Lorsch, 2012).

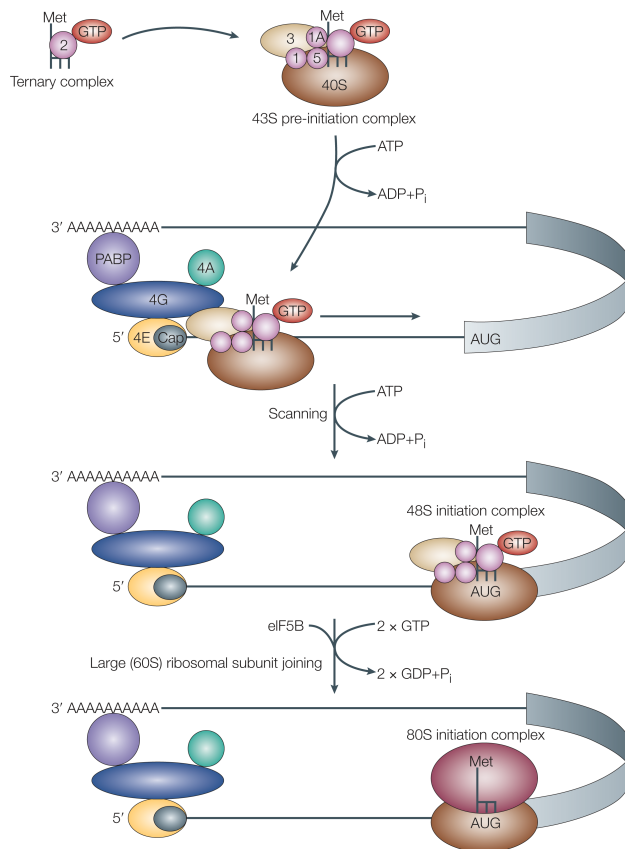


Figure 2. Simplified scheme of cap-mediated translation initiation (taken from (Gebauer and Hentze, 2004)). The ternary complex, composed by the methionine-initiator tRNA and the GTP-bound form of eIF2, binds to the 40S subunit, together with eIF1, eIF1A, eIF5 and eIF3. As a result, the 43S pre-initiation complex is formed. The pre-initiation complex binds the RNA through eIF3 interaction with the eIF4G subunit of eIF4F complex, which also contains eIF4E that binds the cap structure, and eIF4A, an RNA helicase that unwinds secondary structures. eIF4G also interacts with the poly(A)-binding protein (PABP) and the mRNA forms a closed-loop. Then, the 43S pre-initiation complex scans along the 5' UTR until it recognizes the AUG initiation codon. Binding of the 43S to the AUG initiation codon results in the formation of the 48S initiation complex. Following AUG recognition, eIF5 triggers the hydrolysis of the GTP bound to eIF2 and most of the initiation factors are released. Subsequently, the large 60S ribosomal subunit joins in a process that requires GTP hydrolysis on eIF5B.

3.2. Translation elongation

Translation elongation is the process of protein synthesis performed by ribosomes. Three positions for tRNAs are available in the ribosome: an acceptor site (A site), where the aminoacyl-tRNA is placed; the peptidyl site (P site), which contains the tRNA with the growing polypeptide; and the exit site (E site), where the empty tRNA exits the ribosome.

Following translation initiation, an 80S ribosome is positioned in the start codon with the methionine-charged initiator tRNA in the P site. Then, an aminoacyl-tRNA is carried to the empty A site as part of a ternary complex with the eukaryotic elongation factor 1A (eEF1A) and GTP. Codon recognition by the tRNA triggers GTP hydrolysis by eEF1A, which results in eEF1A release and aminoacyl-tRNA accommodation into the A site. Once the correct aminoacyl-tRNA has been positioned in the A site, the ribosomal peptidyl transfer centre positions the substrates for catalysis and a peptide bond is formed between the incoming amino acid and the growing polypeptide. After peptide bond formation, the eukaryotic elongation factor 2 (eEF2) promotes the translocation of the tRNAs and the movement of the mRNA in a process that requires GTP hydrolysis. As a result, the empty tRNA is positioned in the E site and the elongated peptidyl-tRNA in the P site. The A site is then empty and available for binding the next aminoacyl-tRNA. This procedure is repeated until a stop codon is encountered and the process of translation termination is initiated (Dever and Green, 2012; Kapp and Lorsch, 2004).

3.3. Translation termination and ribosome recycling

Translation termination occurs when a stop codon (UAA, UGA or UAG) enters the A site of the ribosome. In eukaryotes, termination is catalysed by two protein factors, eRF1 and eRF3. While eRF1 is responsible for stop codon recognition and peptidyl-tRNA hydrolysis, eRF3 is a translational GTPase required for the deposition of eRF1 to the ribosomal peptidyl transferase centre. Additionally, the ATPase ABCE1 has been shown to promote the rate of peptide release by the eRF1:eRF3 complex (Dever and Green, 2012).

Finally, once translation is terminated, ribosomal subunits need to dissociate and release in order to liberate the mRNA and regenerate the necessary factors for subsequent rounds of translation. Although the exact mechanisms driving ribosomal subunits dissociation in eukaryotes are not clear, ABCE1 has been proposed to be involved in the dissociation process (Dever and Green, 2012).

3.4. The closed-loop model

The closed-loop model refers to the bridging of the 5'-end and the 3'-end of the same mRNA molecule through protein-protein and protein-mRNA interactions, which results in mRNA circularization. mRNA circularization allows the 5' cap and the 3' poly(A) tail to synergistically promote mRNA stability and translation.

Both ends of the mRNA are bridged through the simultaneous interaction of eIF4G with eIF4E, which is bound to the cap, and the PABP, which is bound to the poly(A) tail (Imataka et al., 1998; Wells et al., 1998). The resulting circular conformation of the mRNA enhances translation initiation through the recruitment of the small ribosomal subunit to the mRNA (Sachs et al., 1997; Tarun and Sachs, 1995) (Figure 2). Beyond translation initiation, mRNA circularization plays a role in ribosome recycling upon translation termination. To this end, the termination factors eRF1 and eRF3 contribute to the formation of a stable closed-loop structure after 60S subunit joining through the interaction of eRF3 with PABP. This structure allows the direct re-entry of ribosomes to the translation initiation point, enhancing the translation efficiency (Amrani et al., 2008; Uchida et al., 2002) (Figure 3).

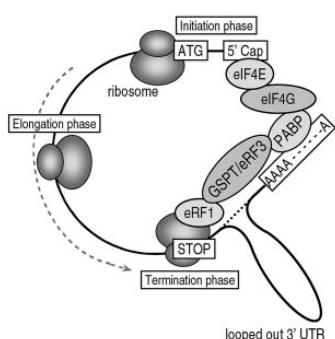


Figure 3. Closed-loop model for ribosome re-initiation (taken from (Uchida et al., 2002)). The interactions between eRF1-eRF3-PABP and 3'poly(A)-PABP-eIF4G-eIF4E-5'cap circularize the mRNA and facilitate ribosome re-initiation.

4. Translational control of gene expression

4.1. Global versus specific control of mRNA translation

Translational control of gene expression is used to rapidly modulate protein levels in a large variety of biological contexts. It is especially relevant during meiosis and early development, when transcription is silent and protein expression relies on maternal mRNAs previously stored in the oocyte.

There are two major modes of translational regulation: the global control of translation that regulates most of the mRNAs in the cell, and the mRNA-specific control that only affects defined groups of mRNAs.

On the one hand, **global control of mRNA translation** is achieved by changes in the availability of factors from the translational machinery. Usually, initiation factors are the most common target for translational control. Two initiation factors subjected to such a control are eIF2 and eIF4E. Under certain stress conditions, the α -subunit of eIF2 is phosphorylated by different kinases such as PKR, PERK, HRI and GCN2. eIF2 phosphorylation reduces the dissociation rate of eIF2 from the guanine nucleotide exchange factor eIF2B, which converts the inactive eIF2-GDP to the active eIF2-GTP. As a consequence, the GDP-GTP exchange in eIF2 does not take place, the assembly of the ternary complex decreases and mRNA translation initiation is inhibited. Exceptionally, the translation of *ATF4* and *GCN4* mRNAs, which encode two transcription factors, is upregulated by eIF2 phosphorylation due to the presence of uORFs in their 5' UTRs. Thus, under conditions with low concentration of ternary complex, ribosomes skip these uORFs and the translation of the main ORF is favoured. Another mechanism for general cap-dependent translation inhibition is performed by eIF4E-binding proteins (4E-BPs), which disrupt eIF4E-eIF4G interaction by competing with eIF4G for binding to eIF4E. Extracellular stimuli like mitogens and growth factors activate signalling cascades that end up with the hyperphosphorylation of 4E-BPs by mTOR. Phosphorylated 4E-BPs are not able to bind eIF4E and, consequently, translation initiation is enhanced (Gebauer and Hentze, 2004; Sonenberg and Hinnebusch, 2007).

On the other hand, **mRNA-specific translational control** is accomplished through specific *cis*-acting elements localized in the 5' and 3' UTRs of particular mRNA subpopulations. The subsequent binding of *trans*-acting factors influences the translation of that particular subset of mRNAs through different mechanisms. Besides controlling mRNA translation, mRNA-specific *cis*-acting elements can specify mRNA localization and local protein synthesis. Local mRNA translation confers high precision in protein localization and supports rapid responses to biological demand, which is particularly important during development and in highly polarized cells like neurons (Jung et al., 2014). For example, 71% of the ≈ 2300 genes analysed during *Drosophila* embryogenesis produce mRNAs that are localized to distinct subcellular compartments (Lécuyer et al., 2007).

Among the mechanisms described to control mRNA-specific translation are eIF4F complex interference by eIF4E binding proteins, ribosomal subunits recruitment and scanning inhibition, post-initiation translation inhibition by miRNAs and regulation of the poly(A) tail length by polyadenylation and deadenylation. The following are some examples of mRNA-specific translational control. First, specific 4E-BPs can inhibit translation of specific mRNAs by precluding the recruitment of eIF4G. This is the case for Maskin, which is recruited by the cytoplasmic polyadenylation element binding protein (CPEB) to CPE-containing mRNAs, and Cup, which is recruited by Smaug or Bruno to control the translation of anterioposterior axis determinants in *Drosophila* (Richter and Sonenberg, 2005). Second, 43S ribosomal complex recruitment can be hindered by steric blockage exerted by RNA-binding proteins bound near the 5'-end cap or by the action of repressing complexes bound to the 3' UTR. An example of this last mechanism is the RNA-binding protein sex-lethal that, together with UNR, blocks the recruitment of the pre-initiation complex. Interestingly, sex-lethal can also inhibit the scanning of the 43S complex when bound to the 5' UTR (Abaza et al., 2006; Beckmann et al., 2005). Furthermore, the recruitment of the 60S ribosomal subunit can also be prevented, for example, by the action of hnRNP K and hnRNP E1 (Gebauer and Hentze, 2004). How miRNAs repress translation is still unclear. Generally, miRNAs function as part of ribonucleoprotein complexes, known as miRNA-induced silencing complexes (miRISCs), which repress translation at initiation, 80S complex assembly or even at post-initiation steps (Fabian et al., 2010).

Translational regulation of mRNAs through changes in the poly(A) tail length will be carefully described in the following section.

4.2. Translational control by poly(A) tail length: cytoplasmic polyadenylation and deadenylation

Beyond the role of the poly(A) tail length in mRNA stability by protecting the mRNA from the degradation machinery, it is clear that changes in the poly(A) tail length is a widespread mechanism of translational control.

The poly(A) tail has been shown to act synergistically with the 5' cap to stimulate cap-dependent translation initiation. Accordingly, the length of the poly(A) tail defines the extent of mRNA translation. Thus, mRNAs with short poly(A) tails (approximately 40 adenosines) will be translationally silent or repressed, whereas mRNAs with long poly(A) tails (approximately 150 adenosines) will be efficiently translated (Richter, 2007). Despite all mRNAs acquire a poly(A) tail of 250 adenosines co-transcriptionally, its length is subsequently modulated by deadenylation and polyadenylation events. This mechanism of translational control fine-tunes protein expression in time and space in different biological contexts, such as meiotic and mitotic cell cycle progression, early development and synaptic plasticity. Particularly relevant is the translational control of maternal mRNAs during oocyte maturation and early development, since transcription is inactive and newly protein synthesis relies on the translational activation through cytoplasmic polyadenylation of previously stored mRNAs.

Whether an mRNA is subjected to translational control through poly(A) tail length regulation is determined by the combination of *cis*-acting elements present, generally, in its 3' UTR.

Deadenylation is usually the first step for the degradation of aberrant or no longer needed transcripts (Parker and Song, 2004). Nevertheless, cytoplasmic deadenylation can also lead to mRNA translational silencing without affecting the stability of the messenger. Hence, deadenylation from ≈ 200 to 20 adenines inhibits mRNA translation, while deadenylation beyond 20 adenines is linked to mRNA decapping and decay (Zhang et al., 2010). RNA-binding proteins bound to specific

sequences on the transcript mediate the recruitment of active deadenylases, being the main ones the Poly(A)-specific ribonuclease (PARN) and the CCR4-NOT complex. Among the *cis*-acting elements promoting deadenylation are AU-rich elements (AREs), embryonic deadenylation element (EDEN), CPEs and miRNA target sites (Weill et al., 2012). First, AREs, which consist of 5'-AUUUA-3' pentamer repeats in U-rich regions, are recognized by a large variety of ARE-binding proteins. One of the best-characterized ARE-binding proteins is tristetraprolin (TTP), which recruits the CCR4-NOT complex. During meiotic progression in *Xenopus* oocytes, a paralog of TTP, C3H-4, promotes CCR4-NOT-mediated deadenylation of ARE-containing mRNAs (Belloc and Méndez, 2008). Second, EDEN is a GU-rich sequence recognized by EDEN-BP that induces deadenylation of mRNAs after fertilization (Graindorge et al., 2008). In mammalian cells, the deadenylase recruited by EDEN-BP is PARN. Third, CPEs, which consensus sequence is 5'-UUUUAU-3' or 5'-UUUUAAU-3', are bound by CPEBs, which in turn can recruit different deadenylases. While CPEB1, when not phosphorylated, recruits PARN in order to translationally repress target mRNAs, CPEB3 mediates mRNA deadenylation and decay through the recruitment of the CCR4-NOT complex (see section 7.2). Finally, miRNAs promote mRNA deadenylation through the miRISC complex and CCR4-NOT deadenylase (Fabian et al., 2010).

In response to certain stimuli, stored deadenylated mRNAs can be reactivated by **cytoplasmic polyadenylation**. The best-characterized mechanism of cytoplasmic polyadenylation is driven by CPEBs, a family of four RNA-binding proteins that bind to CPE elements in the 3' UTR of target mRNAs. Although the consensus CPE sequence is 5'-UUUUAU-3' or 5'-UUUUAAU-3', some variations are found in specific mRNAs (Piqué et al., 2008). The most studied member of the family is CPEB1, which has a dual role in mRNA translational control. As specified before, non-phosphorylated CPEB1 recruits the deadenylase PARN to deadenylate and store mRNAs. However, upon phosphorylation, CPEB1 decreases its binding to PARN and increases its affinity for CPSF and the poly(A) polymerase defective in germline development 2 (Gld-2), which results in the translational activation of CPE-containing mRNA through cytoplasmic polyadenylation. The other members of the CPEB family also regulate mRNA translation through poly(A) tail length control, although the molecular mechanisms are not so well-defined. Interestingly, CPEBs can potentially regulate the 20% of vertebrate genomes, being key players in

biological processes as divergent as meiosis and synaptic plasticity (for details refer to section 7).

In addition to CPEs, other elements have been described to mediate cytoplasmic polyadenylation of mRNAs, such as the Musashi-binding element (MBE), 5'-G/AUnAGU-3', which is recognized and bound by the RNA-binding protein Musashi. It has been suggested that Musashi mediates the cytoplasmic polyadenylation of mRNAs in early meiotic phases of *Xenopus* oocytes through the recruitment of Gld-2 (Arumugam et al., 2010; Charlesworth et al., 2006; Cragle and MacNicol, 2014), although this model is not universally accepted (Weill et al., under review). Ultimately, in *Drosophila*, the cytoplasmic polyadenylation of the mRNA encoding the dorso-ventral determinant Toll is driven by a non-canonical mechanism. Hence, Toll mRNA polyadenylation is independent of the presence of CPEs or PAS and implies a novel but still not-identified machinery (Coll et al., 2010).

4.3. mRNPs and mRNP granules

As already stated, mRNAs are not “naked” nucleic acids but instead are coated by multiple RBPs that determine their processing and fate. Thus, it is more convenient to refer to mRNAs as messenger ribonucleoprotein particles (mRNPs). mRNPs are highly dynamic structures that are subjected to rearrangements that regulate the mRNA fate in response to biological signalling (Gebauer et al., 2012). mRNPs composition is complex and depends on the combination of specific *cis*-acting elements located mainly in the 3' and 5' UTRs. Unveiling the composition of mRNPs, as well as their diversity and dynamics, is relevant to better understand mRNA translational control. Recent system-wide studies have defined the mRNA interactome in mammalian cells and its occupancy profile, identifying more than 800 RBPs with potential roles in mRNA biology. Furthermore, the protein occupancy profiles indicated that extensive regions of the 3' UTRs are targeted by RBPs (Baltz et al., 2012; Castello et al., 2012). These studies ratify the high intricacy of mRNPs.

mRNPs with specific RBP compositions can keep mRNAs translationally inactive (see sections 4.1, 4.2 and 7.2). Many translationally silent mRNPs have the ability to assemble into membraneless cytoplasmic organelles known as mRNP granules. Specific examples of mRNP granules are processing bodies (P-bodies), stress

granules, neuronal granules and germ granules (Buchan, 2014). These two last being specialized granules for mRNA storage and localization in neurons and germ cells respectively. The best-characterized mRNPs granules in somatic cells are P-bodies and stress granules, described thereafter.

P-bodies are present in non-stressed cells and are characterized by the accumulation of proteins involved in translational repression and mRNA decay. Degradation of eukaryotic mRNAs is generally initiated by CCR4/NOT-mediated deadenylation. After deadenylation, mRNAs can be degraded by the exosome from 3' to 5', or, more commonly, mRNAs are decapped by Dcp1/Dcp2 decapping enzyme and then degraded by the exonuclease Xrn1 from 5' to 3'. Alternative specialized mRNA decay pathways are responsible for the degradation of aberrant mRNAs, such as nonsense-mediated decay, non-stop decay and no-go decay (Garneau et al., 2007). P-bodies are enriched in factors involved in these degradation processes, as is the case of the decapping enzyme complex Dcp1/Dcp2, decapping activators, and the CCR4/NOT deadenylation complex. Moreover, P-bodies contain translation repressors as p54, Rap55, eIF4E-T, Pat1 and CPEB1 (Wilczynska et al., 2005), as well as proteins involved in the miRNA repression pathway, like GW182. In consonance with their composition, P-bodies are thought to represent centres for mRNA decay, although not all the mRNAs in P-bodies are degraded but instead can be stored and later returned to a translationally active state (Brenques et al., 2005; Cougot et al., 2004; Parker and Sheth, 2007).

Stress granules, which are formed upon cellular stress, share some components with P-bodies (such as p54, Rap55 and CPEB1) but characteristically contain translation initiation factors like eIF4E, eIF4G, eIF4A, eIF3, eIF2 α , PABP and the 40S ribosomal subunit, and translational repressors like TIA-1 and TIAR. Thus, it seems that stress granules are aggregates of mRNPs stalled at translation initiation. Stress granules have been hypothesized to function in mRNA repression and stabilization during cellular stress (Buchan and Parker, 2009; Decker and Parker, 2012).

Despite the proposed function in mRNA degradation, stabilization and repression of P-bodies and stress granules, mRNP assembly into macroscopic mRNP granules is not rate limiting for none of these processes. Thus, the current hypothesis argues that mRNP granule formation results in an increased local concentration of factors

within granules, which enhances mRNA repression, mRNA decay in the case of P-bodies, or the formation of productive translation complexes in stress granules. At the same time, mRNP granule assembly implies a decrease of the concentration of these same factors in the cytosol, which can be beneficial to avoid promiscuous mRNA decay and to maintain a proper ratio of mRNAs and translation factors (Decker and Parker, 2012; Erickson and Lykke-Andersen, 2011).

The assembly of P-bodies and stress granules is dependent on the pool of non-translating mRNAs. Hence, most probably, they assemble through protein-protein interactions between translationally repressed mRNPs. Low-complexity domains in P-bodies and stress granules factors have been shown to be involved in mRNP granule assembly through self-association (Jonas and Izaurralde, 2013) (further described in section 5).

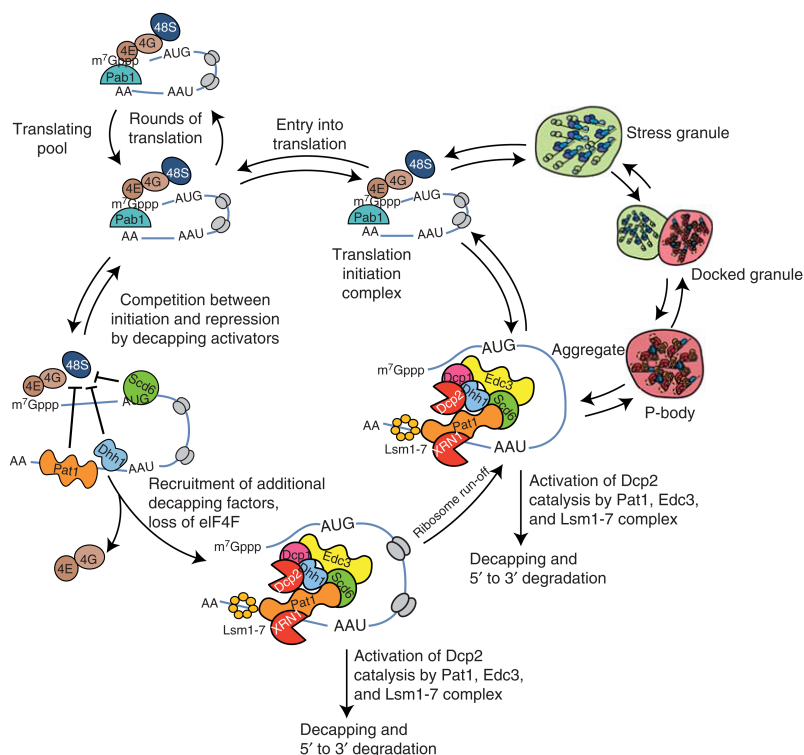


Figure 4. Model for the “mRNP cycle” (taken from (Decker and Parker, 2012)). The movement and remodelling of mRNPs between polysomes, P-bodies and stress granules are represented.

Noteworthy, fluorescence recovery after photobleaching experiments (Kedersha et al., 2000) show that mRNP granules are dynamic structures. In addition, several observations argue that mRNAs can cycle between P-bodies, stress granules and polysomes, which implies that mRNPs must undergo remodelling processes that will ultimately determine the mRNA fate (Figure 4) (Buchan and Parker, 2009; Decker and Parker, 2012; Kedersha et al., 2005).

5. Intrinsically disordered proteins

A considerable portion of eukaryotic proteins contains large regions of disorder, known as intrinsically disordered regions (IDRs). For instance, 44% of human protein-coding genes contain disordered segments of more than 30 amino acids in length. Intrinsically disordered regions are characterized by the lack of a stable, well-defined, globular structure. This feature is linked to a biased amino acid composition and low sequence complexity. Hence, in comparison with structured domains, IDRs contain low proportion of hydrophobic amino acids, whereas are enriched in polar and charged amino acids. Some proteins are mainly disordered. However, the majority of the proteins in eukaryotic proteomes contain both IDRs and structured regions and are referred thereafter as intrinsically disordered proteins (IDPs) (Lee et al., 2014).

The lack of structure provides several advantages to IDPs. First, disordered regions are ideal platforms for multiple interactions. In this sense, IDRs harbour molecular recognition elements and short linear motifs that can fold upon binding to their targets, although some disordered regions seem to function as flexible unstructured linkers. Generally, the interactions mediated by IDRs are characterized by high specificity but modest affinity, allowing rapid signalling responses. Second, IDRs have a high degree of conformational flexibility that grants the interaction with multiple targets. Finally, IDRs are accessible regions for post-translational modification sites. Owing to these features, IDPs are ideal to mediate signalling and

coordinate regulatory events and, frequently, function as central hubs in signalling networks (Wright and Dyson, 2014).

IDPs play essential functions in many cellular processes, including cell cycle, regulation of transcription and translation. According with their biological relevance and their structural properties, the expression of proteins with disordered domains is tightly regulated. IDP-encoding transcripts are generally less abundant than transcripts encoding more structured proteins due to increased decay rates. Moreover, IDPs are less abundant than ordered proteins due to lower protein synthesis rates and shorter half-lives. Finally, as previously mentioned, IDPs are enriched in post-translational modification sites (Gsponer et al., 2008). Miss-regulation of IDPs has been linked to neurodegenerative diseases due to abnormal protein aggregation (Gray and Woulfe, 2013; Uversky et al., 2008).

5.1. Intrinsically disordered regions in RNA-binding proteins

The recently published mRNA interactome revealed that RNA-binding proteins are especially enriched in IDRs, with overrepresentation of low complexity and short repetitive amino acid sequences (Castello et al., 2012). In agreement with this observation, a statistically significant portion of the RBPs precipitated with biotinylated isoxazole chemical, which precipitates components from mRNP granules, contain low complexity sequences, such as the [G/S]Y[G/S] motif (Kato et al., 2012).

These facts suggest that IDRs may have a relevant role in RNA biology.

5.2. Intrinsically disordered regions in the formation of membraneless organelles

IDPs with low-complexity regions, as well as multivalent proteins, can undergo phase transitions that result in the formation of membraneless organelles, which are dynamic aggregates not surrounded by membranes. Membraneless organelles often contain both proteins and mRNAs and are referred as mRNP granules (for details see section 4.3).

Phase transitions rely on multiple weak intermolecular interactions. These low affinity interactions explain the high degree of dynamism of membraneless organelles, which are constantly exchanging components with the surrounding cytoplasm and exhibit liquid-like behaviours (Brangwynne et al., 2009).

Two main molecular features have been related to the capacity of molecules to phase separate. On the one hand, interactions between multivalent macromolecules, including multi-domain proteins and mRNAs, have been shown to produce sharp liquid-liquid demixing phase transitions in aqueous solution. This is exemplified by the Nephtrin-NCK-N-WASP system, where all the components present multiple interacting domains. The Nephtrin-NCK-N-WASP system modulates the activity of the actin-nucleating complex Arp2/3, and, importantly, it undergoes phase transitions that correspond to an increase of actin assembly rate, indicating that the formation of membraneless organelles could favour rate-limiting steps in different processes (Banjade and Rosen, 2014; Li et al., 2012).

On the other hand, low-complexity disordered domains are also able to undergo phase transitions. On that account, two studies from McKnight and colleagues have revealed that low-complexity sequences are necessary and sufficient for the transition to a dynamic hydrogel state composed by relatively unstable amyloid-like fibers. These hydrogels are able to recruit mRNAs when low-complexity regions are fused to an RNA-binding domain (RBD). Thus, a two-component model for mRNA recruitment to membraneless organelles has been proposed, where RNA-binding proteins recruit mRNAs through their RBD and phase separate by multiple intermolecular interactions established between low-complexity sequences (Han et al., 2012; Kato et al., 2012). In agreement with this model, many P-bodies and stress granules components have regions rich in proline, glutamine and asparagine that have the ability to self-interact and are required for mRNP granule assembly (Decker and Parker, 2012; Jonas and Izaurralde, 2013). Nevertheless, the ability of low-complexity sequences to phase separate into hydrogels is not exclusive for RNA-binding proteins and mRNP granules. Instead, phenylalanine/glycine (FG) repeats in nucleoporins have been shown to form a three-dimensional meshwork required for the nuclear pore complex selective transport (Frey and Görlich, 2007; Frey et al., 2006; Schmidt and Görlich, 2015). In addition, the spindle regulatory protein BuGZ undergoes phase transitions around microtubules in order to support

spindle assembly and, again, this ability depends on its low-complexity disordered domain (Jiang et al., 2015).

An important feature of liquid-like or hydrogel-like aggregates is that they are potentially modulated by post-translational modifications. For example, the hydrogels formed by the low-complexity sequence from fused in sarcoma (FUS) RBP are reversible upon phosphorylation by DNA-dependent protein kinase (Han et al., 2012). Moreover, the liquid-like droplets assembled by the IDR of Ddx4 RNA helicase are sustained through electrostatic interactions and reverse upon arginine methylation (Nott et al., 2015). Finally, the phase transition boundary in the Nephrin-NCK-N-WASP system decreases considerably upon Nephrin phosphorylation, in this case, due to the creation of binding sites for NCK SH2 domain (Li et al., 2012). Thus, the dynamic nature of these aggregates makes them susceptible to post-translational regulation.

At this point it is important to emphasize the fact that these liquid-like or hydrogel-like aggregates are different from the amyloid aggregates characteristics of neurodegenerative diseases, which are stable, non-regulated and pathogenic. It is plausible that pathogenic amyloid fibrils represent an aberrant phase transition from liquid-like dynamic aggregates to solid-like static fibrils (Figure 5) (Weber and Brangwynne, 2012), which might be favoured by specific disease-related mutations that enhance fibrillization (Molliex et al., 2015).

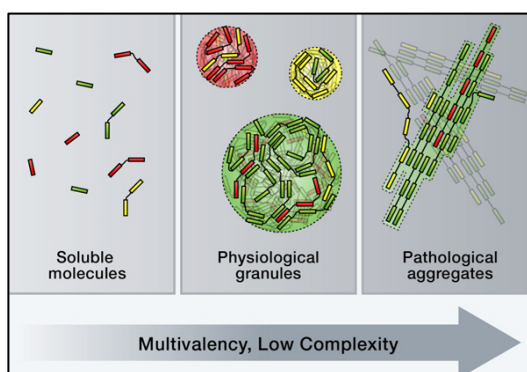


Figure 5. Phase transitions in intracellular biomolecules (from (Weber and Brangwynne, 2012)). Multivalent interaction domains and low-complexity sequences drive phase transitions into physiological liquid-like granules. These aggregates are dynamic and reversible, unlike amyloid pathogenic aggregates found in neurodegenerative disorders that are very stable. Pathological aggregates may represent an aberrant phase transition to fibrils.

6. Protein phosphorylation and hyperphosphorylation

Protein phosphorylation is a very common post-translational modification that regulates protein activity in time and space, and influences almost every cellular process. It consists in the addition of a phosphate group to specific protein residues, which in eukaryotes are serines (S), threonines (T) and tyrosines (Y). Protein kinases are the enzymes responsible for protein phosphorylation, whereas protein phosphatases reverse this reaction. Thence, protein phosphorylation is a rapid and reversible mechanism for the control of protein function.

Protein kinases catalyse the transfer of the γ -phosphate from ATP to the hydroxyl oxygen of S, T or Y. Although all classical kinases are structurally similar, there are some structural features in the kinase active site that confer specificity in substrate recognition. Hence, generally, different kinases recognize different consensus sequences on substrates. For example, cyclin-dependent kinases (Cdks) and p42 mitogen-activated protein kinase (p42MAPK, also known as ERK2) are proline-directed kinases that require the presence of a proline after the S/T phosphorylation site for target recognition. This amino acid composition is disfavoured in non-proline-directed kinases. Besides the local interactions established by the kinase active site and the surrounding amino acids of the substrate phosphorylation site, there are other mechanisms that contribute to kinase specificity. Among them, there are mechanisms to recruit kinases to specific substrates, such as distal docking sites between the kinase and its substrate, conditional docking sites generated by previous phosphorylation events known as priming events, kinase-targeting subunits and scaffolds, which act as platforms that recruit kinases and substrates to the same complex. Kinase localization to certain subcellular compartments also contributes to specificity, as well as the presence of competing substrates (Ubersax and Ferrell, 2007).

Approximately 30% of cellular proteins are phosphorylated in at least one residue and the consequences of such phosphorylation events are very diverse, including modulation of the substrate intrinsic activity, subcellular location, half-life and binding to other proteins (Cohen, 2000).

Protein phosphorylation can induce conformational changes that directly affect the activity of the substrate, for example, by changing the accessibility of the substrate catalytic domain. This can be accomplished by single phosphorylation events. Nevertheless, many proteins are phosphorylated in multiple residues, especially IDPs, which are readily accessible for post-translational modifications. Multisite phosphorylation can influence the conformational propensities of IDPs. For example, it can induce folding of the disordered region, as is the case of 4E-BP2 (Bah et al., 2015), or, otherwise, can prevent the binding and folding of disordered autoinhibitory sequences (Wright and Dyson, 2014). However, it can also produce changes in protein function through bulk electrostatics without the necessity of conformational changes. This is exemplified by Ste5 and Sic1 hyperphosphorylation. First, Ste5, a MAPK scaffold protein, is phosphorylated in eight proline-directed S/T near its membrane-binding domain that prevent its binding to the plasma membrane by electrostatic repulsion (Serber and Ferrell, 2007; Strickfaden et al., 2007). Second, the Cdc2 inhibitor Sic1 only binds to Cdc4 ubiquitin ligase subunit when it is phosphorylated in at least six out of the nine phosphosites, due to the effect of cumulative electrostatic interactions (Borg et al., 2007).

Beyond its role in modulating protein conformation and binding to partners, hyperphosphorylation exerts fine control over cell signalling, contributing to the integration of different signalling pathways, the timing of cellular events and the generation of switch-like ultrasensitive responses.

An ultrasensitive response is defined as “a response to an increasing stimulus that is described as a sigmoidal dose-response curve. Low levels of stimulus produce a poor response but, as the stimulus level increases, there is an abrupt increase in the response to near-maximal levels” (Ubersax and Ferrell, 2007). Thus, ultrasensitivity allows a signal transducer to ignore small stimuli and then respond decisively once the input surpasses a certain threshold. This kind of input-output relationships produces switch-like responses as the ones that drive cell cycle progression. Different mechanisms can generate ultrasensitivity, being cooperativity, enzyme saturation, feed-back loops, substrate competition and hyperphosphorylation some examples (Ferrell and Ha, 2014a, 2014b; Kim and Ferrell, 2007).

In multisite phosphorylation systems, ultrasensitivity can be generated by cooperativity. Thus, if the first phosphorylations favour the later ones, as would be

the case of priming phosphorylations, the response becomes ultrasensitive. Another way of producing ultrasensitivity is by competition. Hence, if the different hypophosphorylated forms of the substrate compete for kinase binding, only in situations where the amount of kinase is able to generate the hyperphosphorylated form, the response will be generated and ultrasensitive (Ferrell and Ha, 2014c; Trunnell et al., 2011). Additionally, in order to produce maximal ultrasensitive responses it is best that only half of the sites are indeed required for activation, since the inessential phosphorylation sites will compete for the kinase and will buffer low kinase activity (Figure 6) (Ferrell and Ha, 2014c; Kim and Ferrell, 2007).

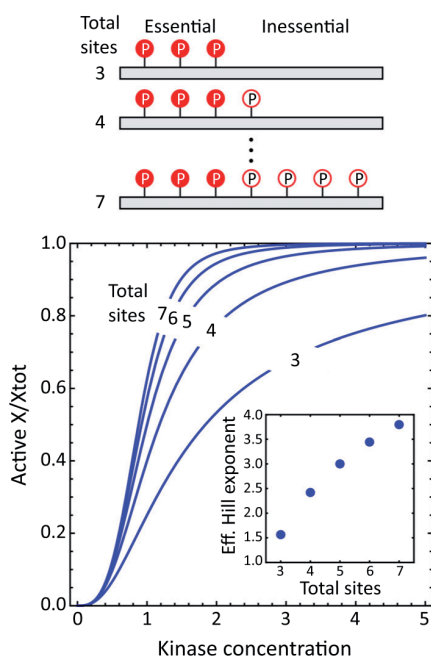


Figure 6. Extra phosphorylation sites increase ultrasensitivity (from (Ferrell and Ha, 2014c)). Hypothetical input-output relationship between a kinase and its substrate X, considering different number of inessential phosphorylation events. Assuming that three phosphorylations are required for the activation of X (essential phosphorylations), when the total number of phosphosites is seven, the ultrasensitivity in the response is higher.

An example in which hyperphosphorylation accounts for ultrasensitivity is the regulation of the phosphatase Cdc25C by Cdc2 (refer to section 7.4 for Cdc25C and Cdc2 function in cell cycle). Clearly, when three out of the five described Cdc2-mediated phosphosites in Cdc25C are mutated, the ultrasensitivity of the response is lost (Trunnell et al., 2011). Ultrasensitive responses like this contribute to the bistability of cell cycle.

7. Cytoplasmic polyadenylation element binding proteins

7.1. The CPEB family of RNA-binding proteins: C-terminal and N-terminal domains

The CPEB family of RNA-binding proteins is composed of four paralogs in vertebrates, CPEB1, 2, 3 and 4. CPEBs are also present in invertebrates, although in different number. For example, in *Drosophila*, there are two CPEB orthologs, Orb and Orb2, in *Caenorhabditis elegans* four (CPB-1, -2 and -3 and FOG-1) and in *Aplysia* one (ApCPEB) (Fernández-Miranda and Méndez, 2012; Ivshina et al., 2014) (Figure 7).

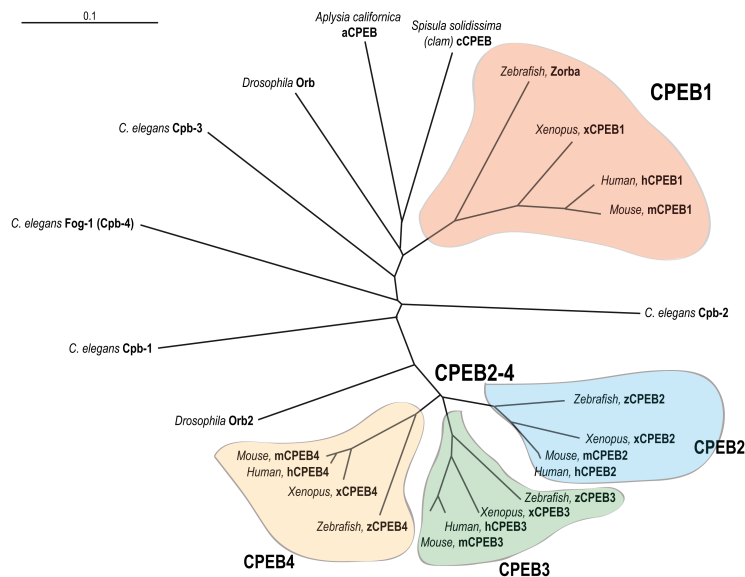


Figure 7. The CPEB family of RNA-binding proteins (from (Fernández-Miranda and Méndez, 2012)). Unrooted phylogenetic tree of the most representative CPEB paralogs and orthologs, based on a multiple sequence alignment. CPEB1 vertebrate orthologs (red) are the most distal members of the family, while CPEB2 (blue), CPEB3 (green) and CPEB4 (yellow) are placed in the same branch.

The sequence conservation between the CPEBs defines two subfamilies, one composed by CPEB1 and the other one by CPEB2, 3 and 4, which are more closely related (Figure 7). Interestingly, the phylogenetic analysis clearly shows that CPEBs are more conserved between orthologs than between paralogs, which provides strong foundation for cross-species predictions (Wang and Cooper, 2010).

All the members of the family contain a C-terminal RNA-binding domain and an N-terminal regulatory domain (Figure 8).

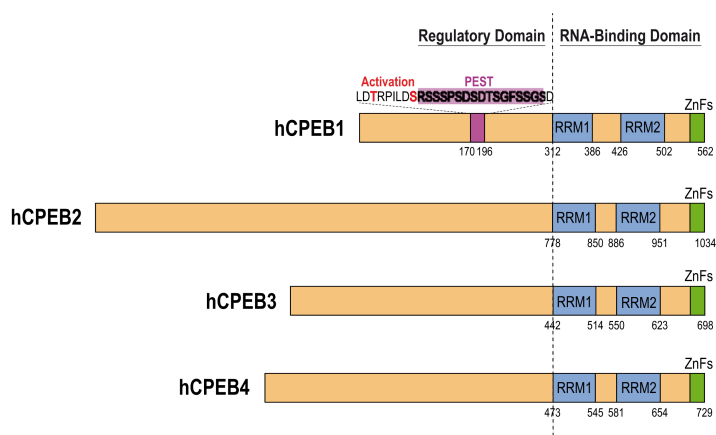


Figure 8. Protein domains of hCPEBs (taken from (Fernández-Miranda and Méndez, 2012)). CPEBs share a conserved C-terminal RNA-binding domain composed of two RNA recognition motifs (RRMs, in blue) and a ZZ domain (green). The N-terminal half of the CPEBs is highly variable and, at least for CPEB1 and CPEB3, is the regulatory domain. hCPEB1 activating phosphorylation sites are highlighted (red), as well as the PEST box (purple) responsible for CPEB1 degradation.

On the one hand, the RBD is composed by two RNA Recognition Motifs (RRM) in tandem followed by a zinc-binding domain (ZZ domain). This region is highly conserved between CPEB paralogs and orthologs, although the sequence identity is much higher between CPEB2, 3 and 4 than to CPEB1 (Huang et al., 2006). Precisely, the sequence identity in this domain is 96% between CPEB2, 3 and 4, and 46% between CPEB1 and the other CPEB family members (Figure 9). RNA recognition and binding is performed by the two RRM, being RRM1 the major

binding domain (Huang et al., 2006). Although it was proposed that the two CPEB subfamilies bind to different sequences on target mRNAs (Huang et al., 2006), more recent studies show that all CPEBs recognize and bind to CPE elements in the 3' UTR of target mRNAs and, therefore, regulate overlapping mRNAs populations (Igea and Méndez, 2010; Novoa et al., 2010; Ortiz-Zapater et al., 2012). The ZZ domain was first characterized as a Zinc Finger (Hake et al., 1998). However, Merkel et al. have shown that it is a ZZ domain that adopts a cross-braced zinc coordination topology (Merkel et al., 2013). Although ZZ domains usually participate in protein-protein interactions, the CPEB1 ZZ domain contributes to RNA binding, although does not confer specificity (Hake et al., 1998; Huang et al., 2006).

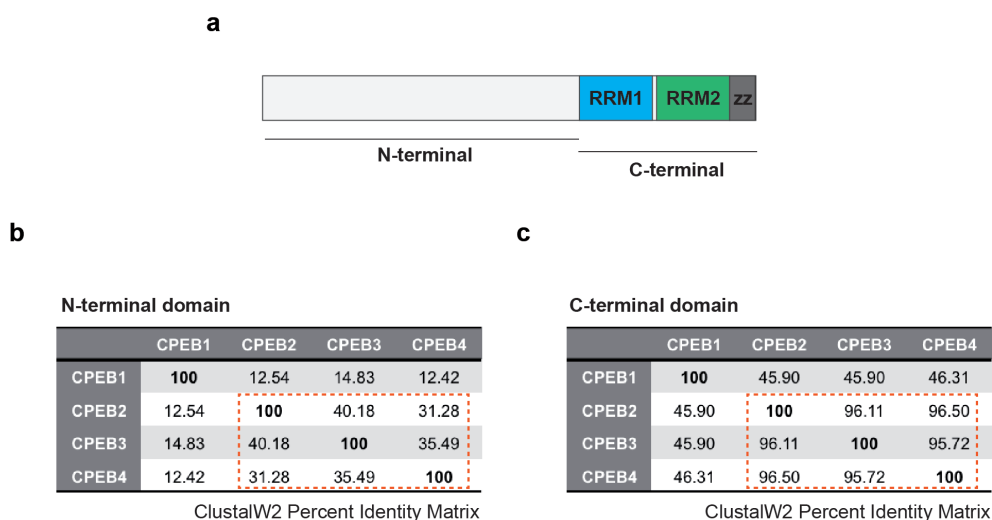


Figure 9. N-terminal and C-terminal domains conservation among hCPEB paralogs. (a) Schematic representation of CPEB N-terminal and C-terminal domains. RRM1 (blue), RRM2 (green) and the ZZ domain (grey) from the C-terminal RNA-binding domain are highlighted. (b) ClustalW2 Percent Identity Matrix of the N-terminal domain of hCPEB paralogs. Note that this region is not conserved among CPEB family members. (c) ClustalW2 Percent Identity Matrix of the C-terminal domain of hCPEB paralogs. This domain shows 96% sequence identity between CPEB2, 3 and 4, and 46% between CPEB1 and the other CPEBs.

On the other hand, the N-terminal domain (NTD) is highly variable across CPEB paralogs, both in length and composition. Note that the sequence identity in this region hardly reaches 40% between CPEB2, 3 and 4, and is just around 14% when comparing CPEB1 with the other members of the family (Figures 8 and 9). This N-terminal region, at least for CPEB1 and CPEB3, is the regulatory domain. In the case of CPEB1, the NTD contains an Aurora A Kinase phosphorylation site responsible for its activation, as well as multiple Cdc2 and Plk1 phosphorylation sites that target CPEB1 for degradation through a PEST-box domain (Mendez et al., 2000a, 2000b, 2002). In CPEB3, the NTD is rich in glutamines and forms amyloid-like aggregates, which are regulated by SUMOylation and monoubiquitination (Driscaldi et al., 2015; Pavlopoulos et al., 2011). These regulatory motifs are not conserved between CPEB paralogs (Theis et al., 2003). Thus, the different CPEBs must be regulated by alternative mechanisms. In agreement with this observation, the NTD from CPEB1 cannot be substituted with that from CPEB3 (Huang et al., 2006). Moreover, although CPEB1 and CPEB4 bind the same target mRNAs, they are not interchangeable in meiosis due to a differential post-translational regulation (Igea and Méndez, 2010). Interestingly, CPEB2, 3 and 4 NTDs, but not CPEB1, contain large regions of disorder (Figure 10).

To conclude, CPEBs share a conserved RBD but differ in their NTD, which confers a differential post-translational regulation to the CPEBs and the ability to differentially respond in a given cellular environment.

CPEBs play a dual role in mRNA translational regulation through cytoplasmic polyadenylation. They can both repress or activate mRNAs for subsequent translation. In the following section, the molecular mechanisms behind CPEB-mediated translational repression or activation are discussed.

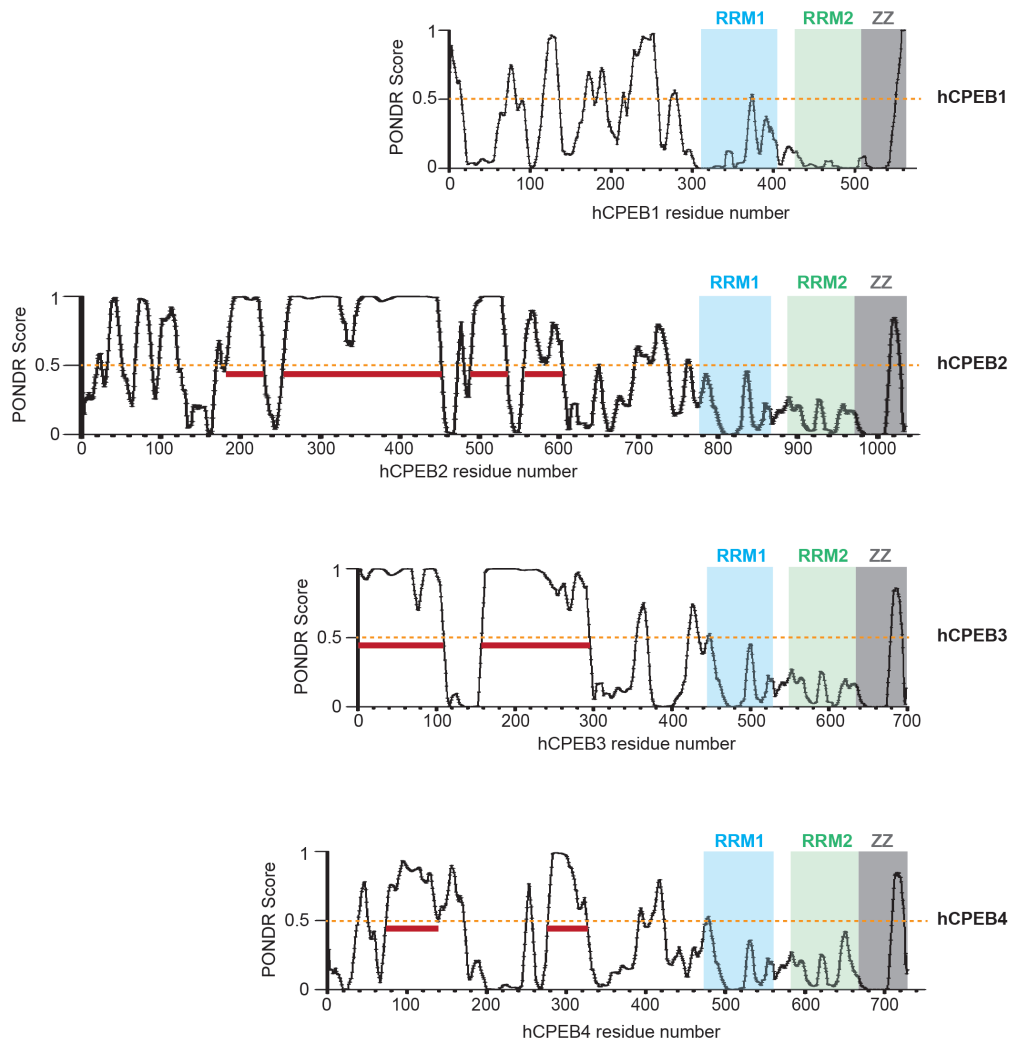


Figure 10. Disorder tendency of hCPEBs calculated with PONDNR® VL-TX predictor. PONDNR Scores above 0.5 indicate disorder, while PONDNR Scores below 0.5 indicate order. Large disordered regions are highlighted with a red line. RRM1 (blue), RRM2 (green) and the ZZ domain (grey) of the RNA-binding domains are shown. Note that while the RNA-binding domain is ordered, the N-terminal domains of CPEB2, 3 and 4 (not CPEB1) contain large disordered regions.

7.2. CPEB mediated translational repression

The majority of the mechanisms behind CPEB-mediated translational repression, as well as activation, have been elucidated in *Xenopus* oocytes. Moreover, the only CPEB studied in depth mechanistically is CPEB1.

CPEB1-mediated repression requires a specific arrangement of CPE elements in the 3' UTR of target mRNAs that consists of two CPEs spaced by less than 50 nucleotides, which most probably reflects the formation of a dimer (Piqué et al., 2008).

Different models for CPEB1 repression have been proposed (Figure 11), however they are mutually exclusive. It is not well known whether the different repression complexes described are transcript-specific, cell cycle phase-specific or otherwise represent intermediary stages in the assembly of a larger repression complex (Fernández-Miranda and Méndez, 2012).

The first model (Figure 11a) proposes that CPEB1 repression complex mediates the shortening of the poly(A) tail acquired in the nucleus by the recruitment of the deadenylase PARN. In this model, CPEB recruits CPSF to the PAS and, together with the scaffolding protein Symplekin, recruit the poly(A) polymerase Gld-2 (Barnard et al., 2004). At the same time, CPEB and Gld-2 recruit PARN, which presents a very robust activity and overrides the polyadenylation activity of Gld-2. Therefore, the poly(A) tail of the target mRNA is shortened by the action of PARN (Kim and Richter, 2006). Importantly, PARN deadenylation is only efficient in capped mRNAs. Moreover, CPEB1 also interacts with the embryonic poly(A)-binding protein (ePAB). This fact, together with the shortening of the poly(A) tail, precludes ePAB from its association with the poly(A) tail and disrupts the cap-eIF4E-eIF4G-ePAB-poly(A) mRNA-circularizing complex (Kim and Richter, 2007). As a consequence, the mRNA is silenced.

The second model (Figure 11b) implies the disruption of the interaction between eIF4E and eIF4G through Maskin, an eIF4E-interacting protein that precludes the recruitment of eIF4G and avoids translation initiation (Stebbins-Boaz et al., 1999).

The third model (Figure 11c) has been identified in early stage oocytes. It describes the assemblage of a CPEB repression complex containing the RNA helicase Xp54, the RNA-binding proteins P100 and RAP55, the eIF4E-binding protein eIF4E-T and

eIF4E1b. In this model, the interaction between eIF4E and eIF4G is affected since the eIF4E protein in this complex is eIF4E1b, which interacts with eIF4E-T rather than binding eIF4G (Minshall et al., 2007). Consistent with a repressing role of the described CPEB mRNP, many of the proteins mentioned are enriched in P-bodies.

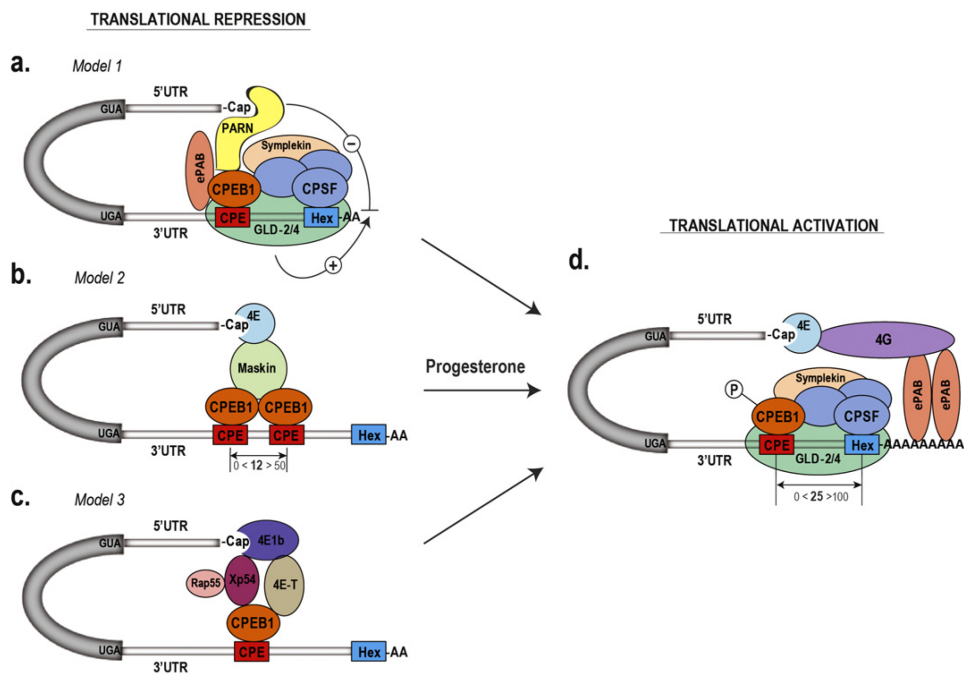


Figure 11. CPEB1-mediated translational control mechanisms (from (Fernández-Miranda and Méndez, 2012)). **(a-c)** Schematic representation of CPEB1 repression complexes. **(a)** Repression complex mediated by CPEB1 interaction with PARN deadenylase. **(b)** Repression complex mediated by CPEB1 interaction with Maskin, which binds to eIF4E and blocks the formation of the cap-binding complex. **(c)** Repression complex mediated by CPEB interaction with Xp54, eIF4E-T and eIF4E1b. **(d)** Upon progesterone stimulation, CPEB is phosphorylated (P) and assembles an activation complex with Gld2/4 polymerase that drives cytoplasmic polyadenylation. The poly(A) tail recruits ePAB, which establishes connections with the cap-binding complex for translation initiation. The distance (in nucleotides) required for translational repression is shown in b. The distance required for translational activation is shown in d. The *cis*-acting elements Cytoplasmic Polyadenylation Element (CPE) and poly(A) signal (Hex) are shown in red and blue respectively. The length of the poly(A) tail is indicated.

These three models are not compatible. For example, PARN-mediated deadenylation requires the interaction with the 5' cap (Gao et al., 2000; Kim and Richter, 2007), which implies that eIF4E should be absent from the complex. Moreover, although the third model is most abundant in early stage oocytes, the interaction between CPEB1 and eIF4E-T is also detected in stage VI oocytes (Minshall et al., 2007). Since both eIF4E-T and Maskin bind eIF4E, the second and the third model are mutually exclusive. Even though, it is clear that CPEB1-mediated translational repression involves mRNA deadenylation and interference with the cap-eIF4E-eIF4G complex formation.

Whether these mechanisms of translational repression are conserved in somatic cells is not clear, but some studies have clarified some aspects of this issue. Although the mammalian ortholog of Maskin (TACC3) does not contain an eIF4E-binding motif, another eIF4E binding protein, Neuroguidin, has been involved in CPEB1-mediated repression together with Gld-2 and PARN in mammalian neurons (Jung et al., 2006; Udagawa et al., 2012).

With respect to the other members of the CPEB family, much less is known. Nevertheless, some studies suggest that they repress mRNA translation through different mechanisms.

First, CPEB3 has been shown to repress mRNA translation when tethered to a specific luciferase reporter and has been proposed to translationally repress the mRNA encoding the AMPA receptor GluR2 in neurons (Huang et al., 2006). Nevertheless, how CPEB3 actively represses mRNA translation is still not known. Hosoda et al. have shown that CPEB3 negatively regulates the expression of target genes by the formation of a ternary complex with the anti-proliferative protein Tob and the deadenylase Caf1, which results in deadenylation and decay of CPEB3 target mRNAs (Hosoda et al., 2011). However, this mechanism implies a regulation of target mRNA abundance and not a direct role in translational repression.

Second, CPEB2 is also able to repress translation in somatic cells. However, CPEB2 does not interfere with the translation initiation step but with elongation. Specifically, CPEB2 interacts with the elongation factor eEF2 to slow down peptide elongation of CPEB2-bound mRNAs (Chen and Huang, 2012). At the moment, the

only CPEB2 target described is *HIF-1α* mRNA (Chen and Huang, 2012; Hägele et al., 2009).

Finally, CPEB4 represses the translation of a large set of mRNAs in terminal erythropoiesis by interacting with the initiation factor eIF3 (Hu et al., 2014).

To conclude, the CPEB family members can repress the translation of specific mRNAs through different mechanisms that include shortening of the poly(A) tail, blocking of the formation of the cap-eIF4E-eIF4G complex or even the reduction of the elongation rate.

7.3. CPEB mediated translational activation

CPEB-mediated translational activation of mRNAs implies the remodelling of the CPEB-mRNP above mentioned in order to drive cytoplasmic polyadenylation. For cytoplasmic polyadenylation of CPE-containing mRNAs, the CPE must be closer than 100 nucleotides from the PAS, being the optimal distance 25 nucleotides (Piqué et al., 2008).

As for repression, the mechanisms behind the translational activation of CPE-containing mRNAs were first described for CPEB1 in the context of meiosis. The switch from a repression to an activation complex is triggered by CPEB1 phosphorylation at S174. This phosphorylation event is catalysed by Aurora A kinase (Mendez et al., 2000a), which in meiosis is activated by progesterone stimulation and subsequent meiotic resumption (Andrésson and Ruderman, 1998). CPEB phosphorylation at S174 increases the affinity of CPEB1 for CPSF (Mendez et al., 2000b) and causes the expulsion of PARN from the complex (Kim and Richter, 2006), while the recruitment of Gld-2 by CPEB1 and CPSF is maintained and even enhanced (Barnard et al., 2004). These facts result in an efficient elongation of the poly(A) tail mediated by Gld-2. Moreover, CPEB1 undergoes early RINGO/Cdc2-catalyzed phosphorylation on six proline-directed sites that dissociate ePAB from CPEB1, allowing ePAB binding to the poly(A) tail (Kim and Richter, 2007). ePAB bound to the newly elongated poly(A) tail associates with eIF4G and displaces Maskin from eIF4E (Cao and Richter, 2002; Stebbins-Boaz et al., 1999). Maskin-eIF4E interaction is also affected by Cdc2-mediated Maskin phosphorylation (Cao et al., 2006). Finally, Maskin dissociation from the complex allows eIF4E and

eIF4G interaction and, as a consequence, mRNA translation initiation takes place (Figure 11d).

This mechanism of polyadenylation-induced translation is conserved in neurons (Udagawa et al., 2012), although in this context Neuroguidin would be the eIF4E interacting factor instead of Maskin and CPEB1 phosphorylation and activation would be mediated by Aurora A kinase (Huang et al., 2002) or CaMKII (Atkins et al., 2004). Furthermore, in human fibroblasts, CPEB1 has been shown to mediate the cytoplasmic polyadenylation of *p53* mRNA through the recruitment of Gld-4 instead of Gld-2 (Burns et al., 2011). However, the specific scenarios in which CPEB1 would act through Gld-2 or Gld-4 non-canonical poly(A) polymerases remain to be determined.

The other members of the CPEB family are also able to mediate translational activation of mRNAs.

CPEB3 function in mRNA translational activation has been studied in the context of synaptic plasticity and long-term memory. In hippocampal neurons, CPEB3 is activated by the E3 ubiquitin ligase Neurilized1, which monoubiquitinates CPEB3 NTD. Monoubiquitinated CPEB3 mediates the translational activation of *GluA1* and *GluA2* mRNAs through cytoplasmic polyadenylation (Pavlopoulos et al., 2011). More recently, it has been shown that CPEB3 activity in cytoplasmic polyadenylation in neurons requires the formation of active prion-like aggregates (Drisaldi et al., 2015; Fioriti et al., 2015; Stephan et al., 2015) (further discussed in section 7.5.1). Alternatively, it has been proposed that *GluA1* and *GluA2* mRNAs are not translationally activated by CPEB3 but, instead, CPEB3-mediated repression is alleviated through CPEB3 cleavage by Calpain 2 (Wang and Huang, 2012).

Regarding CPEB2, its role in mRNA translational activation is not clear. It has been involved in *HIF1-α* mRNA translational stimulation through cytoplasmic polyadenylation (Hägele et al., 2009), but also through its dissociation from eEF2 (Chen and Huang, 2012).

Finally, CPEB4 is able to mediate translational activation of CPE-containing mRNAs through cytoplasmic polyadenylation and the recruitment of the polyadenylation machinery, such as of Gld-2 and CPSF (Igea and Méndez, 2010; Novoa et al., 2010; Ortiz-Zapater et al., 2012).

Certainly, CPEBs are key regulators of mRNA translation, at the level of mRNA repression as well as activation. However, the scheme is much more complex since the timing, the extent and the localization of these events is also tightly regulated, as exposed in the following section about the role of CPEBs in meiosis.

7.4. CPEBs in meiotic progression of *Xenopus* oocytes

The meiotic cell cycle consists of two consecutive cell divisions (M-phases) without an intervening S-phase. Most of the knowledge accumulated to understand meiosis comes from the study of *Xenopus laevis* oocyte maturation.

Fully-grown stage VI oocytes are arrested at the G2/M transition of meiosis I, more concretely at the diplotene stage of prophase I (PI). Previous to this first arrest, oocytes grow in size and store large amounts of maternal mRNAs, absolutely required for meiotic progression since it occurs in the absence of transcription. Progesterone stimulation, provided *in vivo* by the neighbouring follicle cells of the ovary, releases stage VI oocytes from the arrest, allowing them to re-enter the meiotic cell cycle until a second arrest at metaphase II (MII), where the egg awaits for fertilization (Bayaa et al., 2000; Tian et al., 2000). Upon fertilization, MII arrest is released and the subsequent embryonic cell divisions start, characterized by the lack of G1 and G2 phases until the mid-blastula transition, where transcription starts again (Mendez and Richter, 2001; Schmitt and Nebreda, 2002).

The process of oocyte maturation occurs in the absence of transcription and is supported by a complex network of translational repression and activation of the previously stored maternal mRNAs, as well as protein degradation and post-translational modification events. Altogether establish phase-specific peaks of activities required for meiotic phase transitions.

Three key activities are required for meiotic progression of *Xenopus* oocytes: the maturation promoting factor (MPF), an heterodimer composed by Cdc2 and cyclin B required for entry into M-phase; the anaphase promoting complex or cyclosome (APC/C), an E3 ligase multisubunit complex required for cyclin B degradation and metaphase exit; and the cytostatic factor (CSF), which is the activity required for MII arrest (Figure 12).

In the immature oocyte, MPF is catalytically inactive due to inhibitory phosphorylations driven by Myt1. This MPF is called pre-MPF and contains cyclins B2 and B5 as regulatory subunits (Hochegger et al., 2001; Piqué et al., 2008). Upon progesterone stimulation, MPF is activated through two signalling pathways. One involves the phosphatase Cdc25C, which removes the inhibitory phosphorylations on MPF. Cdc25C is activated by the *Xenopus* polo-like kinase xPlk1, which in turn is activated by the upstream kinase kinase xPlkk1 (Perdiguero and Nebreda, 2004). The other pathway required for MPF activation is the Mos/MEK1/MAPK/p90Rsk cascade, which is activated through the translational activation of *c-mos* maternal mRNA and results in Myt1 inactivation through p90Rsk-mediated phosphorylation. The resulting increase in active MPF mediates the transition to Metaphase I (MI) (Nebreda and Ferby, 2000). Metaphase exit is accomplished by the activation of the APC/C complex at metaphase. The APC/C then mediates the polyubiquitination and degradation of cyclin B and the transition to anaphase (Peters, 2006). However, an intermediate level of MPF activity is required in order to avoid replication (Iwabuchi et al., 2000). Intermediate MPF activity in interkinesis is achieved through a high translation rate of cyclins B1 and B4 through cytoplasmic polyadenylation and translational activation of their maternal mRNAs (Hochegger et al., 2001; Piqué et al., 2008). At the end of the first meiotic division, the polar body is extruded with half of the DNA content. Finally, for the entry into MII, APC/C activity decreases through the action of CSF and, as a consequence, MPF activity rises again and is maintained at high levels during MII arrest. The CSF is the activity responsible for the establishment and maintenance of the MII arrest (Tunquist and Maller, 2003; Wu and Kornbluth, 2008). It involves the Mos/MEK1/MAPK/p90Rsk pathway, Emi2 and Cyclin E/cdk2 (Tunquist et al., 2002). These two last CSF components are also newly synthesized through the cytoplasmic polyadenylation of their mRNAs. Emi2 is a well-characterized inhibitor of APC/C that acts through direct APC/C binding. It is very tightly regulated by kinases and phosphatases during CSF-arrest as well as upon fertilization. At MII, Emi2 stability and affinity for APC/C are maintained thanks to the recruitment of the phosphatase PP2A, which counteracts a bunch of inhibitory phosphorylations driven by Cdc2, Plk1 and CK1 kinases. The recruitment of PP2A to Emi2 is established by p90Rsk-mediated phosphorylation of Emi2 (Inoue et al., 2007; Isoda et al., 2011; Nishiyama et al., 2007). Finally, CSF release is triggered by the elevation of intracellular calcium, which activates CaMKII. CaMKII then

phosphorylates and primes Emi2 for the recruitment of Plk1, which in turn phosphorylates Emi2 and targets it for degradation by the proteasome (Hansen et al., 2006; Liu and Maller, 2005). As a result, APC/C activity increases, MPF decreases and meiosis completes.

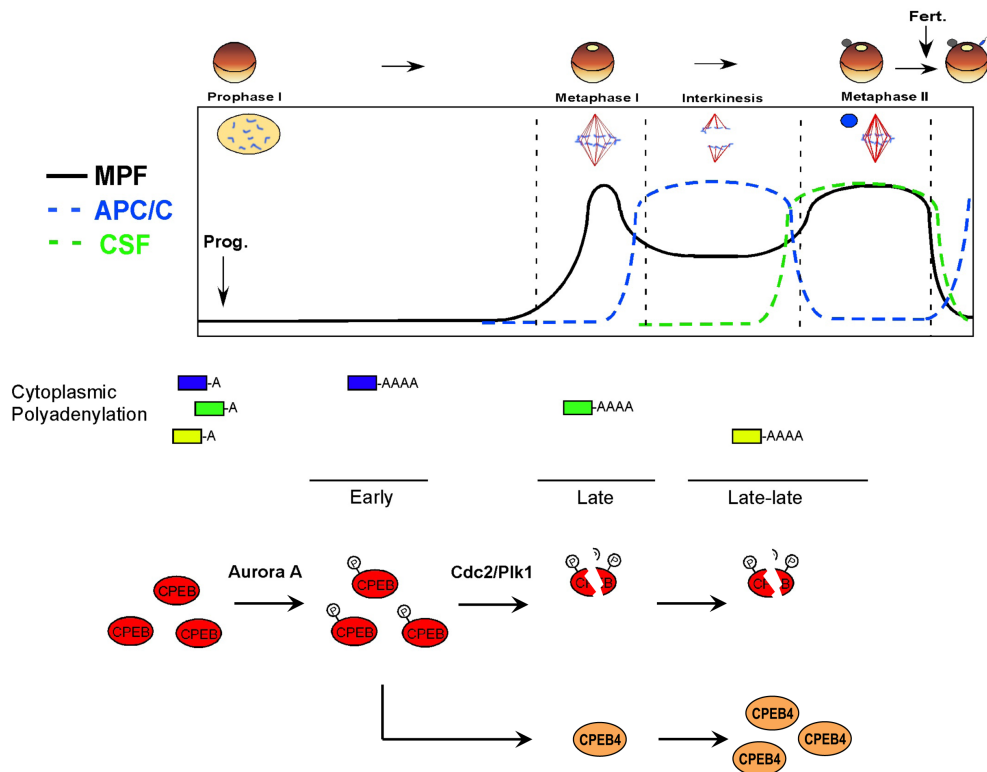


Figure 12. Meiotic cell cycle progression in *Xenopus* oocytes. Schematic representation of meiotic progression from prophase I to fertilization. Maturation promoting factor (MPF), anaphase promoting complex (APC/C) and cytotstatic factor (CSF) activities are indicated in black, blue and green respectively. Stored maternal mRNAs are represented with short poly(A) tails. Long poly(A) tails represent the three cytoplasmic polyadenylation waves (early, late and late-late) driven by CPEB1 and CPEB4. CPEB1 (CPEB, red) levels, as well as its activation by Aurora A kinase and its degradation as a consequence of Cdc2 and Plk1 phosphorylation are depicted. Finally, CPEB4 (orange) synthesis and accumulation are also shown.

7.4.1. A combinatorial code of *cis*-acting elements defines the time and extent of translational control during meiosis

As stated, meiosis relies on the translational repression and activation of previously stored maternal mRNAs. This translational regulation is mediated by the sequential activities of CPEB1 and CPEB4 (Igea and Méndez, 2010). However, not all mRNAs are activated at the same time, neither to the same extent. Instead, different waves of cytoplasmic polyadenylation and deadenylation drive meiotic progression (Belloc et al., 2008) (Figure 12).

CPE-containing mRNAs display specific behaviours during meiosis. The time and extent of translational control is defined by a combinatorial code of *cis*-acting elements localized in the 3' UTR of CPE-containing mRNAs. Thus, the translational behaviour of CPE-regulated mRNAs during meiosis can be predicted according to the combination of *cis*-acting elements present in a given 3' UTR (Belloc and Méndez, 2008; Piqué et al., 2008) (Figure 13):

1. Translational repression requires a cluster of at least two CPEs to recruit a CPEB1 dimer. The distance between adjacent CPEs defines the extent of repression, being the optimal distance 10-12 nucleotides.
2. Translational activation requires at least a single consensus CPE or a non-consensus CPE together with a Pumilio Binding Element (PBE). The CPE must be closer than 100 nucleotides from the PAS but not overlapping.
3. The extent of polyadenylation and translational activation is determined by the distance between the CPE and the PAS, with an optimal distance of 25 nucleotides, which would represent the more relaxed positioning for the CPEB-CPSF complex. Thus, the distance between CPE-PAS defines weak or strong CPEs.
4. The early or Cdc2-independent wave of cytoplasmic polyadenylation, which is mediated by CPEB1 upon its activation by Aurora A, requires CPEs non-overlapping with the PAS. mRNAs encoding Mos, cyclin B2 and B5, C3H-4, Emi1 and CPEB4 are polyadenylated in this early wave of cytoplasmic polyadenylation.
5. The late or Cdc2-dependent polyadenylation is driven by at least two CPEs, one of them overlapping with the PAS. During the transition from PI to MI, when CPEB1 levels are high, the recruitment of CPSF to the PAS is prevented by the presence of

CPEB1 in the overlapping CPE. However, once Cdc2 is activated at MI, most of the CPEB1 is degraded (Mendez et al., 2002) and stochastically only the non-overlapping CPE would recruit CPEB. As a consequence, CPSF would be recruited to the PAS and late mRNAs, such as cyclins B1 and B4, would be polyadenylated.

6. The presence of AU-rich elements (AREs) further defines the polyadenylation behaviour dictated by the CPEs. During meiosis, AREs recruit a zinc-finger protein named C3H-4, which in turn recruits the deadenylase CCR4/Not and opposes CPEB activity on those mRNAs containing CPEs and AREs. The effect of C3H-4-mediated deadenylation on target mRNAs is defined by the arrangement of CPEs. Thus, for an mRNA, such as *emi1*, that contains a weak CPE and is polyadenylated during the early wave of cytoplasmic polyadenylation, the deadenylation overrides the polyadenylation and as a consequence the mRNA is inactivated after MI. For “early-strong” CPEs, polyadenylation is displaced to MI, whereas for mRNAs containing a “late-strong” CPE arrangement, C3H-4 causes a delay in their polyadenylation until interkinesis. Thus, C3H-4 generates a third wave of cytoplasmic polyadenylation in interkinesis that activates the translation of *emi2* and cyclin E mRNAs, classified as late-late mRNAs.

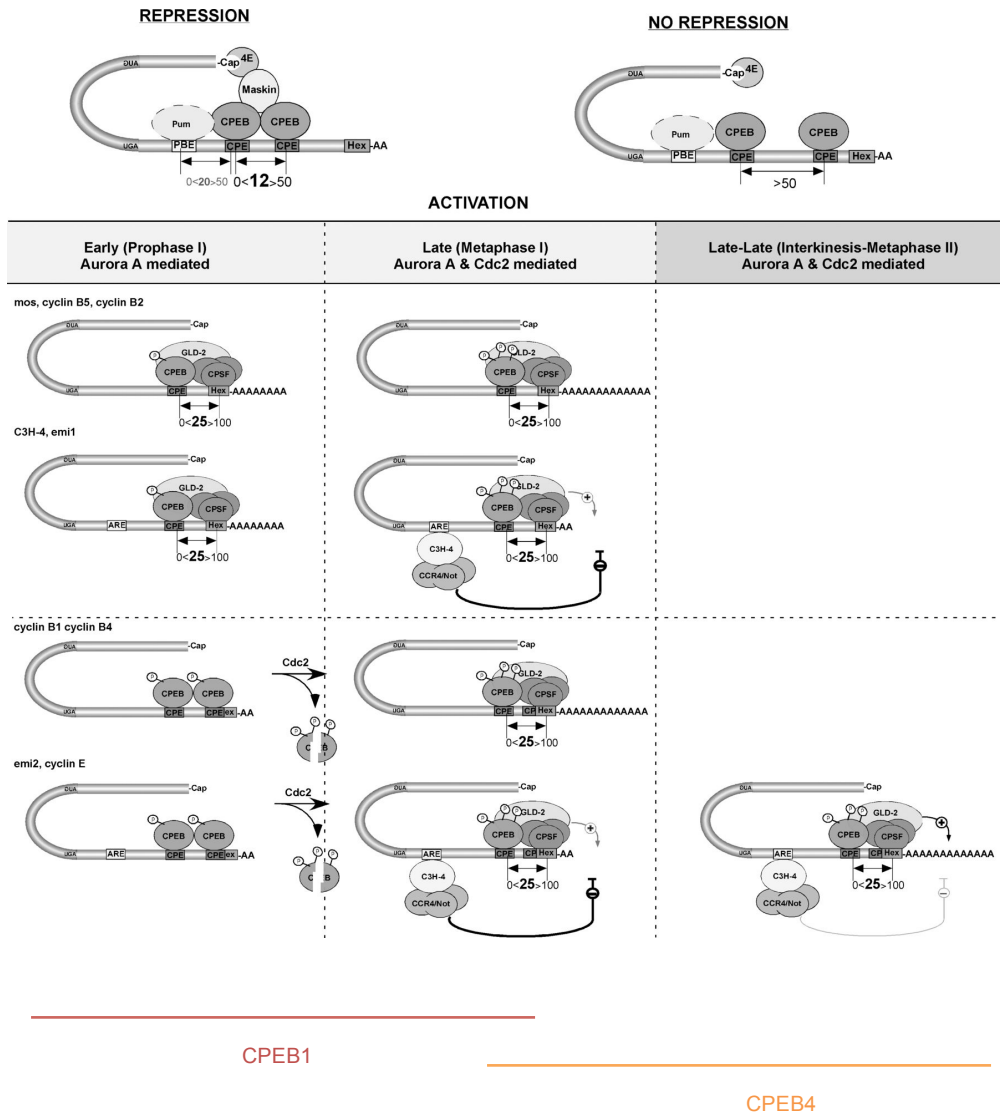


Figure 13. Model for CPE/ARE-mediated translational control (from (Belloc et al., 2008)). Schematic representation of the *cis*-acting elements and *trans*-acting factors required for CPEB-mediated translational repression and activation. The different elements that define the time and extent of CPE-containing mRNAs translational activation are indicated, as well as the three cytoplasmic polyadenylation waves (early, late and late-late). Note that while the early and the late waves are driven by CPEB1, the late-late wave is sustained by CPEB4. The distances (in nucleotides) required for translational repression and activation are also shown.

7.4.2. Sequential waves of polyadenylation and deadenylation drive meiosis

Oocyte maturation is an all-or-none response that ensures meiosis completion. This all-or-none response is accomplished by positive and negative feedback loops as well as by the intrinsic ultrasensitivities of the signalling cascades involved in meiosis, such as MAPK and Cdc2 (see section 6). Ultrasensitivity ensures that biological responses are rapid and robust but only occur once the stimulus reaches a certain threshold (Ferrell, 1999).

The signalling cascades that govern meiotic progression rely on new protein synthesis. The hierarchical translation of specific subpopulations of mRNAs during meiosis is regulated through sequential waves of polyadenylation and deadenylation. From the PI arrest to MI, CPEB1 controls the translational repression and activation of maternal mRNAs during the early and late waves of cytoplasmic polyadenylation. However, from interkinesis to MII it is CPEB4 the one that sustains the translational activation of late mRNAs and activates the translation of late-late mRNAs (Igea and Méndez, 2010) (Figure 14).

In stage VI oocytes arrested at PI, the CPE-regulated mRNAs are either inactive with short poly(A) tails or actively repressed by a dimer of CPEB1 (Barkoff et al., 2000; de Moor and Richter, 1999; Piqué et al., 2008). Upon progesterone stimulation, CPEB1 is phosphorylated by Aurora A (Mendez et al., 2000a) and induces the “early”, or Cdc2-independent, cytoplasmic polyadenylation wave. This first wave activates the translation of mRNAs that encode for proteins required for MPF activation and the transition to MI, such as cyclins B2 and B5, Mos and the APC/C inhibitor Emi1 (Belloc et al., 2008). The switch-like activation of MPF is sustained by multiple positive feedback loops in the MAPK/Cdc2 network (Ferrell, 2002), which also target Aurora A kinase synthesis and activation (Frank-Vaillant et al., 2000; Ma et al., 2003). At this time, *C3H-4* and *CPEB4* mRNAs are also translationally activated by CPEB1. C3H-4-mediated deadenylation inactivates *emi1* translation in MI, generating a negative feedback loop that results in APC/C activation. APC/C, in turn, generates a second negative feedback loop on MPF and allows the transition to interkinesis (Belloc and Méndez, 2008). At MI, CPEB1 is phosphorylated by Cdc2 and Plk1, triggering its partial destruction by the proteasome (Mendez et al., 2002). CPEB1 degradation is required for the second wave of “late”, or Cdc2-dependent, polyadenylation to occur, as well as to prevent

the repression of previously activated mRNAs during interkinesis (Igea and Méndez, 2010). During the second wave of translational activation, cyclins B1 and B4 are synthesized, which are required to maintain an intermediate level of MPF activity during interkinesis and for MPF reactivation at MII. However, CPEB1 degradation results in very low levels of CPEB1 in the second meiotic division. At this time, CPEB1 is replaced by CPEB4 to complete meiosis. CPEB4 is encoded by an “early” maternal mRNA. Nevertheless, the combination of strong CPEs and AREs in its 3' UTR delays its translational activation and protein accumulation until interkinesis, when CPEB4 generates the third wave of “late-late” polyadenylation. During this third wave, the CSF components cyclin E and Emi2 are synthesized and the MII arrest is established. CSF, in turn, inhibits APC/C and allows the full reactivation of MPF to maintain the oocyte arrested until fertilization. Moreover, CPEB4 targets its own mRNA, generating a positive feedback loop to maintain CPEB4 levels (Igea and Méndez, 2010) (Figure 14).

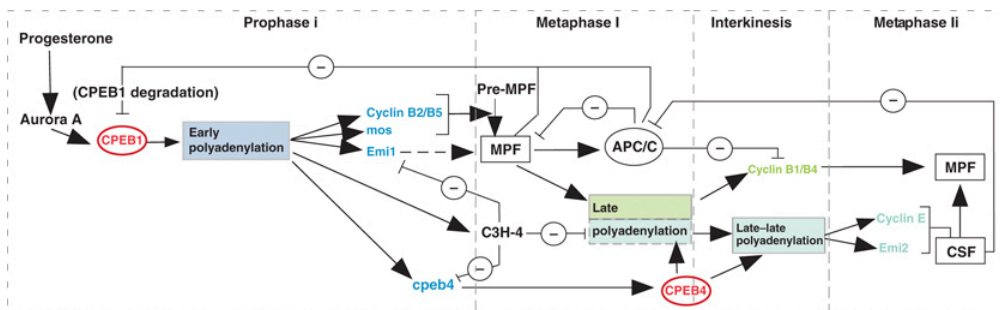


Figure 14. Sequential waves of polyadenylation and deadenylation drive meiosis (from (Igea and Méndez, 2010)). Schematic representation showing the sequential waves of cytoplasmic polyadenylation and deadenylation driving meiotic progression. The three waves of cytoplasmic polyadenylation (early, late and late-late) are depicted with boxes. While CPEB1 drives the cytoplasmic polyadenylation in early meiotic stages, CPEB4 mediates the translational activation of maternal mRNAs from interkinesis to metaphase II arrest. The positive and negative feedback loops that ensure meiotic progression are also indicated.

7.4.3. Why two different CPEBs are required for meiotic progression?

Both CPEB1 and CPEB4 recruit the polyadenylation machinery to CPE-containing mRNAs in order to activate their translation through cytoplasmic polyadenylation (Igea and Méndez, 2010; Novoa et al., 2010). However, they act in different meiotic phases. While CPEB1 regulates mRNA translation during the first meiotic division, CPEB4 does it during the second. Accordingly, CPEB1 and CPEB4 expression patterns are complementary and reflect their phase-specific activities. Thus, CPEB1 is present at high levels until MI, whereas CPEB4 starts to accumulate in interkinesis (Igea and Méndez, 2010).

The requirement of two distinct CPEBs to complete meiosis relies on their differential post-translational regulation. Although CPEB1 and CPEB4 are able to mediate the cytoplasmic polyadenylation of overlapping mRNA populations, they are not functionally exchangeable. Igea et al. showed that a non-degradable form of CPEB1 is not able to compensate for the lack of CPEB4 in the second meiotic division. Moreover, substitution of CPEB4 by CPEB1 results in deadenylation of previously activated mRNAs, such as cyclin B1. Only a constitutively active variant of CPEB1 can replace CPEB4. These results may reflect the differential post-translational regulation of both proteins.

CPEB1 is activated by Aurora A kinase upon progesterone stimulation (Mendez et al., 2000a, 2000b). However, Aurora A is inactive during interkinesis (Ma et al., 2003; Pascreau et al., 2008), which, in addition to PPI-mediated dephosphorylation of CPEB1 (Tay et al., 2003), would result in inactive CPEB1. To overcome the problem of CPEB1 reassembling repression complexes in the second meiotic division, CPEB1 is replaced by CPEB4, which should be activated by an alternative-signalling pathway. In agreement, the Aurora A phosphorylation site is not conserved in the other CPEB family members and CPEB4 contains putative recognition sites for PKA, CaMKII and S6 (Theis et al., 2003).

Different evidences point to a post-translational activation of CPEB4. First, tethering experiments showed that CPEB4 is only able to mediate translational activation of an RNA probe upon progesterone stimulation (Novoa et al., 2010), indicating that CPEB4 is not active by default but needs to be activated. Second, CPEB4 presents mobility changes in response to progesterone without any effects on its stability

(Igea and Méndez, 2010; Novoa et al., 2010), which suggests that it is post-translationally modified upon meiotic resumption. In addition, different high-throughput mass spectrometry screenings have identified up to sixteen phosphorylation sites in human, mouse or rat CPEB4, fourteen in CPEB4 NTD and two in CPEB4 RBD (www.phosphosite.org) (Dephoure et al., 2008; Huttlin et al., 2010; Olsen et al., 2010). The majority of the sites are conserved in *Xenopus laevis* CPEB4 (Figures 15 and 16).

To conclude, although both CPEBs bind the same *cis*-acting element on target mRNAs and recruit the polyadenylation machinery, CPEB1 needs to be replaced by CPEB4 in order to sustain the polyadenylation of the late-late mRNAs and to prevent the deadenylation of the previously activated mRNAs.

| | | | |
|-----------------------|---|-----|-----------|
| Mm_CPEB4 | NARTYGRARRGQSSLFPMEDGFLDDGRGDQPLHSLGSPHCFTHQNGERVERYSRKVFVGG | 478 | RRM1 |
| Rn_CPEB4 | N-----GQSSLFPMEDGFLDDGRGDQPLHSLGSPHCFTHQNGERVERYSRKVFVGG | 470 | |
| Hs_CPEB4 | NARTYGRARRGQSSLFPMEDGFLDDGRGDQPLHSLGSPHCFSHQNGERVERYSRKVFVGG | 478 | |
| Xl_CPEB4 | -----GQSSLFPMEDGFLDDGRSDQPLHSLGSPHCFPHQNGERVERYSRKVFVGG | 451 | |
| ***** , ***** , ***** | | | |
| Mm_CPEB4 | LPPDIDEDEITASFRFRGPLIVDWPDKAESKSYFPPKGYAFLLFQDESSVQALIDACIEE | 538 | RRM2 |
| Rn_CPEB4 | LPPDIDEDEITASFRFRGPLIVDWPDKAESKSYFPPKGYAFLLFQDESSVQALIDACIEE | 530 | |
| Hs_CPEB4 | LPPDIDEDEITASFRFRGPLIVDWPDKAESKSYFPPKGYAFLLFQDESSVQALIDACIEE | 538 | |
| Xl_CPEB4 | LPPDIDEDEITASFRFRGPLIVDWPDKAESKSYFPPKGYAFLLFQDESSVQALIDACIEE | 511 | |
| ***** | | | |
| Mm_CPEB4 | DGKLYLCVSSPTIKDKPVQIRFWNLSDSDFVMDGSQPLDPRKTI FVGGVPRPLRAVELAM | 598 | RRM2 |
| Rn_CPEB4 | DGKLYLCVSSPTIKDKPVQIRFWNLSDSDFVMDGSQPLDPRKTI FVGGVPRPLRAVELAM | 590 | |
| Hs_CPEB4 | DGKLYLCVSSPTIKDKPVQIRFWNLSDSDFVMDGSQPLDPRKTI FVGGVPRPLRAVELAM | 598 | |
| Xl_CPEB4 | DGKLYLCVSSPTIKDKPVQIRFWNLSDSDFVMDGSQPLDPRKTI FVGGVPRPLRAVELAM | 571 | |
| ***** | | | |
| 1 | | | |
| Mm_CPEB4 | IMDRLYGGVCYAGIDTDPELKYPKGAGRVAFSNQQSYIAAISARFVQLQHGSEIDKRVEVK | 658 | ZZ domain |
| Rn_CPEB4 | IMDRLYGGVCYAGIDTDPELKYPKGAGRVAFSNQQSYIAAISARFVQLQHGSEIDKRVEVK | 650 | |
| Hs_CPEB4 | IMDRLYGGVCYAGIDTDPELKYPKGAGRVAFSNQQSYIAAISARFVQLQHGSEIDKRVEVK | 658 | |
| Xl_CPEB4 | IMDRLYGGVCYAGIDTDPELKYPKGAGRVAFSNQQSYIAAISARFVQLQHGSEIDKRVEVK | 631 | |
| ***** | | | |
| Mm_CPEB4 | PYVLDDQLCDECQGARGCGKFAPFFCANVTCLQYYCEYCWAAIHSRAGREFHKPLVKEGG | 718 | ZZ domain |
| Rn_CPEB4 | PYVLDDQLCDECQGARGCGKFAPFFCANVTCLQYYCEYCWAAIHSRAGREFHKPLVKEGG | 710 | |
| Hs_CPEB4 | PYVLDDQLCDECQGARGCGKFAPFFCANVTCLQYYCEYCWAAIHSRAGREFHKPLVKEGG | 718 | |
| Xl_CPEB4 | PYVLDDQLCDECQGARGCGKFAPFFCANVTCLQYYCEYCWAAIHSRAGREFHKPLVKEGG | 691 | |
| ***** | | | |
| 1 | | | |
| Mm_CPEB4 | DRPRHISFRWN | 729 | |
| Rn_CPEB4 | DRPRHISFRWN | 721 | |
| Hs_CPEB4 | DRPRHISFRWN | 729 | |
| Xl_CPEB4 | DRPRHISFRWN | 702 | |
| ***** | | | |

Figure 16. Mass spectrometry identified phosphorylation sites in CPEB4 RNA-binding domain. The sequence alignment between CPEB4 orthologs (*Mus musculus*, Mm; *Rattus norvegicus*, Rn; *Homo sapiens*, Hs; *Xenopus laevis*, Xl) performed with ClustalW2 is shown. The identified phosphosites and the number of records describing each modification are highlighted in orange (information compiled in PhosphoSitePlus). CPEB4 RRM1 (blue), RRM2 (green) and ZZ domain (grey) are shown.

7.5. CPEBs beyond meiosis

In the last years, the studies describing CPEB function in other biological processes than meiosis have increased considerably. Accordingly, the CPEBs are expressed in a large variety of tissues and have the potential to regulate up to 20% of the genome (Belloc and Méndez, 2008; Piqué et al., 2008). Interestingly, the different members of the CPEB family present specific tissue distribution, both at the level of mRNA (Krupp et al., 2012; Theis et al., 2003) and protein (Human Proteome Map, <http://www.humanproteomemap.org>), although they overlap in certain tissues. Therefore, different tissues and cell types present different composition of CPEBs, which most probably has important functional implications.

Apart from mediating mRNA repression and activation through cytoplasmic polyadenylation, all CPEBs are nucleocytoplasmic shuttling proteins and at least CPEB1 and CPEB4 mediate specific nuclear functions. Thus, CPEB1 regulates pre-mRNA alternative splicing (Lin et al., 2010) and alternative 3' UTR processing in the nucleus (Bava et al., 2013). Regarding CPEB4, its shuttling to the nucleus has been shown to be required for cell survival (Kan et al., 2010).

As mentioned, CPEBs are key regulators of mRNA translation in different physiological and pathological processes, briefly commented thereafter (D'Ambrogio et al., 2013; Fernández-Miranda and Méndez, 2012; Ivshina et al., 2014).

CPEB1 is required for embryonic cell divisions, controlling the polyadenylation and translational activation of cyclin B1 mRNA, which is essential for M-phase progression (Groisman et al., 2002). Moreover, CPEB1 and CPEB4 are involved in cell proliferation by synergistically controlling phase-specific changes in poly(A) tail length of hundreds of mRNAs in tumour derived cells (Novoa et al., 2010). Surprisingly, CPEB1 is also required to induce senescence in primary cells through the translational regulation of *Myc* and *TP53* mRNAs (Burns and Richter, 2008; Burns et al., 2011; Groisman et al., 2006; Groppo and Richter, 2011).

Considering the roles of CPEBs in cell proliferation and senescence, it is not unexpected that they are involved in cancer. CPEBs expression is altered in cancers from different aetiologies (D'Ambrogio et al., 2013). CPEB4 is heightened in pancreatic ductal adenocarcinoma and glioblastomas, where it supports tumour growth, vascularization and invasion through the translational activation of tissue plasminogen activator (*tPA*) mRNA (Ortiz-Zapater et al., 2012). Furthermore, CPEB1 knock out mice are more prone to tumourigenesis (Burns and Richter, 2008) and CPEB1 is down-regulated in several types of human tumours, suggesting a tumour suppressor role of CPEB1.

CPEB1 is also involved in the establishment of cell polarity in mammary epithelial cells by localizing *ZO1* mRNA (Nagaoka et al., 2012), as well as in cell metabolism (Alexandrov et al., 2012; Burns and Richter, 2008; Oruganty-Das et al., 2012).

Finally, CPEBs are highly expressed in the nervous system, where they regulate synaptic plasticity and hippocampal-dependent memories. CPEB1 regulates mRNA transport (Huang et al., 2003) and local protein synthesis at dendrites (Huang et al.,

2002; Udagawa et al., 2012). Hence, it is involved in long-term potentiation and memory extinction (Alarcon et al., 2004; Berger-Sweeney et al., 2006). CPEB3 also mediates learning and memory and its function has been linked to the formation of active prion-like aggregates, as is the case of its orthologs in *Aplysia* and *Drosophila*. In the following section, the requirement of CPEB prion-like multimers for long-term memory is described in detail.

7.5.1. CPEBs and multimer formation

Prions are proteins that can exist in at least two different conformations, one of which is dominant and self-perpetuating. Most of the prions form stable and structured aggregates known as amyloids, which are mainly composed by β -strands (Newby and Lindquist, 2013).

The prion-like properties of CPEBs were first described for a neuronal-specific isoform of CPEB in *Aplysia californica*, ApCPEB. It has been postulated that long-term memory requires the existence of a synaptic tag to mark the activated synapses as sites for local protein synthesis in order to maintain the synaptic changes over time (Frey and Morris, 1997). ApCPEB, which is required for local protein synthesis and for maintaining long-term synaptic facilitation (Si et al., 2003a), has been proposed to function as a synaptic tag through a prion-like mechanism. The NTD of ApCPEB presents two features that resemble yeast prion domains. On the one hand, it has a high glutamine (Q) and asparagine (N) content. On the other hand, it has not predicted secondary structure, which would confer flexibility to switch from one putative state to another one. The same way as prions, ApCPEB presents two functionally distinct heritable states in yeasts, one of which is multimeric, dominant and self-perpetuating. However, while the prionic forms are generally inactive, in the case of ApCPEB, the prion-like aggregated state is the active state of the protein, being the one with RNA-binding capacities (Raveendra et al., 2013; Si et al., 2003b). Importantly, ApCPEB functions as an active prion-like multimer in sensory neurons in response to synaptic stimulation with serotonin (Si et al., 2010). Moreover, the specific block of ApCPEB multimers results in an impairment of the persistence of long-term facilitation, which indicates that the multimer state is the functional one (Si et al., 2010). Although not being very

common, active-prions are not completely unprecedented (Fowler et al., 2007; Newby and Lindquist, 2013).

More recently, the prion-like conformational changes of ApCPEB have been characterized. Purified recombinant ApCPEB undergoes a conformational switch from a soluble state composed by α -helix-rich oligomers to an insoluble state rich in β -sheet amyloid fibers. These amyloid-like aggregates bind CPE-containing RNAs more efficiently than the soluble ApCPEB. Thus, the authors propose that the aggregates formed through the prion-like domain represent a platform for the coordinated polyadenylation of CPE-containing mRNAs (Raveendra et al., 2013).

Interestingly, orthologs for the *Aplysia* neuronal CPEB exist in *Drosophila*, mouse, and humans (Si et al., 2003b; Theis et al., 2003), which suggests that an NTD with such characteristics has an evolutionarily conserved function.

The *Drosophila* ortholog Orb2 also contains a glutamine-rich (Q-rich) region in its NTD that is present in both isoforms, Orb2A and Orb2B. Interestingly, transgenic flies with a specific deletion of Orb2 Q-rich region present specific defects in long-term courtship memory, which shows that the Q-rich region is required for long-term memory but not essential for other Orb2 functions in development (Keleman et al., 2007). The critical role of Orb2 oligomers for long-term memory was nicely assayed by Majumdar et al. They clearly showed *in vivo* that Orb2 exists as an amyloid-like oligomeric state enriched in the synaptic region and enhanced upon neuronal stimulation. Although both isoforms Orb2A and Orb2B form endogenous Orb2 oligomers, the Orb2A isoform is required for the formation of the oligomers. Specifically, the first 8 amino acids of Orb2A catalyze the oligomerization while the Q-rich region is the oligomerization substrate. A specific mutation F5Y that disrupts oligomer formation interferes with the long-term persistence of memory. These results show that Orb2 oligomers, as ApCPEB multimers, are required for memory persistence (Majumdar et al., 2012). Krüttner et al. further characterized the requirement of Orb2 in long-term memory. The authors reported genetic and biochemical data showing that both Orb2 isoforms are required for long-term memory, although they exert their functions through different mechanisms. Orb2B function in development and long-term memory requires its RNA-binding domain as conventional CPEBs. However, the RBD from Orb2A is dispensable for long-term

memory and it is its Q-rich domain the one essential since it seeds the formation of functional Orb2A:Orb2B complexes upon neuronal stimulation (Krüttner et al., 2012).

As it has been already mentioned, the prion-like domain or Q-rich domain from ApCPEB and Orb2 is conserved in other orthologs, as is the case for CPEB3 (Theis et al., 2003). In fact, Orb2A Q-rich domain can be substituted biochemically and functionally by that from mCPEB3 (Krüttner et al., 2012). In mammals, these prionic features are restricted to CPEB3. CPEB1, 2 and 4 do not contain such prion-like domains and moreover do not form amyloid fibers when purified (Stephan et al., 2015).

Recently it has been shown that CPEB3, similar to ApCPEB and Orb2, is a functional prion-like protein required for the persistence of memory. Consistently, the ability of CPEB3 to form amyloid heritable aggregates relies on its NTD. Beside the relevance of proving that the same mechanism described in *Aplysia* and *Drosophila* is maintained in mammals, these studies provide a mechanism for the regulation of the aggregation through SUMOylation. In basal conditions, CPEB3 is SUMOylated and remains majorly soluble. However, upon neuronal stimulation, CPEB3 levels increase and SUMOylation decreases, resulting in CPEB3 aggregation. CPEB3 aggregation is then required for the translational activation of *GluA1* and *GluA2* mRNAs, which encode two AMPAR subunits essential for memory persistence (Drisaldi et al., 2015; Fioriti et al., 2015; Stephan et al., 2015).

This is not the only mechanism proposed for CPEB aggregation regulation. In fact, Orb2A oligomerization is regulated by the fine control of Orb2A protein levels at specific activated synapses (White-Grindley et al., 2014). Upon neuronal stimulation, Orb2A is newly synthesized and stabilized by the Transducer of Erb-B2 (Tob) and Lim Kinase. These events enhance Orb2 oligomerization, required for long-term memory.

To conclude, the function of ApCPEB, Orb2 and CPEB3 in long-term memory is linked to the formation of functional prion-like aggregates. Due to the ability of the aggregates to self-perpetuate and mediate local protein synthesis in activated synapses, it has been proposed that these prion-like aggregates could constitute the synaptic tag required for long-term memory.

OBJECTIVES

Unveiling how the different CPEBs are regulated at a post-translational level is crucial for understanding how they respond to different stimuli, as well as their interconnections in particular scenarios of co-existence. At the moment, it is known that CPEB1 is activated by Aurora A kinase and targeted for ubiquitin-mediated degradation by Cdc2 and Plk1. In addition, CPEB3 activity is controlled by monoubiquitination and SUMOylation, which regulate the transition from the polyadenylation-inactive monomeric form of the protein to an active beta-amyloid-like aggregate. How CPEB2 and CPEB4 activities are controlled is unknown.

The aim of this study is to determine how CPEB4 activity in cytoplasmic polyadenylation is regulated by phosphorylation during cell cycle. Our specific objectives are:

1. Determine if xCPEB4 is phosphorylated in a cell cycle specific pattern
2. Study the phosphorylation pattern of xCPEB4 along the meiotic cell cycle
3. Identify the kinase/s responsible for xCPEB4 post-translational regulation
4. Identify xCPEB4 phosphorylation sites
5. Study the relevance of the identified phosphorylation sites for xCPEB4 function in cytoplasmic polyadenylation and meiotic progression
6. Explore the molecular mechanism behind xCPEB4 activity regulation by phosphorylation

In addition, in collaboration with Frédéric H.-T. Allain and colleagues, we have performed the functional validation of CPEB1 and CPEB4 RNA-binding domain structures in order to uncover the similarities and differences in RNA binding between the different CPEB paralogs.

RESULTS

1. Functional validation of CPEB1 and CPEB4 tandem RRM structures

In order to understand how CPEBs bind to CPE-containing mRNAs and how they assemble repression and activation complexes, Afroz et al. solved the structure of the tandem RRMs of one representative member from each CPEB subfamily, hCPEB1 and hCPEB4.

On the one hand, the solution structure of the tandem RRMs in their free state was determined by nuclear magnetic resonance (NMR). The overall structure of the tandem RRMs from hCPEB1 and hCPEB4 resulted to be similar, although some structural differences were observed. In both cases, the two RRMs adopt a compact and V-shaped structure. When compared to canonical RRMs, the ones from hCPEB1 and hCPEB4 present an extended β -sheet surface. In the case of RRM1, this extension comes from the insertion of two conserved, anti-parallel β -strands (β_a and β_b), whereas for RRM2 the extension comes from the inter-domain linker, which forms an additional β -strand. The fixed orientation of the two RRMs arises from interactions driven mainly by residues outside the RRMs per se. Specifically, the inter-domain linker acts as a hinge to fix the position of the two RRMs, making key interactions to position RRM2 relative to RRM1. In hCPEB1, the region immediately upstream of RRM1, corresponding to the N-terminal domain, strengthens this positioning of one RRM with respect to the other by interacting with the inter-domain linker and by forming a parallel β -strand that directly interacts with RRM2. This region is not conserved among CPEB paralogs and, in the case of hCPEB4, it remains flexible and does not interact with RRM2 (Figure 17).

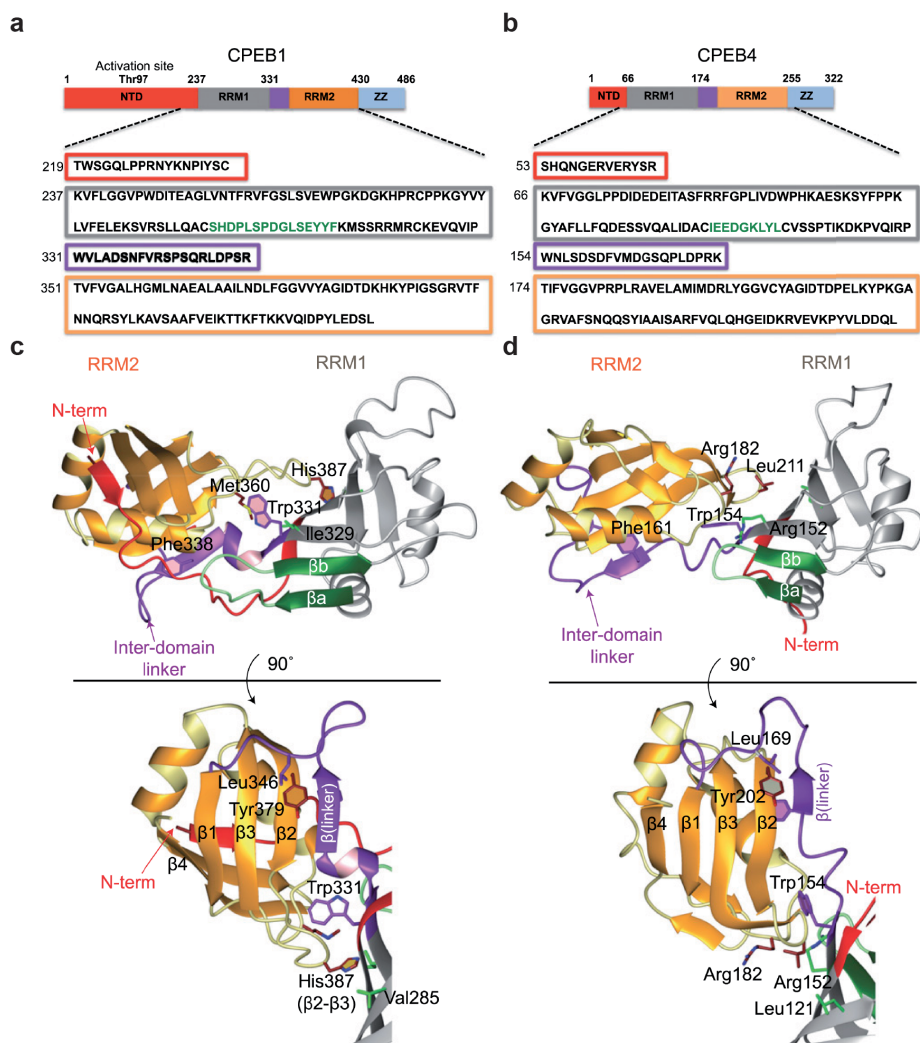


Figure 17. Solution structures of CPEB1 and CPEB4 tandem RRM in the free state (performed by Afroz et al.). (a, b) Schematic representation of full-length hCPEB1 and hCPEB4 proteins. The N-terminal domain, RRM1, the inter-domain linker, RRM2 and the ZZ domain are shown in red, grey, purple, orange and blue, respectively. The residues in RRM1 corresponding to βa and βb are highlighted in green (c, d) Representative structure of hCPEB1 and hCPEB4 tandem RRM in ribbon representation. Below, a 90° rotation of the structures is shown. The color-coding is the same used for Figure 17a and 17b.

On the other hand, the solution structures of hCPEB1 and hCPEB4 tandem RRM s in complex with RNA were solved to enlighten the mRNA recognition and binding modes of the CPEBs. Beside using the consensus CPE sequence 5'-UUUUAU-3' as RNA, Afroz et al. also used the RNA 5'-CUUUA-3', which, although was bound with lower affinity, resulted in better NMR data. The structures revealed that RRM1 is the major RNA-binding domain, being responsible for binding the first four nucleotides (U1 or C1, U2, U3 and U4), while RRM2 binds the last nucleotide A5. Despite the path that the RNA follows through the RRM s is the same for hCPEB1 and hCPEB4, the residues involved in RNA binding and, consequently, the surface charge and the interactions at the protein-RNA interface differ between both proteins. This fact affects primary the binding pocket of A5. While in hCPEB1 this region could accommodate a cytosine (present in non-consensus CPEs 5'-UUUUCAU-3'), in hCPEB4 the hydrophobic contacts established with A5 could not be established with a cytosine. Interestingly, although the individual RRM s fold equally in complex with RNA as in the unbound state, RNA binding results in a conformational change where RRM2 rotates 45° toward RRM1 and closes the RNA-binding cleft (Figure 18).

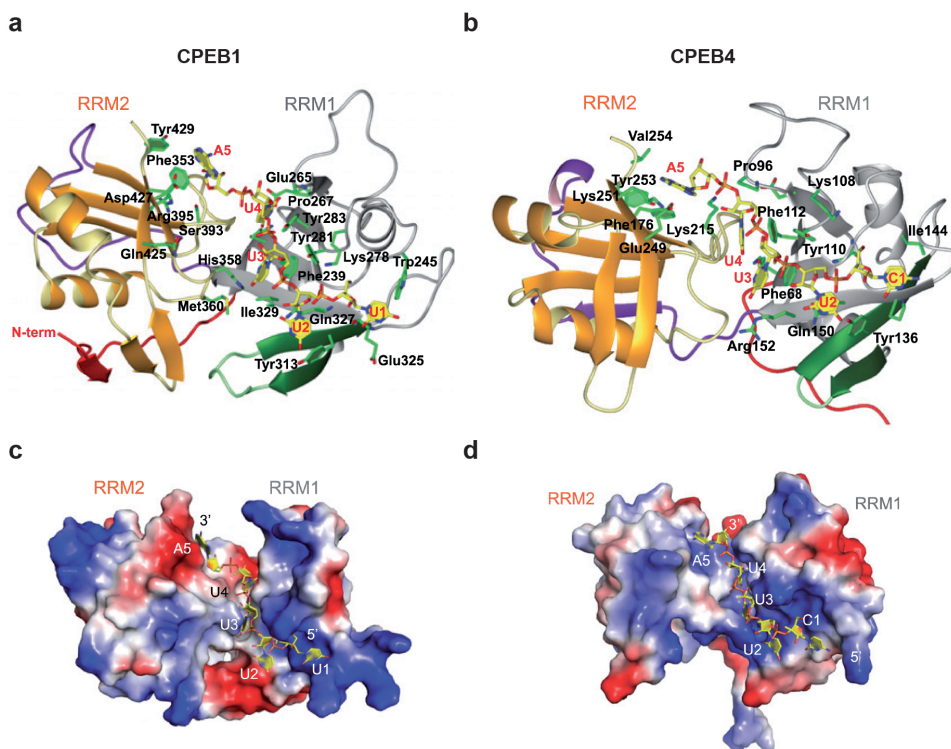


Figure 18. Structures of CPEB1 and CPEB4 tandem RRM domains in complex with RNA (performed by Afroz et al.). (a) Stereo view of the structural model of hCPEB1 RRM12 in complex with 5'-UUUUA-3'. The protein is shown in ribbon representation. The RNA is shown in yellow stick representation and the bases are labelled. (b) Stereo view of the structure of hCPEB4 RRM12 in complex with 5'-CUUUA-3'. Protein is shown in ribbon, while the RNA is shown in yellow stick representation. (c, d) Surface charge (positive – blue, negative – red) representation of hCPEB1 and hCPEB4 RRM12 in complex with RNA.

In order to validate the structural results obtained by NMR and highlight their functional relevance *in vivo*, we set up a competition assay in *Xenopus laevis* oocytes. This assay consists in competing endogenous CPEBs with a truncated protein variant just harbouring the CPEB RNA-binding domain (the tandem RRM domains followed by the ZZ domain, namely RRM12ZZ). These truncated variants are able to specifically bind CPE-containing mRNAs. However, since the whole N-terminal domain is missing, they cannot interact with the cytoplasmic polyadenylation machinery and, as a consequence, act as dominant-negative variants of CPEB-mediated cytoplasmic polyadenylation. We used RRM12ZZ of xCPEB1 and

xCPEB4, which share 99% sequence identity with their human orthologs, as competitors and the 3' UTR of *emi2* (early mitotic inhibitor-2) as a probe to follow its polyadenylation upon progesterone addition. The rationale of the experiment is that the overexpression of wild type RRM12ZZ in oocytes will result in a reduced polyadenylation of *emi2* 3' UTR radioactive probe. However, the overexpression of RRM12ZZ harbouring point mutations that affect either the structure of CPEB tandem RRM or the residues involved in RNA binding would not affect the polyadenylation of the probe (Figure 19a). Accordingly, overexpression of xCPEB1 or xCPEB4 wild type RRM12ZZ results in the competition of the polyadenylation of the probe, compared to the MS2 negative control (Figure 19b). Nevertheless, xCPEB1 and xCPEB4 RRM12ZZ show different competition behaviours. Whereas the overexpression of xCPEB1 RRM12ZZ results in a fraction of RNA completely deadenylated, when xCPEB4 RRM12ZZ is overexpressed it is the length of the poly(A) tail the one that is affected (Figure 19b). This fact could reflect a difference in affinity between CPEB1 and CPEB4.

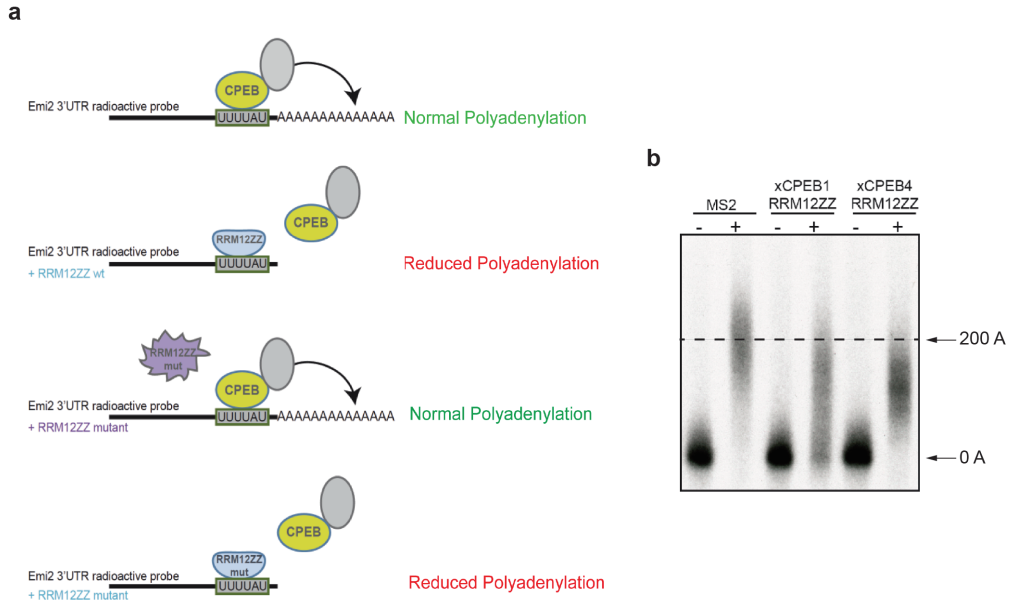


Figure 19. *In vivo* competition assay to validate CPEB1 and CPEB4 tandem RRM structures (in collaboration with Belloc E.). (a) Schematic diagram to illustrate how the *in vivo* functional assay was performed in *X. laevis* oocytes. Oocytes were first injected with a polyadenylated RNA encoding xCPEB1 or xCPEB4 RRM12ZZ in order to overexpress these protein variants. After O/N incubation, these same oocytes were injected with a radioactive *emi2* 3' UTR RNA probe and incubated in the absence or presence of progesterone. Finally, total RNA was extracted and analysed by gel electrophoresis followed by autoradiography. The different conditions and the resulting outcome are depicted. *Emi2* 3' UTR probe is shown in black, with a grey box highlighting a CPE sequence (for clarity, the three CPEs present in the 3' UTR have been simplified to one). Endogenous CPEBs are shown in yellow, the polyadenylation machinery in grey and the overexpressed truncated proteins in blue (those able to bind RNA) and purple (those that lose the capacity to bind RNA). (b) 4% acryl-urea gel showing *emi2* 3' UTR probe polyadenylation in the absence (-) or presence (+) of progesterone in oocytes overexpressing MS2 protein (negative control), xCPEB1 RRM12ZZ or xCPEB4 RRM12ZZ. Migration of non-polyadenylated RNA (0 A) and polyadenylated RNA (200 A) is shown. The dashed line marks the median polyadenylation in the control MS2.

To evaluate the effect of the different mutants, we established a method to calculate the percentage of competition of each variant. In the case of xCPEB1 RRM12ZZ, we calculated the percentage of deadenylated probe, whereas for xCPEB4 RRM12ZZ the distance of the median polyadenylation was taken into account. In both cases, the percentage of competition of the wild type variants was set at 100% and the negative control MS2 was set at 0% (Figures 20 and 21).

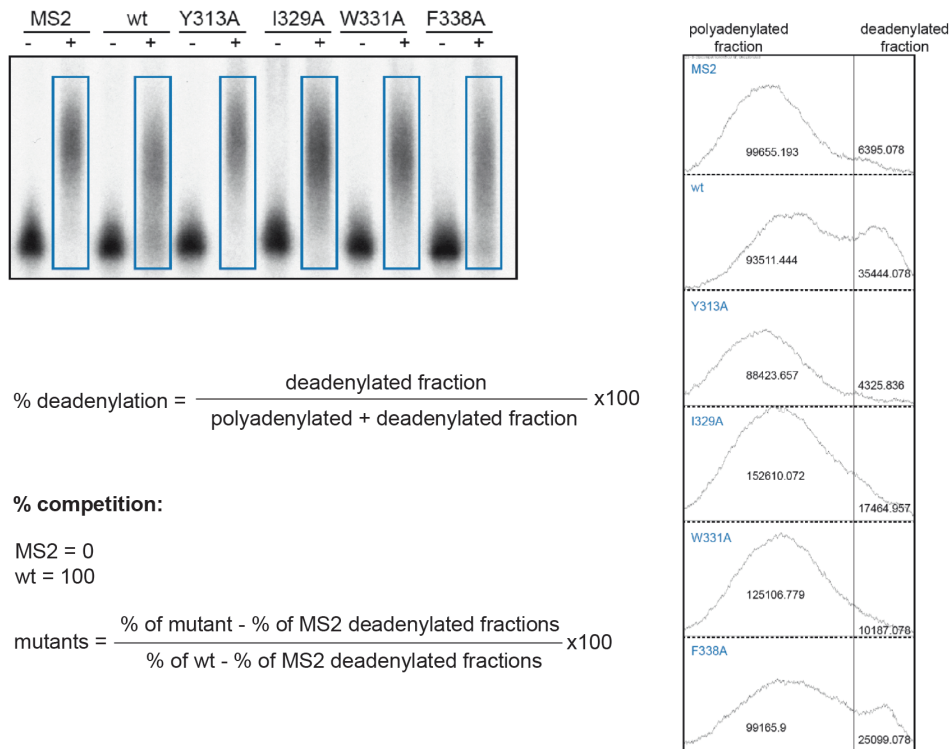


Figure 20. Quantification method to determine the percentage of competition of CPEB1 RRM12ZZ and mutants. Using the Fiji software, the areas depicted with a blue rectangle (upper, left gel) were selected to plot the intensity profiles of the lanes (right panel). A line was traced in these profiles to distinguish the polyadenylated from the deadenylated fraction of the probe. Next, the area of each fraction was obtained in order to apply the formulas shown to calculate the percentage of competition.

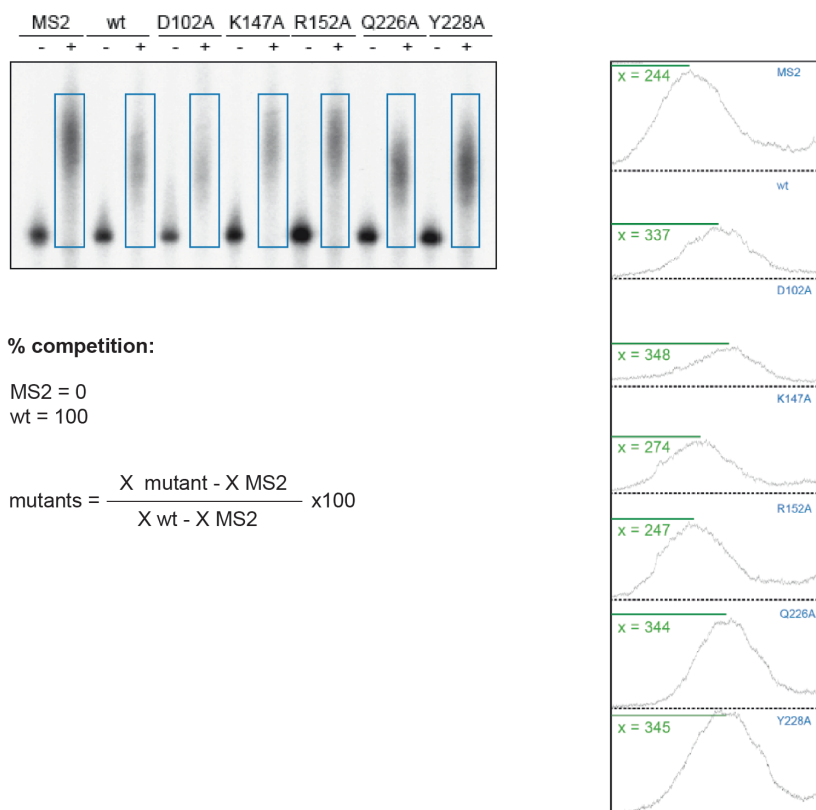


Figure 21. Quantification method to determine the percentage of competition of CPEB4 RRM12ZZ and mutants. Using the Fiji software, the areas depicted with a blue rectangle (upper, left gel) were selected to plot the intensity profiles of the lanes (right panel). The distance from the top of the lane to the peak of maximum intensity of the lane was obtained (X) and used in the formula shown to calculate the percentage of competition.

Competition experiments with xCPEB1 RRM12ZZ and RRM12, which contains both RRMs but lacks the ZZ domain, demonstrate that to efficiently compete with endogenous CPEBs, the RRMs require the presence of the downstream ZZ domain (Figure 22b-d). This result is in agreement with previous reports that show that this domain is required for RNA binding in gel shift assays (Hake et al., 1998). However, more recently it was reported that the ZZ domain is a potential protein-protein interaction domain (Merkel et al., 2013). To clarify the function of the ZZ domain, Afroz et al. solved the solution structure of the domain and generated a structural

model that includes CPEB1 tandem RRM s and the ZZ domain (Figure 22a). The structure revealed a $\beta\alpha\beta$ fold that coordinates two zinc ions in a cross-brace fashion. The hydrophobic helical surface could be suitable for protein interaction, while the β -strands expose aromatic and positively charged residues that could bind nucleic acids. The resulting model shows that the ZZ model is positioned in proximity to the β -sheet of RRM2, therefore there is the possibility that the ZZ domain, although has not the ability to bind to CPE elements by its own, could interact with nucleotides downstream the CPE element. The fact that the ZZ domain is required for efficient competition *in vivo* supports its role in RNA binding (Figure 22).

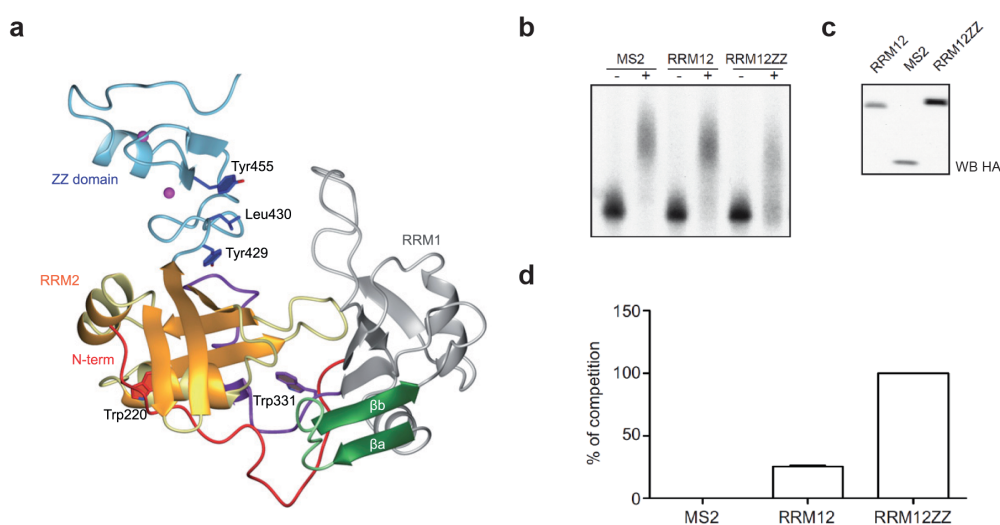


Figure 22. The ZZ domain is required for efficient competition of mRNA polyadenylation (in collaboration with Afroz et al. and Belloc E.). (a) Structural model of hCPEB1 tandem RRM s and the ZZ domain. RRM1 is shown in grey, RRM2 in orange and the ZZ domain in blue. The two zinc ions are shown as purple spheres. (b) 4% acryl-urea gel showing *emi2* 3' UTR probe polyadenylation in the absence (-) or presence (+) of progesterone in oocytes overexpressing MS2 (negative control), xCPEB1 RRM12 or xCPEB1 RRM12ZZ. (c) Western blot anti-HA that shows the levels of overexpression of the proteins. (d) Percentage of competition of polyadenylation calculated from three independent experiments. Results are shown as means and s.d.

Once the *in vivo* competition experiment was set up, we proceeded to validate the structural characterization of CPEB1 tandem RRM. Point mutants of residues important for the positioning of RRM2 in proximity to RRM1 [W220A (N-terminal region upstream of RRM1), W331A (inter-domain linker) and F338A (β -strand from inter-domain linker)] lost their ability to compete cytoplasmic polyadenylation. Furthermore, mutants on residues of RRM1 described to interact with the first four nucleotides of the RNA (F239A, Y281A, Y283A, Y313A, Q327A and I329A) also showed a reduced ability to compete. Finally, the mutation of F353 from RRM2 predicted to interact with the A5 of the RNA also affected the competition efficiency of xCPEB1 RRM12ZZ. Control mutations in RRM1 (N254A) and RRM2 (R402A) did not affect competition (Figure 23).

Regarding CPEB4, similar results were obtained. Mutations in the inter-domain linker that alter the positioning of the two RRMs (W154A and F161A), in RRM1 that affect the interaction with C1, U2, U3 and U4 (F68A, K108A, Y110A, F112A, Y136A, K147A, Q150A and R152A) and in RRM2 that disrupt the binding of A5, resulted in a reduction of the competition mediated by xCPEB4 RRM12ZZ. Control mutation in RRM1 (D102A) and in RRM2 (Q249A and Y228A) showed the same level of competition as the wild type variant (Figure 24).

These results confirm that the residues predicted to be relevant for the folding of CPEB1 and CPEB4 tandem RRMs and for the interaction with the RNA are indeed essential in a physiological context.

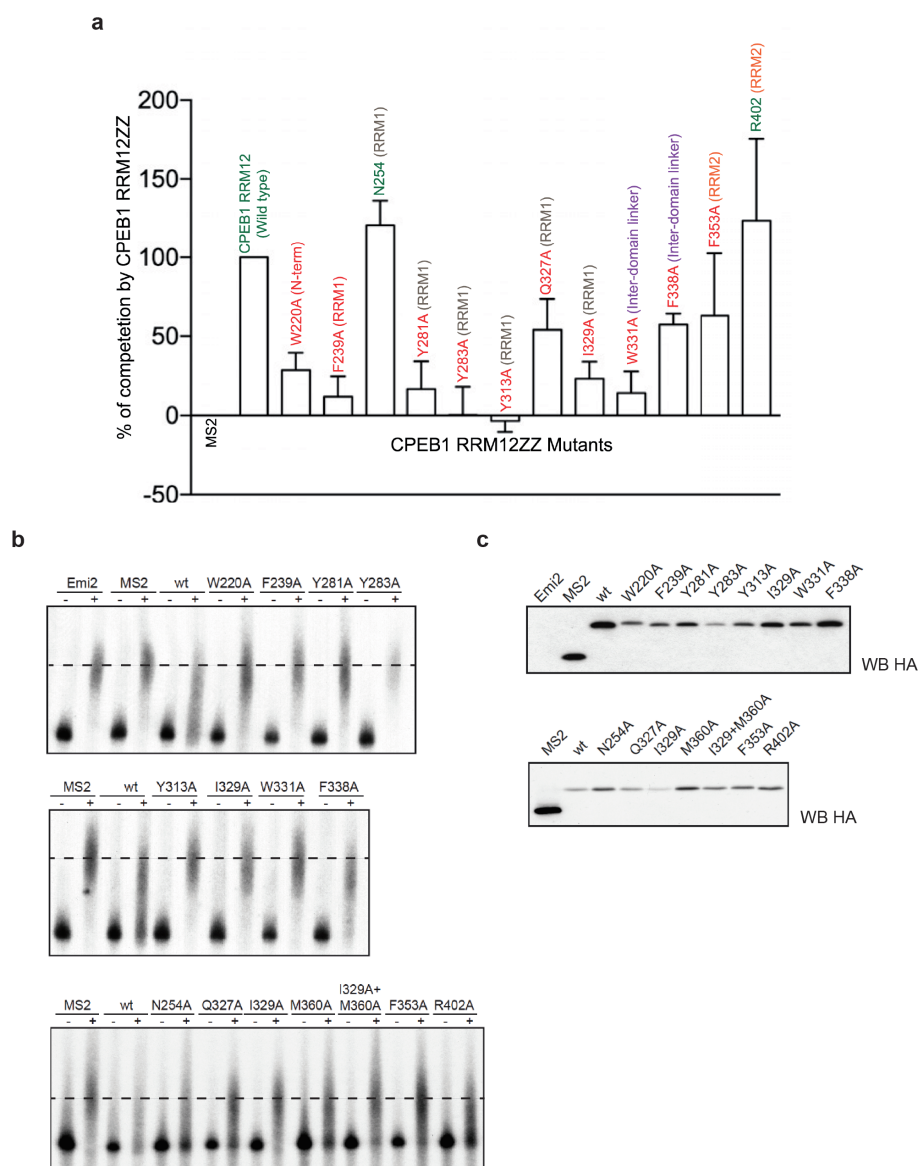


Figure 23. *In vivo* competition assay to validate CPEB1 residues involved in RRM folding and RNA binding (in collaboration with Belloc E.). (a) Percentage of competition of polyadenylation exerted by xCPEB1 RRM12ZZ, wild type or mutants, calculated from three independent experiments. Results are shown as means and s.d. Positive controls and wild type are labelled in green, while mutants are labelled in red. (b) 4% acryl-urea gel showing *emi2* 3' UTR probe polyadenylation in the absence (-) or presence (+) of progesterone in oocytes without protein overexpression (Emi2), or overexpressing MS2 (negative control), xCPEB1 RRM12ZZ wild type (wt) or mutants. The dashed line marks the median polyadenylation in the control MS2. (c) Western blots anti-HA showing the expression level of the overexpressed proteins. Note that residues are numbered according to hCPEB1 sequence.

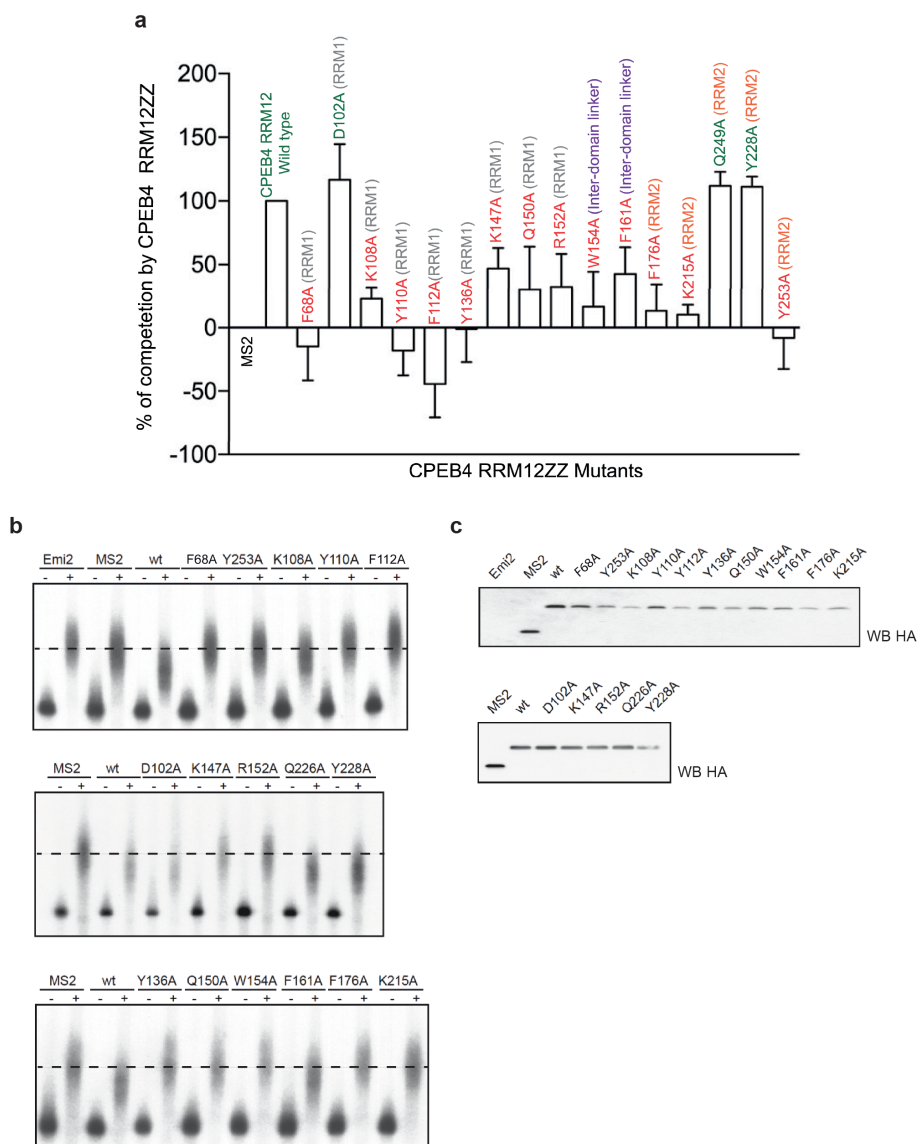


Figure 24. *In vivo* competition assay to validate CPEB4 residues involved in RRM folding and RNA binding (in collaboration with Belloc E.). (a) Percentage of competition of polyadenylation exerted by xCPEB4 RRM12ZZ, wild type or mutants, calculated from three independent experiments. Results are shown as means and s.d. Positive controls and wild type are labelled in green, while mutants are labelled in red. (b) 4% acryl-urea gel showing *emi2* 3' UTR probe polyadenylation in the absence (-) or presence (+) of progesterone in oocytes without protein overexpression (Emi2), or overexpressing MS2 (negative control), xCPEB4 RRM12ZZ wild type (wt) or mutants. The dashed line marks the median polyadenylation in the control MS2. (c) Western blots anti-HA showing the expression level of the overexpressed proteins. Note that residues are numbered according to hCPEB1 sequence.

2. CPEB4 is highly phosphorylated in the N-terminal domain during meiosis

To investigate whether xCPEB4 is regulated by phosphorylation during meiosis, we first performed a λ -phosphatase (λ -PPase) assay in HA-CPEB4 overexpressing *X. laevis* oocytes. When compared to stage VI oocytes, HA-CPEB4 presented a mobility shift at metaphase I [MI; corresponding to the germinal vesicle breakdown (GVBD)], which was maintained 1h after GVBD and at metaphase II (MII). This band retardation disappeared when the extracts were treated with λ -PPase, which indicates that xCPEB4 is phosphorylated in response to progesterone (Figure 25a).

After, to further define the regions of xCPEB4 that are phosphorylated, we subdivided the protein in four different fragments (1, 2, 3 and RBD) (Figure 25b) and conducted an *in vitro* kinase with MII oocyte extracts as the source of kinases. xCPEB4 full-length protein and the three fragments located in the N-terminal disordered domain (fragments 1, 2 and 3) were very efficiently phosphorylated. Per contra, only a residual phosphorylation close to background was detected for the C-terminal RBD fragment (Figure 25c). This result already suggests that xCPEB4 is phosphorylated in multiple residues localized in the N-terminal domain. In order to unveil the phase-specificity of these phosphorylation events, we carried out a time course *in vitro* kinase assay with oocyte extracts collected at different meiotic time points. The progression through the meiotic phases was followed by Histone H1, which is phosphorylated by Cdc2. None of the proteins tested was phosphorylated at prophase I (stage VI). However, all of them were phosphorylated in response to progesterone. xCPEB4 full-length and fragment 1 maintained the same phosphorylation level from MI to MII. Fragment 3 phosphorylation followed Cdc2 kinase activity profile, which peaks at MI and MII and maintains intermediate levels during interkinesis. Fragment 2 presented an intermediate kinetic (Figure 25d). Altogether, these results illustrate that xCPEB4 N-terminal domain is phosphorylated in multiple residues and that its phosphorylation is driven by at least two kinases with different activity profiles along meiosis, being Cdc2 a good candidate.

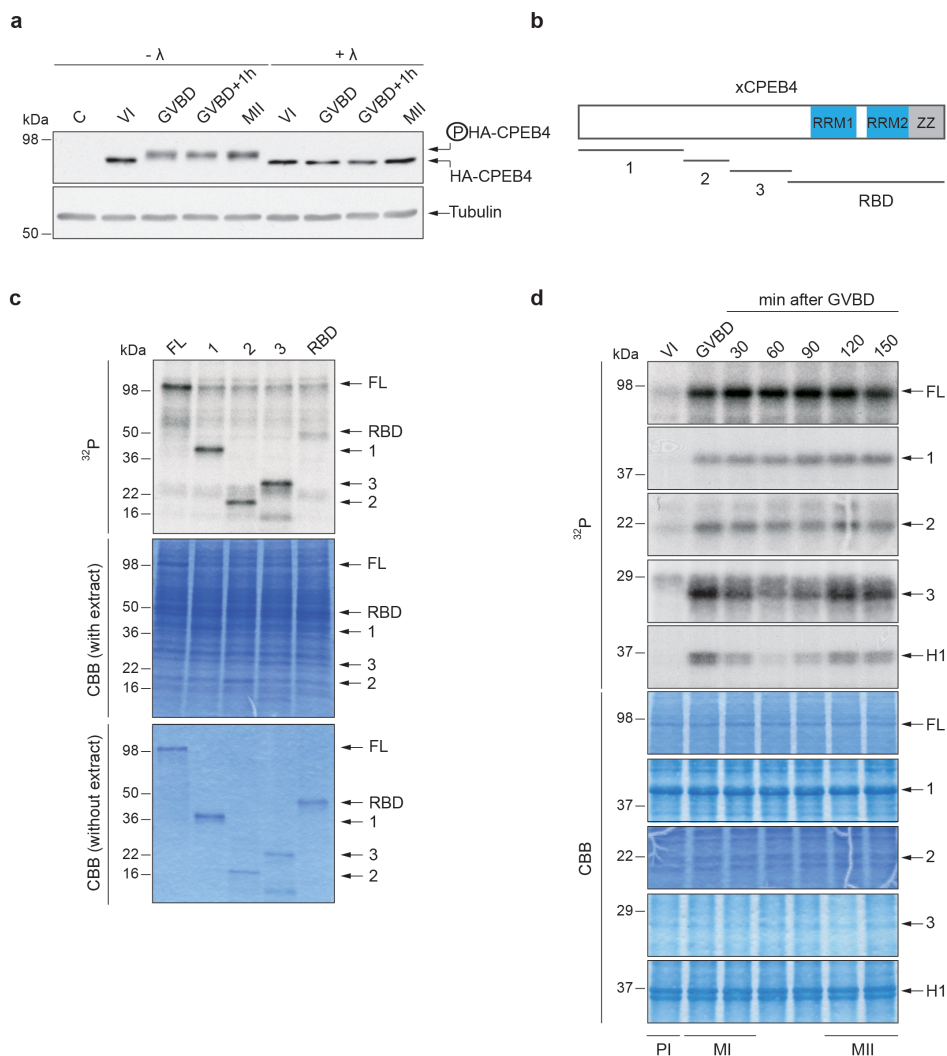


Figure 25. xCPEB4 is highly phosphorylated in its N-terminal domain in a phase-specific manner. (a) Lambda-phosphatase assay (λ) of overexpressing HA-CPEB4 *Xenopus* oocytes collected at indicated times (stage VI; GVBD, germinal vesicle breakdown; MII, metaphase II). The phosphorylation status of xCPEB4 was determined by western blot with anti-HA. C, non-injected oocytes. (b) Schematic representation of xCPEB4 protein. The four protein fragments used (1, 2, 3 and RBD) are outlined. RRM1 and RRM2 are highlighted in blue and the ZZ domain in grey. (c) *In vitro* kinase assay of xCPEB4 full-length (FL) or fragments (1, 2, 3 and RBD), phosphorylated with metaphase II oocyte extracts. Upper panel shows the autoradiography (32 P). Middle panel corresponds to the coomassie stained gel (CBB with extract). In the lower panel equivalent protein amounts used in the assay were loaded as control (CBB without extract). (d) Time course *in vitro* kinase assay of xCPEB4 full-length (FL) or fragments (1, 2 and 3) with oocyte extracts collected at indicated times. Upper panels show the autoradiographies (32 P). Lower panels correspond to the coomassie stained gels (CBB). Histone H1 phosphorylation was used to define prophase I (PI), metaphase I (MI) and metaphase II (MII).

We confirmed that xCPEB4 N-terminal domain is phosphorylated in at least twelve phosphorylation sites by two-dimensional (2D) phosphopeptide maps. xCPEB4 fragments 1, 2 and 3 were *in vitro* phosphorylated with oocyte extracts from MI (GVBD), interkinesis (GVBD+1h) and MII, re-purified and in-gel digested with trypsin and chymotrypsin. The resulting peptides were solved by thin-layer electrophoresis followed by thin-layer chromatography. In the resulting 2D maps, each spot represents one phosphopeptide (pp). Fragment 1 presented four different phosphopeptides (pp 1-4) (Figure 26a), with an extra one (pp 5) only present in higher exposures (see Figures 27 and 29). Fragment 2 showed one phosphopeptide (pp 6) and fragment 3 six phosphopeptides (pp 7-12) (Figure 26a). All of the phosphopeptides detected were present in the three meiotic phases assessed, although as previously shown for fragment 3 the efficiency of the phosphorylation events can vary between phases. Moreover, to rule out the probability that we were missing phosphorylation events due to the truncation of the protein, as would be the case of phosphorylations that require priming events, we tested the whole N-terminal domain (fragment 1-409). Despite this fragment was not further characterized, we could not detect more than twelve phosphopeptides in the 2D phosphopeptide maps (Figure 26b). Therefore, we conclude that xCPEB4 N-terminal domain is phosphorylated in at least twelve phosphorylation sites and in a phase specific manner along meiosis.

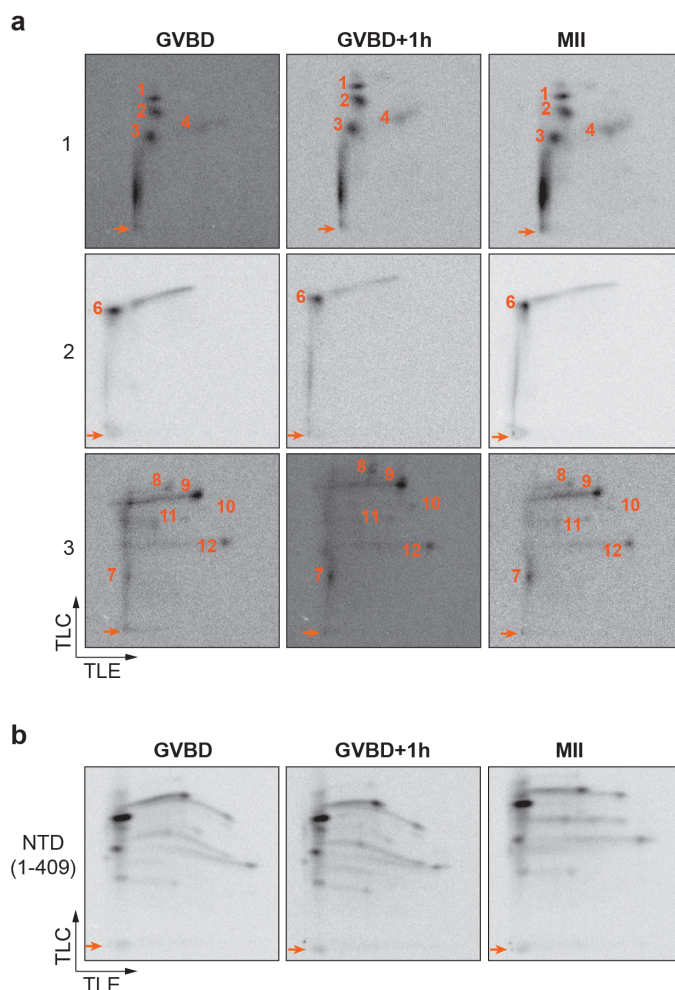


Figure 26. xCPEB4 N-terminal domain is phosphorylated in at least twelve residues. (a, b) Two-dimensional phosphopeptide maps of (a) xCPEB4 fragments 1, 2 and 3 or (b) fragment NTD (1-409 aa), phosphorylated with oocytes extracts collected at indicated times (GVBD, germinal vesicle breakdown, corresponding to metaphase I; GVBD+1h, interkinesis; MII, metaphase II). Phosphopeptides were solved by thin-layer electrophoresis (TLE) followed by thin-layer chromatography (TLC) and visualized with Phosphorimager. Arrows indicate sample origin. Phosphopeptides have been labelled with a number.

3. p42MAPK and Cdc2 kinases drive xCPEB4 phosphorylation

Taking into account that xCPEB4 N-terminal fragments 1, 2 and 3 follow different phosphorylation kinetics along meiosis, most probably different kinases are responsible for xCPEB4 phosphorylation. In order to identify the kinases that phosphorylate xCPEB4, we conducted a small kinase inhibitor screening. Hence, a kinase assay with xCPEB4 full-length recombinant protein and MII oocyte extracts treated with different kinase inhibitors was performed. When compared to the DMSO control, Roscovitine (Cdc2 inhibitor) decreased xCPEB4 phosphorylation to a 75%, BI-2536 (Plk1 inhibitor) to a 58% and FR180204 (ERK1 and ERK2 inhibitor) to a 25%. Otherwise, SL0101 (p90Rsk inhibitor) and U0126 (MEK1 and MEK2 inhibitor) did not affect xCPEB4 phosphorylation. We conclude that Cdc2, p42MAPK (ERK2) and Plk1 are potential xCPEB4 kinases (Figure 27a). The same experiment was performed using xCPEB4 N-terminal fragments 1, 2 and 3 in pursuance of delimiting the regions of xCPEB4 NTD phosphorylated by each kinase. Fragments 1 and 2 were mainly affected by the ERK inhibitor, while fragment 3 was mainly affected by the Cdc2 inhibitor and to a lesser extent by the ERK inhibitor. The effect of Plk1 inhibition on the phosphorylation of the fragments was not as evident as for the full-length protein (Figure 27b). To assess if all the phosphopeptides detected by 2D phosphopeptide maps could be mediated by Cdc2 and p42MAPK, we performed new 2D phosphopeptides maps with fragments 1, 2 and 3 phosphorylated by recombinant p42MAPK or Cdc2/cyclin B. After, the 2D maps generated with recombinant kinases were compared with the ones performed with MII oocyte extracts. For fragment 1, the five phosphopeptides detected with MII extracts were present when the fragment was phosphorylated with p42MAPK (pp 1-5). Upon Cdc2/cyclin B phosphorylation, pp 1-3 could also be detected, although the efficiency of phosphorylation was lower and other phosphopeptides not present in the MII 2D map were observed. For fragment 2, the only phosphopeptide detected with MII extracts was also detected with p42MAPK. In this case, Cdc2/cyclin B was able to phosphorylate fragment 2 but in a different residue not detected with oocyte extracts. For fragment 3, the majority of the phosphopeptides detected at MII

appeared upon Cdc2/cyclin B phosphorylation (pp 8, 9, 11 and 12). Nevertheless, p42MAPK phosphorylated pp 10 very efficiently. Phosphopeptide 7 could not be detected with any of the kinases (Figure 27c).

Taking these results together, we conclude that xCPEB4 fragment 1 and 2 are phosphorylated by p42MAPK, while fragment 3 is phosphorylated by a combination of p42MAPK and Cdc2, having Cdc2 the major role. Interestingly, this result is consistent with the phosphorylation kinetics along meiosis of the different fragments. Hence, fragment 1 follows p42MAPK activity, which peaks at MI and is maintained until MII; fragment 3 is phosphorylated following Cdc2 activity that peaks at MI, decreases in interphase and peaks again at MII; and fragment 2 shows an intermediate kinetic of phosphorylation, albeit resembles more p42MAPK kinetic than Cdc2.

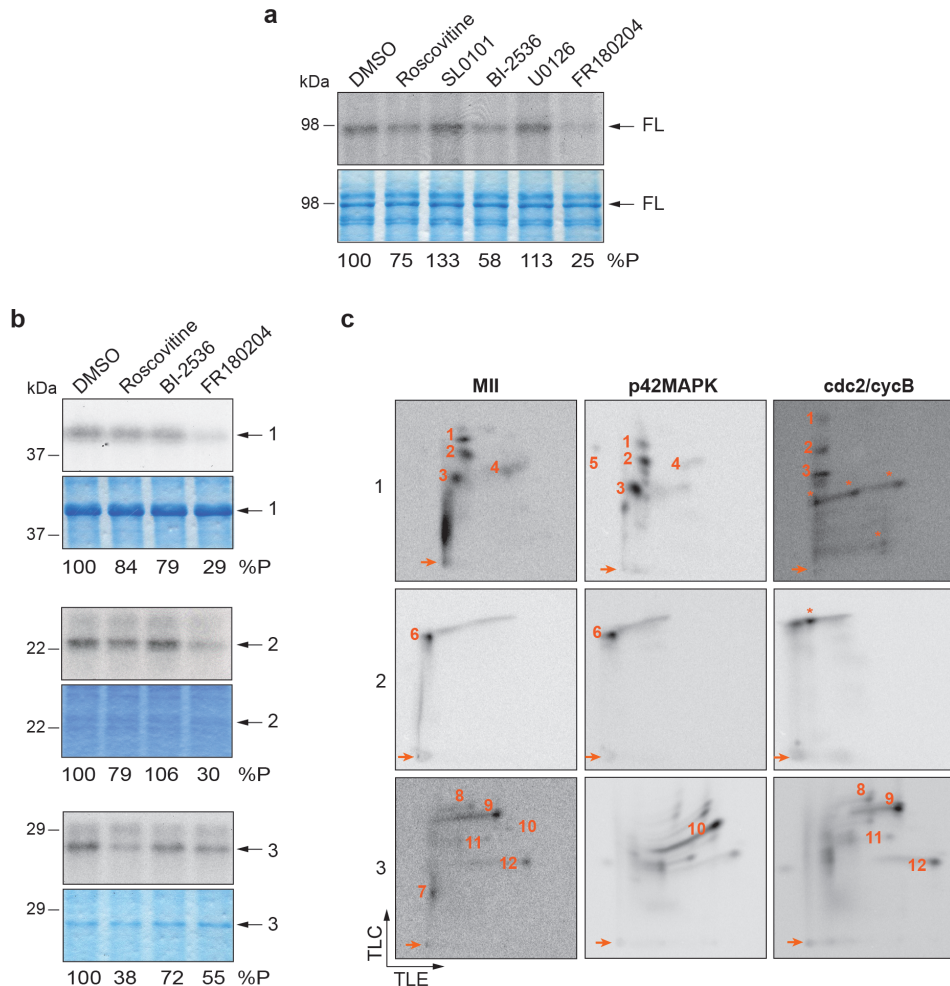


Figure 27. xCPEB4 N-terminal domain is phosphorylated by p42MAPK and Cdc2. (a, b) *In vitro* kinase assay of xCPEB4 (a) full length or (b) fragments (1, 2 and 3), with metaphase II oocyte extracts treated with specific kinase inhibitors (Roscovitine, Cdc2 inhibitor; SL0101, p90Rsk inhibitor; BI-2536, PIk1 inhibitor; U0126, MEK inhibitor; FR180204, ERK inhibitor). Upper panels, autoradiography. Lower panels, coomassie stained gels. Arrows indicate the band corresponding to each protein. DMSO was used as negative control. The percentage of phosphorylation compared to the DMSO control was calculated and shown in the bottom of the gels (% ^{32}P). (c) Two-dimensional phosphopeptide maps of xCPEB4 fragments (1, 2 and 3) phosphorylated with metaphase II oocyte extracts (MII), recombinant p42MAPK or recombinant Cdc2/cyclin B. Phosphopeptides were solved by thin-layer electrophoresis (TLE) followed by thin-layer chromatography (TLC) and visualized with Phosphorimager. Arrows indicate sample origin. Phosphopeptides detected in MII have been labelled with a number. Asterisks (*) indicate phosphopeptides generated with recombinant kinases not present in MII.

4. Identification of xCPEB4 phosphorylation sites by mass spectrometry

We followed a mass spectrometry approach in order to identify the specific phosphorylation sites of xCPEB4. On the one hand, recombinant xCPEB4 full-length protein or the N-terminal fragments 1, 2 and 3 were *in vitro* phosphorylated with MII oocyte extracts, re-purified from the kinase reaction and sent for mass spectrometry analysis. Nine phosphorylation sites were identified, all of them located in the NTD: S38, S97, S250, S253, S328, S330, S351, S357 and S362. Consistent with the fact that the RBD was not *in vitro* phosphorylated with oocyte extracts, we did not identify any phosphorylation sites in this domain although peptides covering this region were detected. On the other hand, we also performed a mass spectrometry analysis of fragments 1, 2 and 3 phosphorylated with the two identified kinases involved in xCPEB4 phosphorylation, Cdc2 and p42MAPK. Three new phosphosites were identified: S18 and S40, driven by p42MAPK, and T324, mediated by Cdc2. Moreover, we specifically detected S328 and S330 in the Cdc2 reaction and S351 in the p42MAPK reaction. Therefore, a total of twelve phosphorylation sites were identified: S18, S38, S40, S97, S250, S253, T324, S328, S330, S351, S357 and S362 (Figure 28a). Taking into account this result, as well as the previously described phosphorylation kinetics, kinase inhibitors assays and 2D phosphopeptide maps, we could assign each phosphorylation site to its kinase. S18, S38, S40, S97, S250 and S253 were assigned to p42MAPK since these sites are located in fragments 1 and 2, which are phosphorylated by p42MAPK. S351 from fragment 3 was also assigned to p42MAPK as this site was specifically detected in the mass spectrometry analysis of fragment 3 phosphorylated with p42MAPK. The rest of the identified residues, T324, S328, S330, S357 and S362, which belong to fragment 3, were assigned to Cdc2 considering that all of the phosphopeptides from this fragments were generated by Cdc2 phosphorylation, except one corresponding to S351.

If we consider the disorder tendency of xCPEB4 predicted with PONDR® VL-TX, it is interesting to notice that all the phosphorylation sites identified, excluding S97, flank the two large disordered regions of xCPEB4 N-terminal domain (Figure 28b).

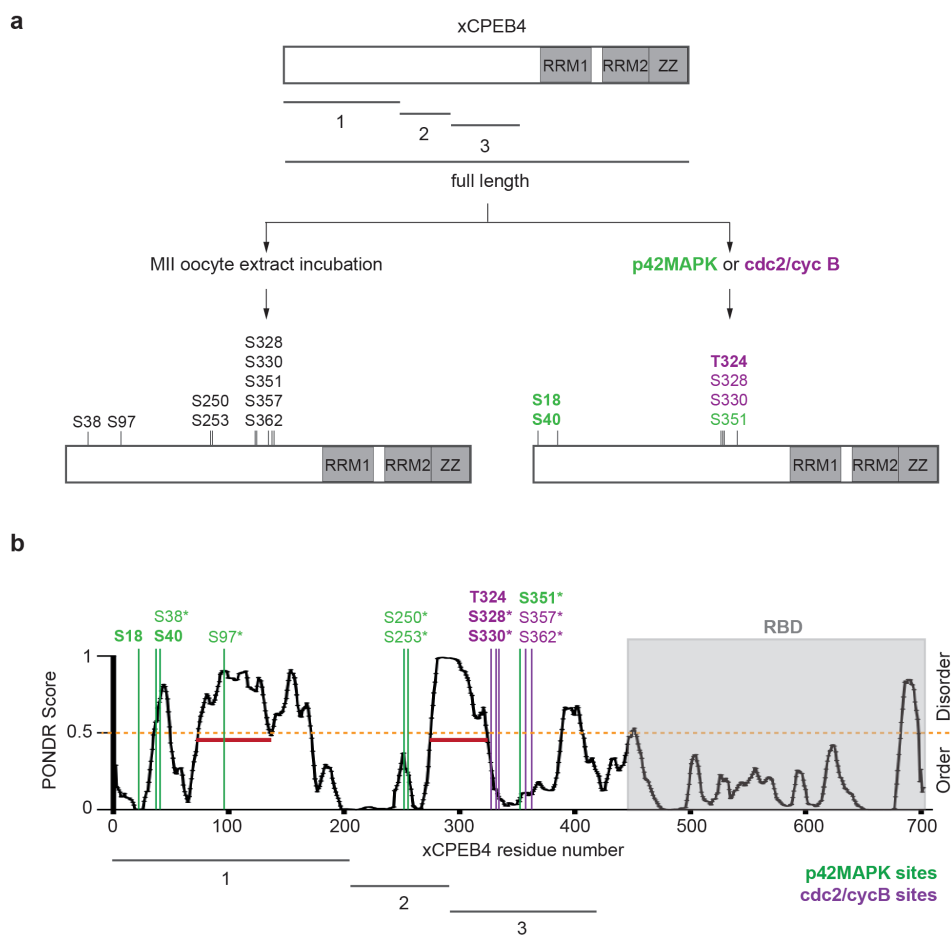


Figure 28. xCPEB4 phosphorylation sites identification by mass spectrometry. (a) xCPEB4 full-length of N-terminal fragments 1, 2 and 3 were phosphorylated with metaphase II (MII) oocyte extracts or recombinant p42MAPK (green) or Cdc2/cyclin B (purple). The identified sites by each of the procedures are shown. **(b)** Disorder tendency of xCPEB4 calculated with PONDR® VL-TX predictor. Red lines represent large disordered regions. Identified xCPEB4 phosphorylation sites are shown. Asterisks (*) indicate phosphosites identified with MII extracts. Bold letters indicate phosphosites identified with either p42MAPK or Cdc2/cyclin B. Green indicates p42MAPK assigned phosphorylation sites, while purple indicates Cdc2/cyclin B assigned phosphorylation sites. xCPEB4 fragments used are outlined.

Importantly, all of the identified xCPEB4 phosphorylations, except S40, are conserved between CPEB4 mammalian orthologs (*Mus musculus*, *Rattus norvegicus* and *Homo sapiens*). Moreover, S97, S250, S253, T324, S328 and S330 have been identified as phosphopeptides in high-throughput mass spectrometry studies from *Mus musculus*, *Rattus norvegicus* and *Homo sapiens* samples.

Subsequently, a validation of the identified phosphosites was carried out to unravel whether the majority of xCPEB4 phosphorylation sites had been identified. We expressed and purified fragments 1, 2 and 3 containing the identified phosphosites mutated to aspartic acid. Then, we performed 2D phosphopeptide maps with MII oocyte extract or recombinant kinases (p42MAPK or Cdc2/cyclin B). The majority of the phosphopeptides detected in wild type conditions disappeared upon mutation of the identified sites. However, phosphopeptides 1, 2 and 7 remained phosphorylated, indicating that beyond the twelve phosphorylation sites described, there are at least three more phosphorylation events (Figure 29a-b). Accordingly, when a 12A mutant version of xCPEB4, where the twelve phosphorylation sites have been mutated to alanine, was overexpressed in oocytes, it still presented a mobility shift upon progesterone stimulation. Moreover, this mobility shift of the 12A mutant disappeared with λ -PPase treatment, confirming that xCPEB4 is phosphorylated in more than twelve residues *in vivo* (Figure 29c).

Altogether, xCPEB4 is hyperphosphorylated in its N-terminal domain in twelve phosphorylation sites, seven of them driven by p42MAPK and five by Cdc2. Nevertheless, *in vitro* and *in vivo* experiments show that xCPEB4 is potentially further phosphorylated.

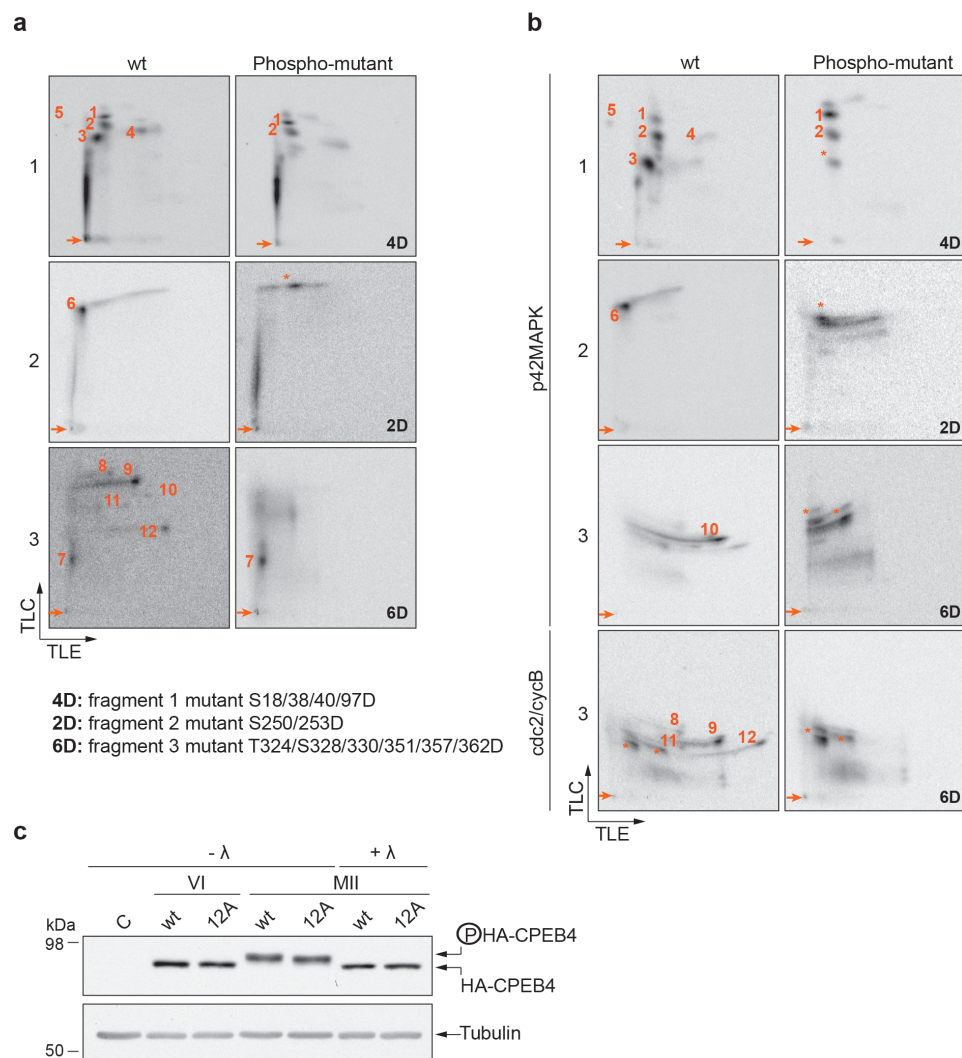


Figure 29. xCPEB4 phosphorylation sites validation shows that there are at least three non-identified phosphosites. (a, b) Two-dimensional phosphopeptide maps of xCPEB4 fragments (1, 2 and 3), wild type or phosphorylation mutants, phosphorylated with (a) metaphase II oocyte extract or (b) recombinant p42MAPK or Cdc2/cyclin B. Phosphopeptides were solved by thin-layer electrophoresis (TLE) followed by thin-layer chromatography (TLC) and visualized with Phosphorimager. Arrows indicate sample origin. Phosphopeptides detected in wild type conditions have been labelled with a number. Asterisks (*) indicate unspecific phosphopeptides only present in xCPEB4 mutants but not detected in wild type conditions. The specific mutations are specified at the bottom of panel a. (c) Lambda-phosphatase assay (λ) of overexpressing HA-CPEB4 *Xenopus* oocytes collected at indicated times (stage VI; MII, metaphase II). Wild type (wt) HA-CPEB4 and the 12A mutant (the twelve phosphorylation sites have been mutated to alanine) were analysed. The phosphorylation status of xCPEB4 was determined by western blot with anti-HA antibody. C, non-injected oocytes.

5. xCPEB4 hyperphosphorylation is essential for xCPEB4 function in meiosis

Once we had identified the phosphorylation sites of xCPEB4 and the responsible kinases, we addressed the functional implication of these phosphorylation events.

5.1. Analysis of xCPEB4 functional phosphorylation sites by MS2-tethering experiments

Our first approach was to test xCPEB4 phosphorylation mutants by MS2-tethering in *Xenopus laevis* oocytes. It was described that hCPEB4, when tethered with the MS2 system, is able to activate the cytoplasmic polyadenylation and subsequent translation of a given luciferase reporter (Novoa et al., 2010). Therefore, we tested the ability of MS2-HA-xCPEB4 to mediate the translational activation of a B1-123 3' UTR luciferase reporter containing MS2 binding sites. This reporter harbours the 3' UTR of cyclin B1 with the three CPE elements mutated. Thus, it is not translationally activated upon progesterone stimulation unless a MS2 fusion protein able to activate its translation targets it. As a control of oocyte quality, the B1 luciferase reporter, which contains three CPEs and responds to endogenous CPEBs, was used. In some experiments, we detected translation stimulation of the B1-123 reporter when MS2-HA-xCPEB4 or MS2-xCPEB1 were tethered, compared to the negative control MS2-GFP. Moreover, the translation stimulation of the B1-123 was abolished when the PAS from the luciferase reporter was mutated (-H), indicating that the increase of luciferase activity detected was due to the cytoplasmic polyadenylation of the reporter (Figure 30). However, we found a lot of variability between experiments and it was difficult to evaluate the twelve xCPEB4 phosphorylation sites with this assay. The lack of reproducibility might be due to the strong binding of the MS2 to MS2-binding sites or to the fact that the MS2 dimerizes and even oligomerizes at high concentrations (Keryer-Bibens et al., 2008), which may alter the dynamics of xCPEB4 mRNP.

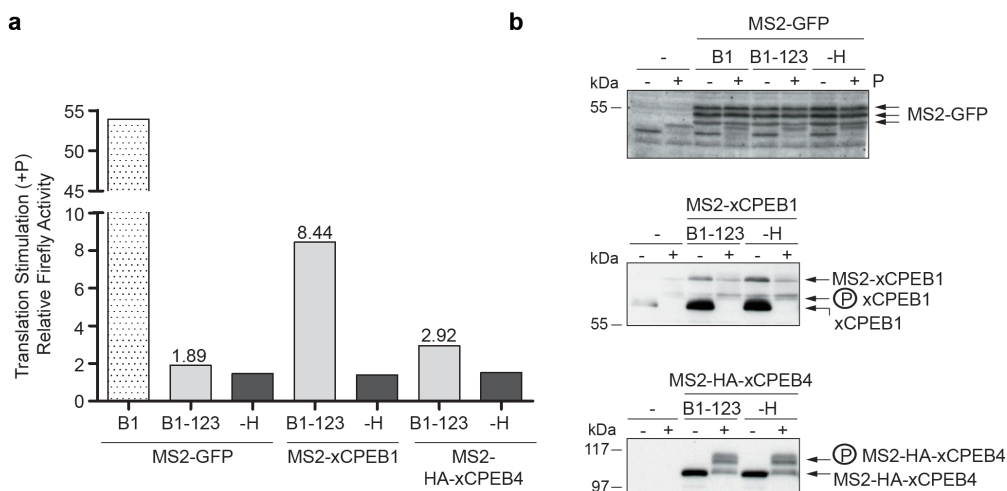


Figure 30. MS2-HA-xCPEB4 tethering experiment. (a) Translational stimulation of firefly luciferase reporters B1, B1-123 or B1-123-H (-H) containing MS2-binding sites in oocytes overexpressing MS2-GFP (negative control), MS2-xCPEB1 (positive control) or MS2-HA-xCPEB4. Renilla luciferase was co-injected with the firefly luciferase reporters as normalizing RNA. Oocytes were treated or not with progesterone. The fold increase upon progesterone stimulation is shown. **(b)** Western blot anti-GFP (upper panel), anti-xCPEB1 (middle panel) or anti-HA (lower panel) to show the levels of overexpression of the MS2 fusion proteins in the different conditions tested.

5.2. Analysis of xCPEB4 functional phosphorylation sites by competition experiments

5.2.1. xCPEB4 hyperphosphorylation in the N-terminal domain is required for cytoplasmic polyadenylation

We tested the functional relevance of the identified xCPEB4 phosphorylation sites by competition assays in *Xenopus* oocytes, similar to the strategy used for the functional validation of CPEB1 and CPEB4 tandem RRM structures. This assay is based in the out-competition of endogenous CPEBs by the overexpression of full-length HA-xCPEB4, wild type or specific phosphorylation mutants. *Emi2* 3' UTR radioactive probe was used to follow its polyadenylation status upon progesterone

stimulation of the oocytes. Ideally, xCPEB4 wild type overexpression, despite being able to displace endogenous CPEBs, will not cause any effect on the polyadenylation of the reporter, since its capability to mediate cytoplasmic polyadenylation of mRNAs should be maintained. The same would happen with the overexpression of active xCPEB4 variants. However, the overexpression of inactive xCPEB4 variants will result in a decrease of the poly(A) tail length. Hypothesizing that xCPEB4 phosphorylation sites are required for its ability to mediate cytoplasmic polyadenylation of mRNAs, then, phospho-null mutants (alanine mutants) will be inactive and will cause a reduction in *emi2* 3' UTR probe poly(A) tail length, while phospho-mimetic mutants (acid aspartic mutants) will be active and will not affect the cytoplasmic polyadenylation of the reporter (Figure 31).

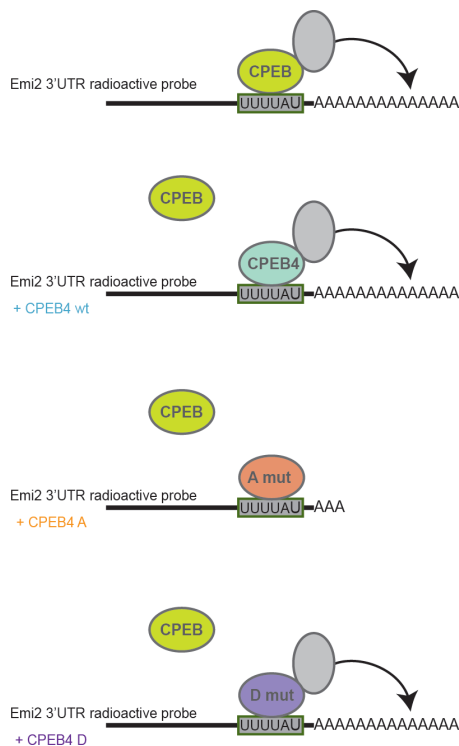


Figure 31. Setting up competition assays for xCPEB4 phosphorylation sites functional evaluation. Schematic diagram illustrating how the competition experiment was performed. xCPEB4, wild type (cyan), phospho null mutants (labelled as “A mut” in orange) or phospho-mimetic mutants (labelled as “D mut” in purple), were overexpressed in *X. laevis* oocytes. After O/N incubation, the oocytes were injected with a radioactive *emi2* 3'-UTR RNA probe in order to follow its polyadenylation upon progesterone stimulation. The *emi2* 3'-UTR radioactive probe is shown in black, with a grey box highlighting a CPE sequence (the three CPE elements present in the probe have been simplified to one). The polyadenylation status of the RNA probe under the specific conditions is shown. Endogenous xCPEBs are depicted in yellow and the polyadenylation machinery in grey.

In order to objectively quantify the percentage of competition, we measured the distance of the median polyadenylation for every condition and assigned 0%

competition to the wild type variant and 100% competition to the xCPEB4 12A variant, which contains the twelve phosphorylation sites mutated to alanine and shows the major effect in competition assays. The percentage of competition of the other phosphorylation mutants was calculated and normalized according to these values (Figure 32).

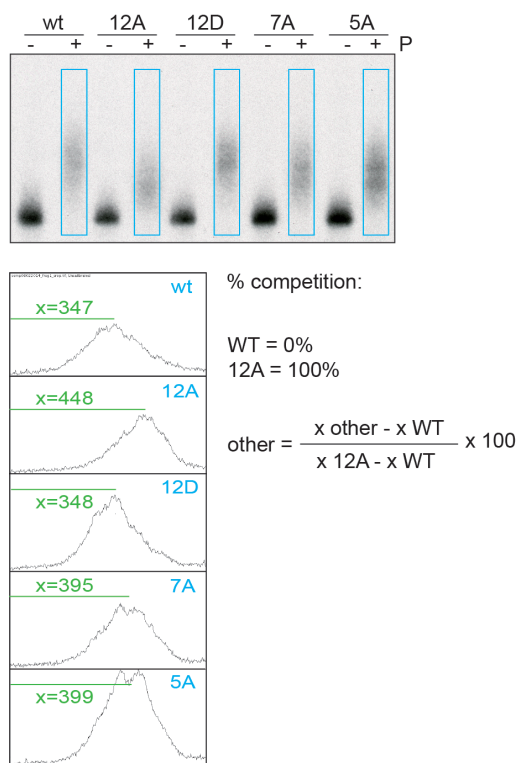


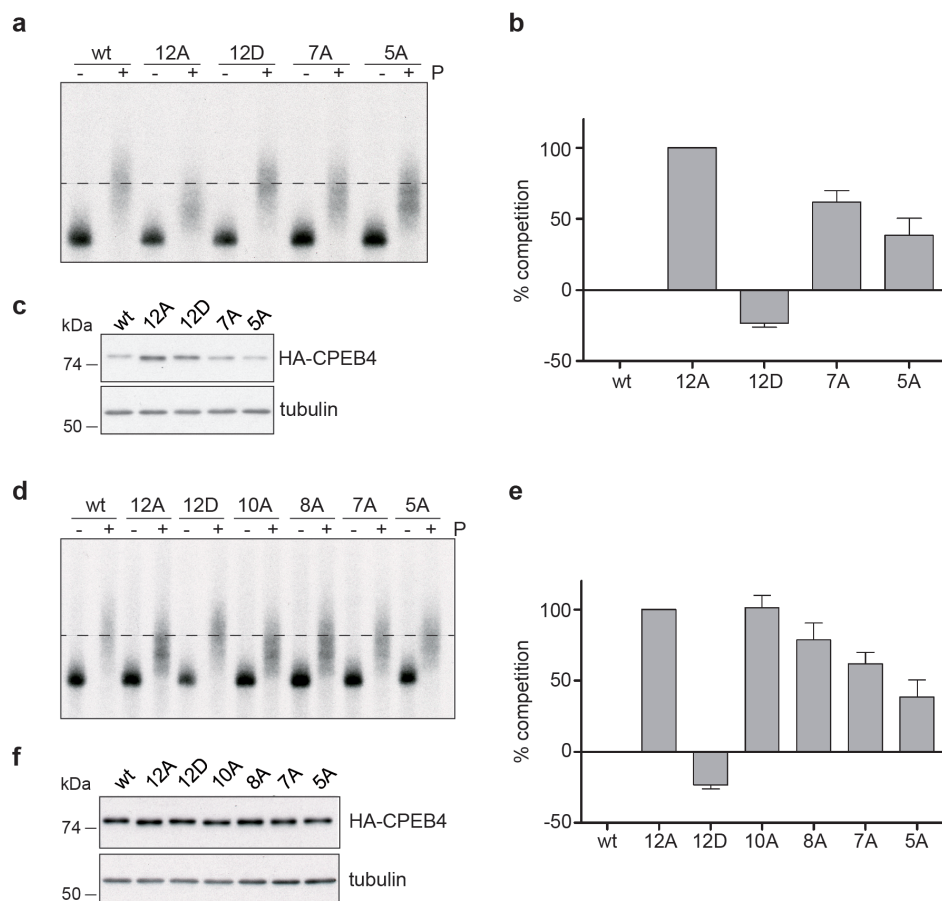
Figure 32. Quantification method to determine the percentage of competition of xCPEB4 phosphorylation mutants. Using the Fiji software, the intensity profiles of the blue rectangles were plotted (lower panel). The distance from the top of the lane to the peak of maximum intensity was obtained (x) and used in the formula shown in order to calculate the percentage of competition.

To start with, we tested the effect of HA-xCPEB4 12A and 12D mutants, which contain the twelve identified xCPEB4 phosphorylation sites mutated to alanine (A) or acid aspartic (D). As expected for an activating role of the phosphorylation events, the phospho-null mutant 12A significantly reduced *emi2* 3' UTR polyadenylation, while the 12D behaved as the wild type variant or even resulted in a longer poly(A) tail of the probe (Figure 33). We then tested the requirement of p42MAPK and Cdc2 phosphorylation events for xCPEB4 function. To this end, we tested HA-xCPEB4 7A and 5A mutants, in which the seven p42MAPK or the five Cdc2 phosphorylation sites were mutated to alanine respectively. None of these mutants was able to

compete to the same extent as the 12A mutant, indicating that both kinases are required to activate xCPEB4 (Figure 33a-c). Moreover, two additional mutants were evaluated, the 10A mutant, which contains all the phosphosites except S18 and S40 mutated to alanine (S18 and S40 were not identified when xCPEB4 was phosphorylated with oocyte extracts but just with recombinant kinases) and the 8A mutant, which contains the phosphosites flanking the second large disordered region mutated to alanine (S250, S253, T324, S328, S330, S351, S357 and S362A). While the 10A mutant was able to compete to the same extent as the 12A mutant, the 8A mutant did not. Interestingly, when all the tested mutants were compared, an additive effect of the phosphorylation events for xCPEB4 activation was unveiled (Figure 33d-f).

To demonstrate that the competition effect perpetrated by the phospho-null mutants depends on RNA binding and is not due to the sequestration of CPEB cofactors, we generated a 12A mutant with two additional mutations in the tandem RRM domains described to disrupt RNA binding (Y490A and K595A) (Afroz et al., 2014). This RNA-binding defective mutant (12Am) was not able to compete the polyadenylation of *emi2* 3' UTR probe, corroborating that the competition effect is due to direct mRNA binding (Figure 34). In fact, other dominant-negative variants described for CPEBs also act through RNA binding (Mendez et al., 2000a). It should be noted that wild type HA-xCPEB4, when compared to the 12Am mutant, showed some degree of competition. Most probably this effect can be explained by a post-translational misregulation of xCPEB4 resulting from its overexpression. In agreement with this hypothesis, the 12D mutant competed less than the wild type variant (Figure 34).

Conclusively, xCPEB4 needs to be phosphorylated in its N-terminal domain by p42MAPK and Cdc2 in at least ten residues in order to be fully active and mediate the cytoplasmic polyadenylation of target mRNAs.



Partial mutants tested:

10A: S38, 97, 250, 253, T324, S328, 330, 351, 357, 362A

8A: S250, 253, T324, S328, 330, 351, 357, 362A

7A: S18, 38, 40, 97, 250, 253, 351A (p42 MAPK sites)

5A: T324, S328, 330, 357, 362A (cdc2 sites)

Figure 33. xCPEB4 hyperphosphorylation is required for its function in cytoplasmic polyadenylation. (a, d) *In vivo* competition assays. 4% acryl-urea gel showing *emi2* 3' UTR probe polyadenylation in the absence (-) or presence (+) of progesterone (P) in oocytes overexpressing HA-xCPEB4 wild type (wt) or different phosphorylation mutants (specified at the bottom of the figure). The dashed line marks the median polyadenylation in wt. (b, e) Percentage of competition of polyadenylation calculated from three independent competition experiments. 0% competition was assigned to wild type and 100% to the 12A mutant. Results are shown as means and s.d. (b) Related to figure 33a. (e) Related to figure 33d. (c, f) Western blot with anti-HA antibody and anti-tubulin (loading control) to show protein expression levels (one-oocyte equivalents were loaded per lane). (c) Related to figure 33a. (f) Related to figure 33d.

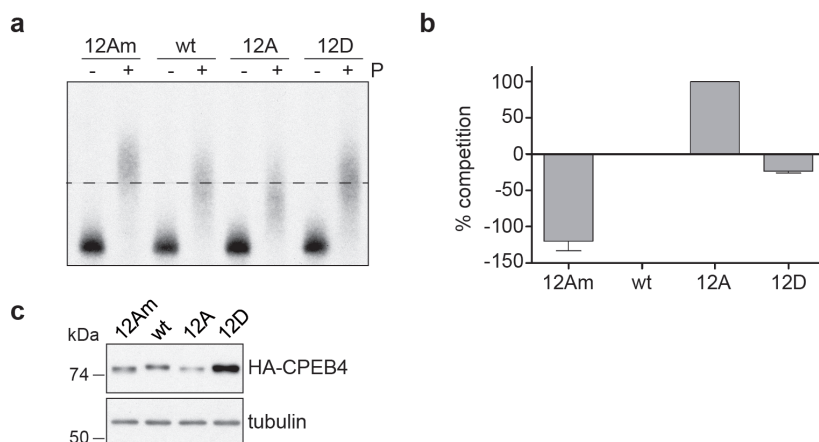


Figure 34. Mutation of xCPEB4 RRM domains abrogates the competition effect caused by the phospho-null mutant 12A. (a) *In vivo* competition assay. 4% acryl-urea gel showing *emi2* 3' UTR probe polyadenylation in the absence (-) or presence (+) of progesterone (P) in oocytes overexpressing HA-xCPEB4 wild type (wt) or different mutants (12A, the twelve phosphorylation sites have been mutated to alanine; 12D, the twelve phosphorylation sites have been mutated to aspartic acid; 12Am, 12A mutant with two additional mutations that disrupt RNA binding, Y490A and K595A). The dashed line marks the median polyadenylation in wt. **(b)** Percentage of competition of polyadenylation calculated from three independent competition experiments. 0% competition was assigned to wild type and 100% to the 12A mutant. Results are shown as means and s.d. **(c)** Western blot with anti-HA antibody and anti-tubulin (loading control) to show protein expression levels (one-oocyte equivalents were loaded per lane).

5.2.2. Non-phosphorylated xCPEB4 has the ability to repress mRNA translation

To uncover whether non-phosphorylated xCPEB4 is just inactive or, otherwise, has the ability to actively repress mRNA translation, we compared the ability of the xCPEB4 12A mutant to compete polyadenylation with the one exerted by the RBD of xCPEB4. The RBD acts as a dominant-negative variant through RNA binding. However, since it lacks the whole NTD it does not recruit CPEB cofactors and therefore does not actively repress mRNAs. Competition experiments showed that the full-length 12A mutant competed the polyadenylation of the probe more efficiently than the RBD. This result proves that xCPEB4 phospho-null mutant not only is not active in cytoplasmic polyadenylation but also is able to actively repress mRNA translation (Figure 35).

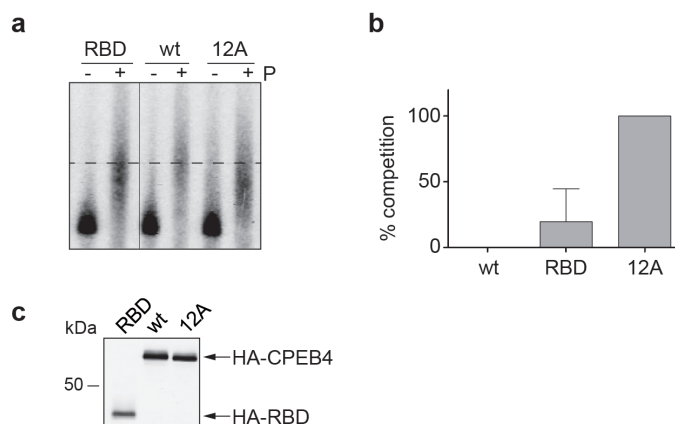


Figure 35. xCPEB4 phospho-null mutant 12A actively represses mRNA polyadenylation. **(a)** *In vivo* competition experiment. *emi2* 3' UTR probe polyadenylation in the absence (-) or presence (+) of progesterone (P) in oocytes overexpressing HA-xCPEB4 wild type (wt), the phospho-null mutant 12A (the twelve phosphorylation sites mutated to alanine) or the truncated variant RBD (RNA-binding domain). The dashed line marks the median polyadenylation in wt. **(b)** Percentage of competition of polyadenylation calculated from three independent competition experiments. 0% competition was assigned to wild type and 100% to the 12A mutant. Results are shown as means and s.d. **(c)** Western blot with anti-HA antibody to show protein expression levels (one-oocyte equivalents were loaded per lane).

5.2.3. xCPEB4 RRM2 phosphorylation does not affect xCPEB4 function

Notwithstanding we had not identified any phosphorylation event in xCPEB4 RNA-binding domain, Y608 located in RRM2 has been found to be phosphorylated in high-throughput mass spectrometry studies for hCPEB4 (www.phosphosite.org). To rule out any relevance of this phosphorylation event for xCPEB4 function, we tested the effect of Y608F mutation by competition experiments. It is important to point out that in this experiments we used the RBD, instead of full-length xCPEB4, to test whether this phosphorylation event affects the ability of this domain to bind RNA (see Figure 19 for methods details). The RBD Y608F mutant was able to bind *emi2* 3' UTR radioactive probe and compete its polyadenylation as efficiently as the wild type RBD. Thus, we conclude that phosphorylation on Y608 does not affect xCPEB4 tandem RRMs structure and binding to mRNA (Figure 36).

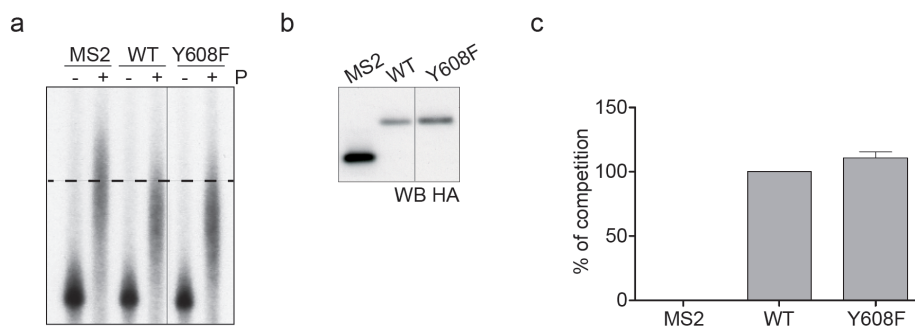


Figure 36. xCPEB4 Y608 phosphorylation is not required for RNA binding. (a) *In vivo* competition experiment. *emi2* 3' UTR probe polyadenylation in the absence (-) or presence (+) of progesterone (P) in oocytes overexpressing MS2 (negative control), xCPEB4 RRM12ZZ wild type (wt) or the phosphorylation mutant Y608F. The dashed line marks the median polyadenylation in the control MS2. (b) Western blot with anti-HA antibody to show protein expression levels (one-oocyte equivalents were loaded per lane). (c) Percentage of competition of polyadenylation calculated from three independent competition experiments. 0% competition was assigned to MS2 control and 100% to xCPEB4 RRM12ZZ wt. Results are shown as means and s.d.

5.3. xCPEB4 hyperphosphorylation is required for meiotic progression

To analyse the requirement of xCPEB4 hyperphosphorylation for meiotic progression, we explored the ability of different xCPEB4 phosphorylation mutants to compensate for the depletion of endogenous xCPEB4. xCPEB4 depletion in oocytes with an antisense oligonucleotide targeting xCPEB4 3' UTR has no effect in the first meiotic division but causes premature exit from the MII arrest, leading to DNA replication and apoptosis (Igea and Méndez, 2010). We used the same strategy to deplete xCPEB4 but collected and fixed the oocytes for metaphase plate visualization 2 h after GVBD (Igea et al. collected the oocytes 10 hours after reaching MII). Under these conditions, we detected a defect in chromosomes alignment in the second metaphase, which most probably is the origin of the long-term effects observed by Igea et al. Precisely, 45% of the oocytes had the chromosomes scattered in the cytoplasm instead of correctly aligned in a single metaphase plate. In order to rescue this phenotype, xCPEB4 variants under the control of xCPEB4 3' UTR but not targeted by the antisense were expressed in oocytes. We first tested the ability of wild type, 12A and 12D variants to rescue

xCPEB4 depletion. Whereas wild type HA-xCPEB4 and the phospho-mimetic mutant 12D rescued the phenotype (near 80% of the oocytes presented a normal metaphase plate), the phospho-null mutant 12A did not (Figures 37a and 37c). Moreover, when p42MAPK and Cdc2 mediated phosphorylation sites were mutated to alanine separately (7A mutant for p42MAPK sites and 5A mutant for Cdc2 sites), none of these mutants was able to rescue the phenotype observed upon xCPEB4 depletion (Figures 37b and 37d). These results confirm that xCPEB4 hyperphosphorylation driven by p42MAPK and Cdc2 is essential for correct meiotic progression.

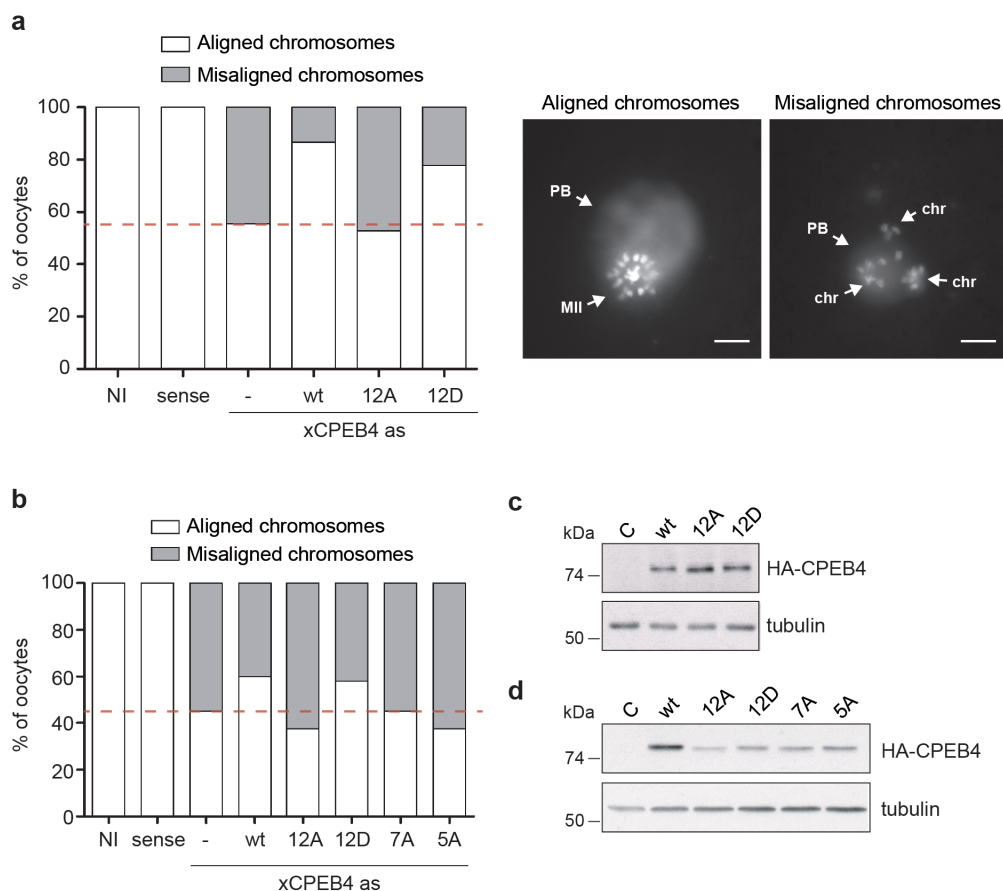


Figure 37. xCPEB4 hyperphosphorylation is required for correct metaphase II arrest. (a, b) *In vivo* rescue experiment. Oocytes were injected with xCPEB4 sense or antisense (as) oligonucleotides. After 16h, oocytes were injected with mRNAs encoding HA-xCPEB4 wild type (wt) or phosphorylation mutants (12A or 12D, the twelve phosphorylation sites have been mutated to alanine (A) or aspartic acid (D); 7A, p42MAPK sites have been mutated to A; 5A, Cdc2 sites have been mutated to A). Oocytes were collected 2 h after GVBD, fixed and stained with Hoechst. A representative image of each phenotype observed (aligned vs. misaligned chromosomes) is shown (PB, first polar body; MII, second metaphase plate; chr, misaligned chromosomes). Scale bar 10 μ m. The percentage of oocytes with each phenotype is plotted in the graph ($n > 15$). The red line marks the percentage of oocytes with aligned chromosomes in the antisense condition. (c, d) Western blot with anti-HA and tubulin (loading control) to show protein expression levels (one-oocyte equivalents were loaded per lane). (c) Relative to Figure 37a. (d) Relative to Figure 37b.

6. xCPEB4 hyperphosphorylation does not regulate the interaction with cofactors

Taking into account that CPEB1 phosphorylation by Aurora A kinase causes the switch from a repression to an activation complex (Barnard et al., 2004; Kim and Richter, 2006; Mendez et al., 2000b), we hypothesized that CPEB4 phosphorylation could also be affecting the recruitment of cofactors. Therefore, we performed co-immunoprecipitation experiments in oocytes overexpressing HA-xCPEB4 wild type, 12A and 12D mutants. First, we evaluated the co-immunoprecipitation of the poly(A) polymerase Gld-2, a known partner for xCPEB4 (Igea and Méndez, 2010). We could not detect any differential interaction between xCPEB4, wild type or phosphorylation mutants, and Gld-2, neither in interphase nor in MII (Figure 38a). Then, we conducted an unbiased approach to detect xCPEB4 cofactors which interaction depends on xCPEB4 phosphorylation status. Thus, we immunoprecipitated HA-xCPEB4 12A and 12D mutants and analysed by mass spectrometry the interacting proteins. We detected chaperones (Hspd1) and RNA helicases (Ddx1 and Ddx20) specifically in the xCPEB4 12A condition. However, the majority of the identified proteins co-immunoprecipitated equally with both mutants (Appendix 1), which shows that their interaction does not depend on xCPEB4 phosphorylation. In fact, no differential silver-stained bands were observed when xCPEB4 12A and 12D co-immunoprecipitations were compared (Figure 38b). Therefore, we conclude that xCPEB4 hyperphosphorylation regulates its activity by a different mechanism than affecting CPEB4 mRNP composition.

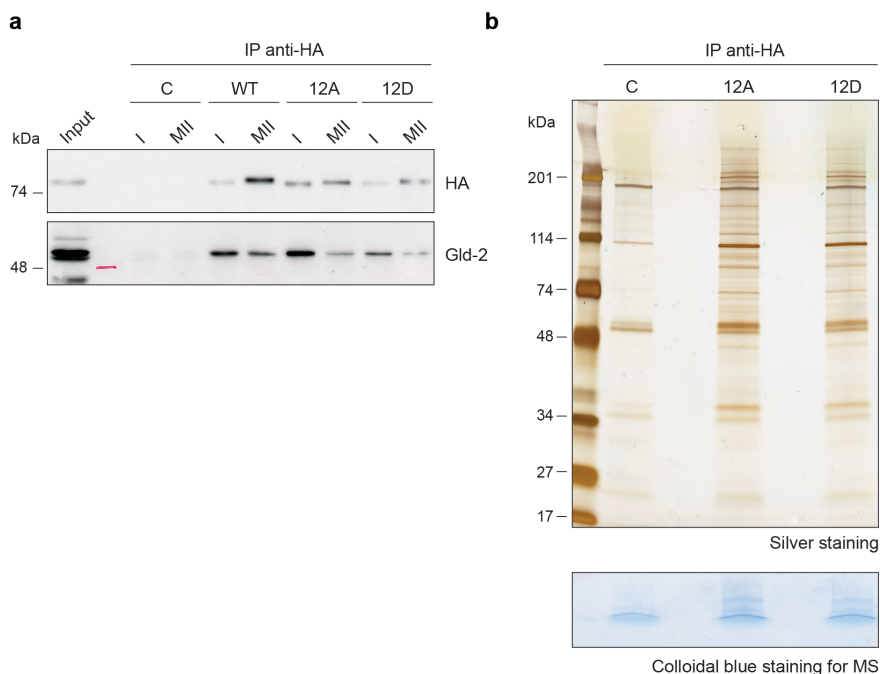


Figure 38. xCPEB4 phospho-mimetic or phospho-null mutants do not differentially interact with Gld-2 or other proteins. (a) Immunoprecipitation of HA-CPEB4, wild type (WT) or phospho-mutants (12A or 12D, the twelve phosphorylation sites have been mutated to alanine (A) or aspartic acid (D)) with anti-HA antibody. Two different meiotic stages were analysed (I, interkinesis; MII, metaphase II). The co-immunoprecipitation of Gld-2 was assessed by western blot. Input corresponds to WT in MII. (b) Immunoprecipitation of HA-CPEB4 12A and HA-CPEB4 12D in MII with anti-HA antibody. In the upper panel, half of the immunoprecipitation was resolved in a 4-20% gradient SDS-PAGE and stained with silver staining (no differential bands between conditions were detected). In the lower panel, the other half of the samples was loaded in SDS-PAGE but not resolved. The gels were excised and analysed by mass spectrometry. C, non-injected oocytes.

7. xCPEB4 hyperphosphorylation modulates its aggregation properties

Considering that ApCPEB, Orb2 and mCPEB3 have been described to form functional amyloid-like oligomers (Fioriti et al., 2015; Majumdar et al., 2012; Si et al., 2010), we wondered if xCPEB4 phosphorylation regulates its activity through an aggregation mechanism.

7.1. xCPEB4 aggregation properties could not be adequately evaluated in *Xenopus laevis* oocytes

To unveil if xCPEB4 is regulated through an aggregation mechanism, we started analysing how HA-xCPEB4 12A and 12D mutants overexpressed in oocytes migrated through sucrose gradients. To this end, we overexpressed both xCPEB4 variants in *Xenopus* oocytes, lysed the oocytes and obtained a clarified extract. Afterwards, the oocyte extracts were loaded and solved on 5%-40% sucrose gradients. Although there were not striking differences in the migration of the 12A and the 12D variants through the gradients, we could observe that the 12A mutant migrated one or two fraction below (denser) than the 12D mutant (Figure 39a-b), which could indicate that the 12A has a stronger tendency to dimerize or oligomerize.

Furthermore, when *in vitro* transcribed cyclin B1 3' UTR mRNA, which contains three CPEs, was added to the extracts, the 12A mutant as well as the 12D migrated one or two fraction below than without mRNA, indicating that both mutants are able to bind RNA under these conditions. Interestingly, when the B1 3' UTR was added to the 12D overexpressing extract, the 12D migrated exactly as the 12A without mRNA. This fact could represent an scenario in which the 12A is forming dimers that migrate equally as two monomeric 12D molecules bound to the same B1 3' UTR mRNA (Figure 39c-d). Moreover, when two out of the three CPEs of cyclin B1 3' UTR were mutated (B1 -23) (Piqué et al., 2008), the change in migration for the 12A mutant upon mRNA addition was less. Hence, the fact that both mutants migrated in

denser fractions upon B1 3' UTR addition was not exclusively due to the mRNA itself but due to the binding of more than one CPEB on the mRNA (Figure 39e-f). Altogether, these experiments, although not being conclusive, suggest that the difference in migration through sucrose gradients observed for the 12A and 12D xCPEB4 variants could be due to the 12A mutant, and not the 12D, forming dimers or small oligomers. Additionally, we do not discard the possibility that xCPEB4 bigger oligomers were lost during the extract preparation.

In order to further analyse the aggregation properties of xCPEB4 we changed of system and moved to cell lines, which are more suitable for microscopy studies.

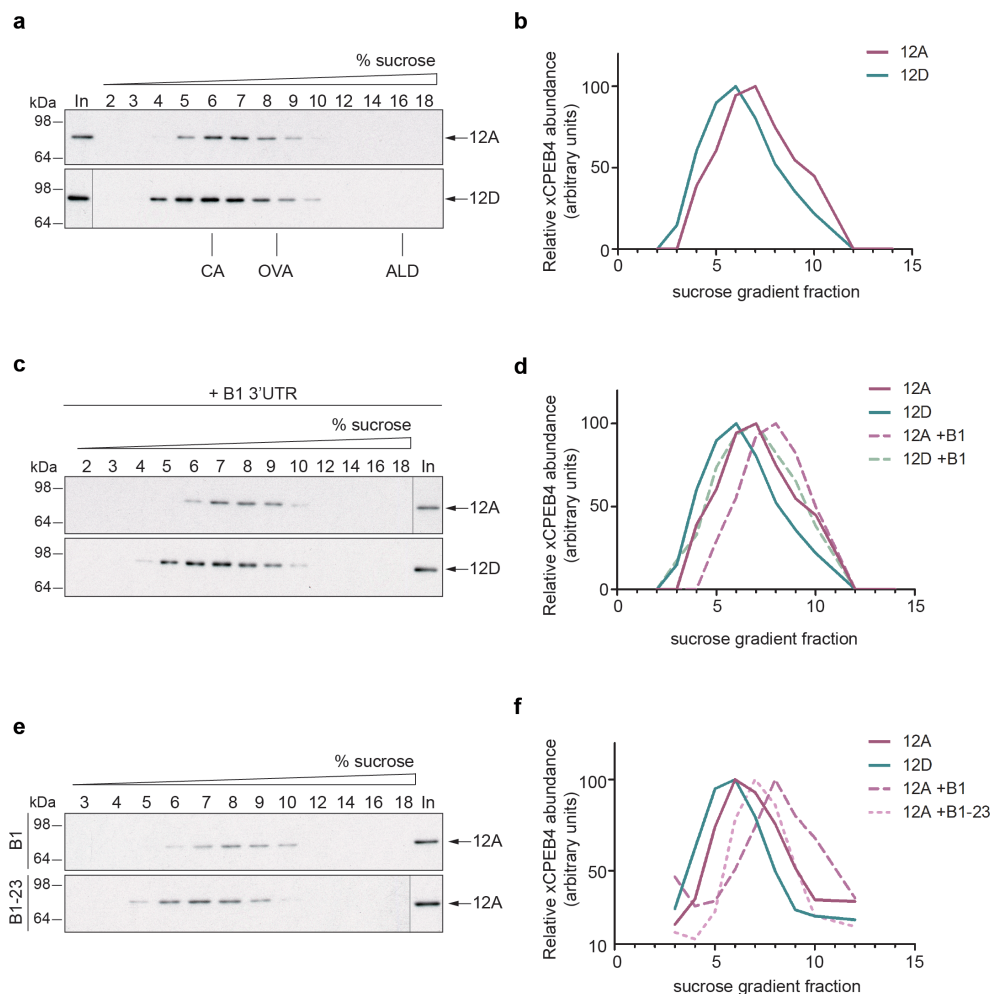


Figure 39. Sucrose gradient analysis of xCPEB4 12A and 12D mutants suggests that the 12A oligomerizes while the 12D remains monomeric. (a, c, e) Western blot with anti-HA of the indicated sucrose gradient fractions. HA-xCPEB4 12A and 12D (the twelve phosphorylation sites have been mutated to alanine (A) or aspartic acid (D)) were overexpressed in oocytes and the resulting oocyte extract was analysed by sucrose gradients, in the absence (a) or presence of B1 (b, c) or B1-23 3' UTR (c). In panel (a) the migration of conalbumin (CA, 75 kDa), ovalbumin (OVA, 44 kDa) and aldolase (ALD, 158 kDa) in the gradient is shown. (b, d, f) Quantification of xCPEB4 12A or 12D abundance along the sucrose gradients. The fraction with maximum signal in the western blot was set to 100 and the relative abundance of the other fractions was calculated. (b) Relative to Figure 39a. (d) Relative to Figure 39c. (f) Relative to Figure 39e.

7.2. Non-phosphorylated xCPEB4 distributes in cytoplasmic granules in U2OS cells

To study xCPEB4 aggregation properties, we overexpressed xCPEB4 fused to eGFP in U2OS cells. While near 80% of the cells overexpressing eGFP-xCPEB4 wild type or the 12A mutant presented a cytoplasmic and punctuated distribution of the GFP signal, in the case of the 12D mutant 80% of the cells showed a diffuse pattern (Figure 40a-b). To exclude the possibility that these granules are a consequence of xCPEB4 binding endogenous mRNAs and translocating, for instance, to P-bodies or stress granules, we tested the ability of xCPEB4 N-terminal domain to form aggregates when overexpressed in U2OS cells. We found that xCPEB4 NTD wild type and the 12A mutant also distributed in cytoplasmic granules, whereas the 12D mutant did not. Instead, xCPEB4 RBD presented the same distribution as eGFP (Figure 40c-d). In addition, we found no co-localization of eGFP-xCPEB4 WT or 12A with P-bodies or stress granules markers (eIF4E-T, which is a component of P-bodies, and p54, which localized in both P-bodies and stress granules) (Figure 41). Thus, although in response to arsenite CPEB4 relocates to stress granules (Chang and Huang, 2014), in non-stressed cells inactive CPEB4 forms aggregates distinct from P-bodies or stress granules. As a result, we conclude that non-phosphorylated xCPEB4 forms aggregates through its NTD. Moreover, most probably this aggregation is regulated by the hyperphosphorylation of the NTD, since the phospho-mimetic mutant 12D has not the ability to aggregate.

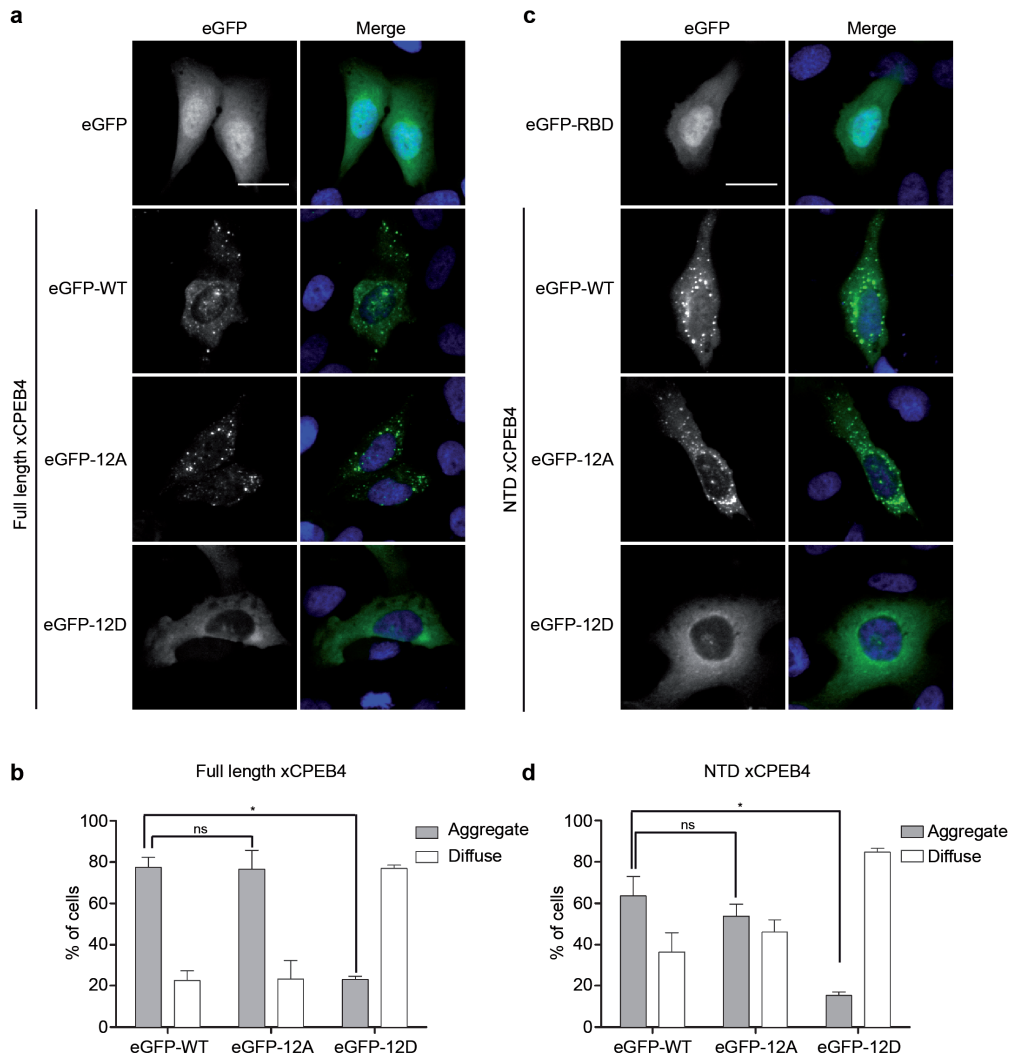


Figure 40. Non-phosphorylated xCPEB4 distributes in cytoplasmic granules in U2OS cells through its N-terminal domain. (a, c) Representative image of eGFP-xCPEB4 (a) full length or (c) N-terminal domain, wild type (WT) or phosphorylation mutants (12A or 12D, the twelve phosphorylation sites have been mutated to alanine (A) or aspartic acid (D)), transfected in U2OS cells. As controls, eGFP and eGFP-RBD (RNA-binding domain) were used. Merge images show eGFP in green and Dapi in blue. Scale bar, 25 μ m. (b, d) Quantification of the different expression patterns observed in (b) Figure 40a and (d) Figure 40c. 100-300 cells were analysed and classified as aggregate (grey bars) or diffuse (white bars) expression pattern. The percentage of cells with each phenotype was calculated from three independent experiments. Significance was addressed with a Sidak's multiple comparisons test, (*) $p < 0.05$, (ns) non significant.

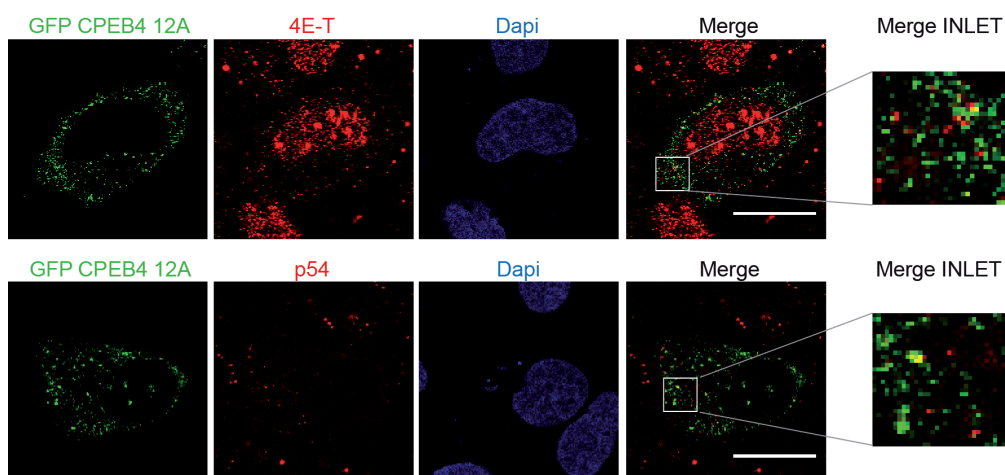


Figure 41. xCPEB4 cytoplasmic granules do not co-localize with P-bodies or stress granules markers. Immunofluorescence of eIF4E-T and p54 in overexpressing eGFP-xCPEB4 12A U2OS cells (the twelve phosphorylation sites of xCPEB4 are mutated to alanine). eGFP is shown in green; 4E-T and DDX6 in red; Dapi in Blue. Merge of eGFP and 4E-T or DDX6 is shown. Scale bar, 20 μ m.

7.3 Purified xCPEB4 N-terminal domain forms aggregates *in vitro* that are regulated by p42MAPK and Cdc2 phosphorylation

To prove that xCPEB4 has the intrinsic property to aggregate through its N-terminal domain, we expressed and purified the NTD, wild type or mutated to alanine or acid aspartic on the twelve identified phosphorylation sites, and analysed its aggregation tendency by three different methods: size exclusion chromatography, dynamic light scattering (DLS) and transmission electron microscopy (TEM).

Purification of the NTDs was performed under denaturing conditions and the proteins were dialyzed against a 2 M urea-containing buffer. Under these conditions, the three NTD variants (wild type, 12A and 12D) behaved equally in size exclusion chromatography and eluted in the expected volume for a disordered monomer

(Figure 42a). However, when urea concentration was decreased to 0.2 M, the wild type and the 12A NTD did not elute, meaning that they were forming aggregates that did not even enter the column. Differentially, the 12D NTD variant eluted at the expected volume (Figure 42b).

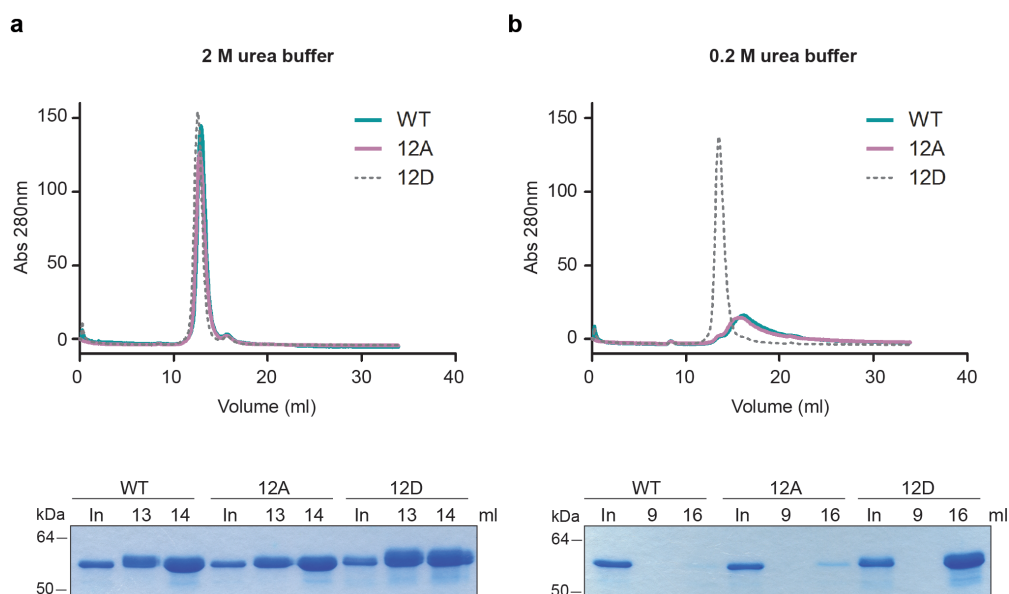
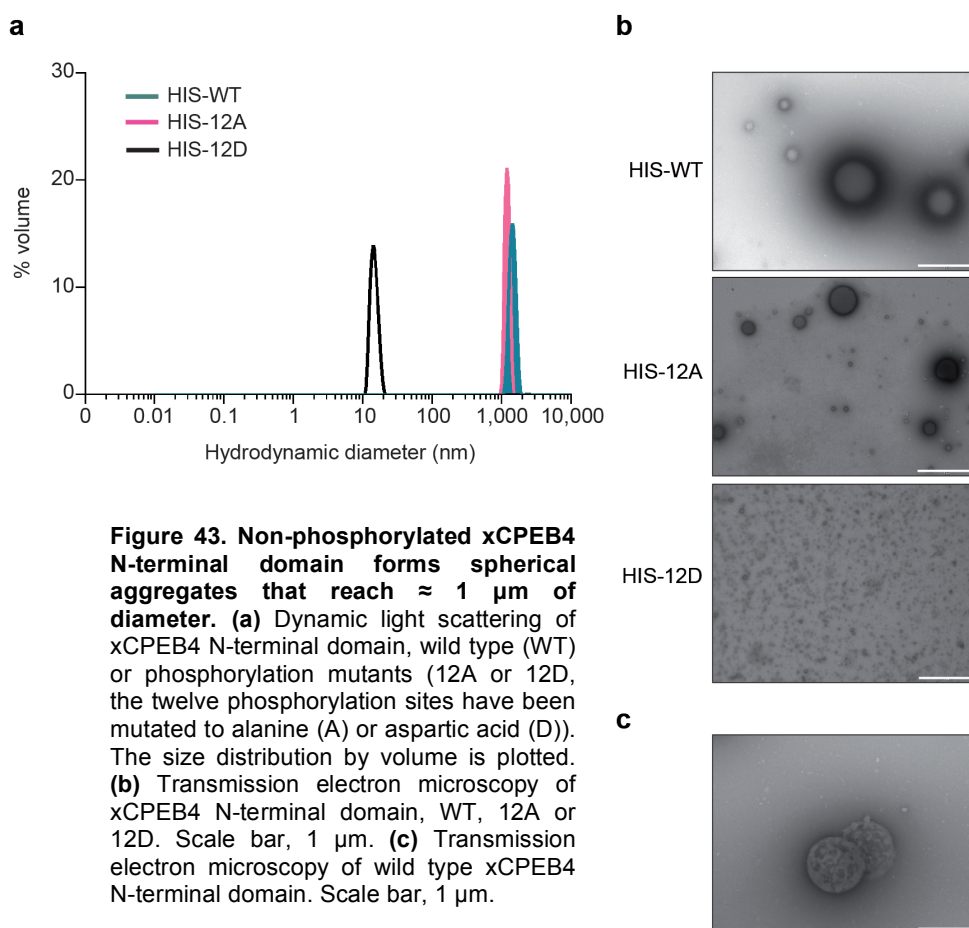


Figure 42. Non-phosphorylated xCPEB4 N-terminal domain forms aggregates *in vitro* at 0.2 M urea, while the phospho-mimetic mutant 12D remains monomeric. (a, b) Size-exclusion chromatography of purified xCPEB4 NTD, wild type (WT), 12A or 12D (the twelve phosphorylation sites have been mutated to alanine (A) or acid aspartic (D)) at 2 M urea (a) or 0.2 M urea (b). In the upper panels, the absorbance at 280 nm for the different elution volumes is represented. In the lower panels, 30 μ l of the indicated elution volumes were solved by SDS-PAGE and stained with coomassie. In, input.

Furthermore, when the purified xCPEB4 NTD variants were subjected to DLS, a technique for measuring the size distribution of molecules and particles, the WT and the 12A mutants presented a hydrodynamic diameter > 1000 nm, while the 12D mutant size was ≈ 10 nm (Figure 43a). This result clearly shows that xCPEB4 NTD non-phosphorylated forms large aggregates. To further characterize these aggregates, we performed TEM of the same samples subjected to DLS.

Interestingly, we observed large spherical structures for WT and 12A NTD that were not present in the phospho-mimetic mutant 12D (Figure 43b). In some cases, some internal structure of these spherical aggregates could be observed (Figure 43c), suggesting that they are build by non-amyloid protein networks.

Altogether, we conclude that xCPEB4 NTD forms large spherical aggregates when is not phosphorylated. Moreover, since these aggregates are not present in the 12D mutant, most probably they are regulated by hyperphosphorylation.



To confirm that the observed NTD aggregates are indeed regulated by phosphorylation, we *in vitro* phosphorylated WT and 12A NTDs with p42MAPK and Cdc2/cyclin B. First, size exclusion chromatography under 0.2 M urea conditions showed that the WT NTD, when phosphorylated by these two kinases, entered the column and eluted in the expected volume as efficiently as the 12D mutant (13-14 ml). Conversely, for the 12A mutant, although more protein eluted at 13-14 ml upon phosphorylation, the recovery was not complete (Figure 44).

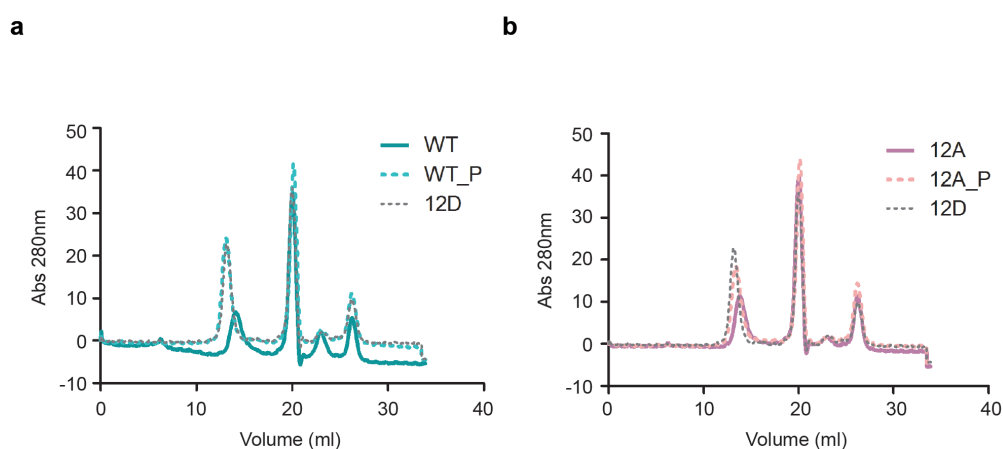


Figure 44. xCPEB4 N-terminal domain aggregates dissolve upon p42MAPK and cdc2/cyclin B phosphorylation. Size-exclusion chromatography of purified xCPEB4 NTD at 0.2 M urea upon *in vitro* phosphorylation with p42MAPK and Cdc2/cyclin B. The absorbance at 280 nm for the different elution volumes is represented. **(a)** xCPEB4 NTD wild type (WT). **(b)** xCPEB4 NTD 12A (the twelve phosphorylation sites have been mutated to alanine). xCPEB4 12D is plotted as a reference.

Second, DLS analysis revealed that the WT NTD size changed from > 1000 nm to \approx 10 nm upon phosphorylation (Figure 45a). However, the 12A variant, which is still phosphorylated by these two kinases but not in the identified residues (Figure 45b), still presented a hydrodynamic diameter > 1000 nm (Figure 45a). Finally, the spherical aggregates observed by TEM for un-phosphorylated WT and 12A were not present in the phosphorylated WT, while large aggregates were still observed for phosphorylated 12A (Figure 45c).

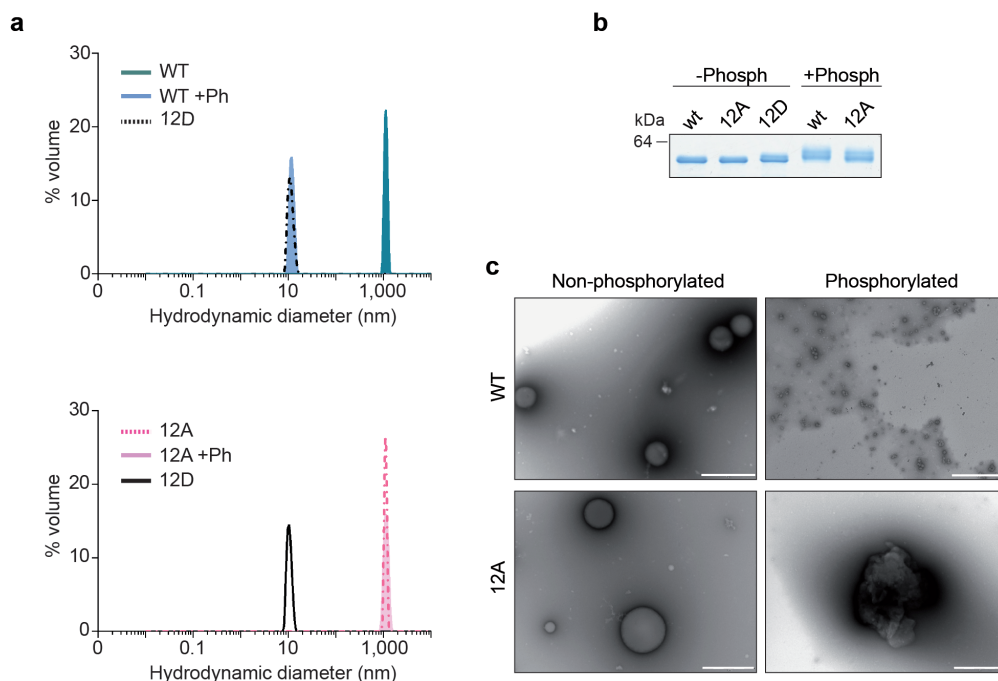


Figure 45. Purified xCPEB4 N-terminal domain forms spherical aggregates that dissolve upon p42MAPK and Cdc2/cyclin B phosphorylation. (a) Dynamic light scattering of purified xCPEB4 N-terminal domain, wild type (WT, upper panel) or phospho-null mutant (12A, lower panel) upon phosphorylation by p42MAPK and Cdc2/cyclin B. The size distribution by volume is plotted. (b) Coomassie stained SDS-PAGE gel of purified xCPEB4 NTD, wild type (wt) or phosphorylation mutants (12A and 12D) upon phosphorylation by p42MAPK and Cdc2/cyclin B (+Phosph). Not phosphorylated proteins are also shown (-Phosph). (c) Transmission electron microscopy of purified xCPEB4 NTD, WT or 12A, upon phosphorylation by p42MAPK and Cdc2/cyclin B. Scale bar, 1 μ m.

These results clearly show that non-phosphorylated xCPEB4 NTD forms large aggregates that are reversible by p42MAPK and Cdc2-mediated phosphorylation on the twelve identified phosphosites.

8. xCPEB4 aggregates recruit CPE-containing mRNAs

Given that the xCPEB4 12A mutant has the ability to actively repress *emi2* 3' UTR polyadenylation and that non-phosphorylated xCPEB4 NTD forms large aggregates, we hypothesized that these aggregates could recruit and repress specific mRNAs.

To prove this hypothesis, we first tried an *in vivo* approach. In this assay, we fractionated cellular extracts from overexpressing GFP-xCPEB4 U2OS cells by sucrose gradients and performed an RNA-immunoprecipitation of the aggregated fraction of GFP-xCPEB4. Western blot analysis of the sucrose gradient fractionation showed that GFP-xCPEB4 was present in the densest fraction of the gradient (fraction 24), which suggests that it is forming large and dense aggregates in U2OS cells. Interestingly, endogenous hCPEB4 was also present in the last fraction of the gradient. Other proteins such as α -tubulin and the unspecific bands detected with anti-hCPEB4 antibody were detected in the first fractions of the gradient, indicating that the gradients were well formed and that the presence of CPEB4 in the last fraction was not a consequence of gradient collapse. In order to check for RNA binding of these aggregates, we performed an RNA-immunoprecipitation with beads specifically recognizing GFP and checked for known CPEB4 mRNA targets by RT-qPCR (Figure 46). However, we did not manage to obtain a specific immunoprecipitation when compared to the negative control (fraction 24 from non overexpressing cells). We suspect that the presence of sucrose or large aggregates in the samples is affecting the specificity of the immunoprecipitation.

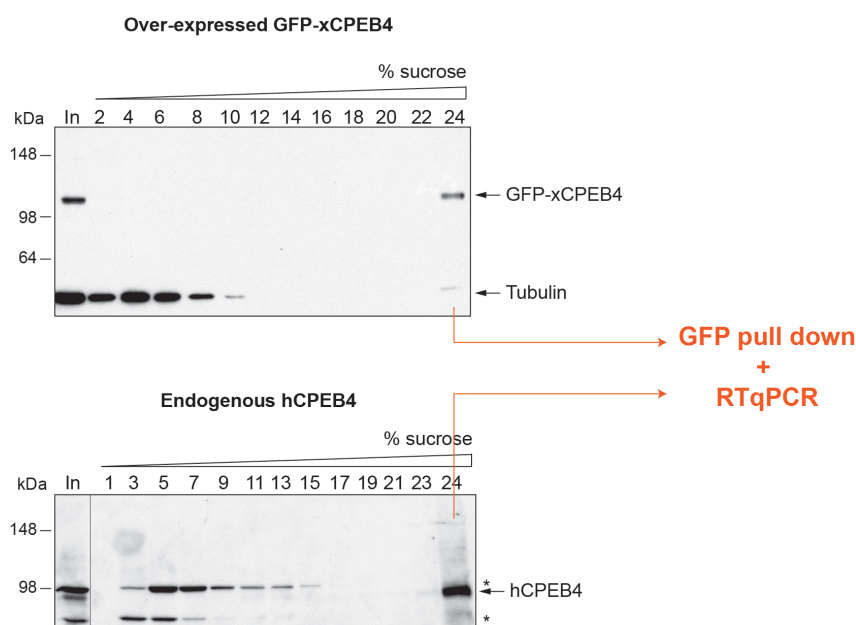


Figure 46. *In vivo* RNA-immunoprecipitation of aggregated GFP-xCPEB4 in U2OS cells. Upper panel, sucrose gradient fractionation of GFP-xCPEB4 overexpressing cells. A western blot anti-GFP of the selected sucrose gradient fractions is shown. Tubulin was used as control. Lower panel, sucrose gradient fractionation of U2OS cells followed by western blot against hCPEB4. Fraction 24 from both conditions was subjected to GFP pull down followed by RT qPCR.

Due to these technical difficulties, we decided to address the question by an alternative *in vitro* approach with purified xCPEB4 full-length protein. In this experiment, we incubated xCPEB4 full-length, or the NTD as control, with radioactive RNA probes corresponding to cyclin B1 or B1-123 (contains the three CPEs mutated) 3' UTRs (Piqué et al., 2008). After, we filtered the samples through a 0.22 μm pore cellulose acetate filter so that the aggregates were retained in the filter. As a prove of principle, we analysed the input and the flow-through obtained after filtration by SDS-PAGE. The totality of the full-length protein was retained in the filter, as well as the majority of the NTD, showing that both variants form aggregates that do not cross the 0.22 μm pores. Upon p42MAPK and Cdc2/cyclin B phosphorylation of xCPEB4 full-length protein, we observed a portion of the protein in the flow-through, which indicates that these aggregates are also reversible by

hyperphosphorylation (Figure 47a). Nevertheless, the disassembly of the full-length aggregates was not complete, most probably because first, not all the molecules were hyperphosphorylated to the same extent and, second, because some of the full-length protein was not correctly folded and formed amorphous aggregates (observed by TEM, data not shown).

To check for RNA binding in the aggregates, we exposed the filters and quantified the signal coming from the radioactive probes B1 and B1-123. The full-length protein significantly retained more B1 probe than the control NTD, which, although forming aggregates, cannot bind RNA. Upon phosphorylation, when full-length aggregates are partially dissolved, we observed a proportional decrease of B1 retention. Moreover, the RNA binding exerted by xCPEB4 aggregates was specific, since no binding of the B1-123 probe was observed (Figure 47b-c).

Therefore, we conclude that xCPEB4 aggregates have the ability to specifically bind CPE-containing mRNAs.

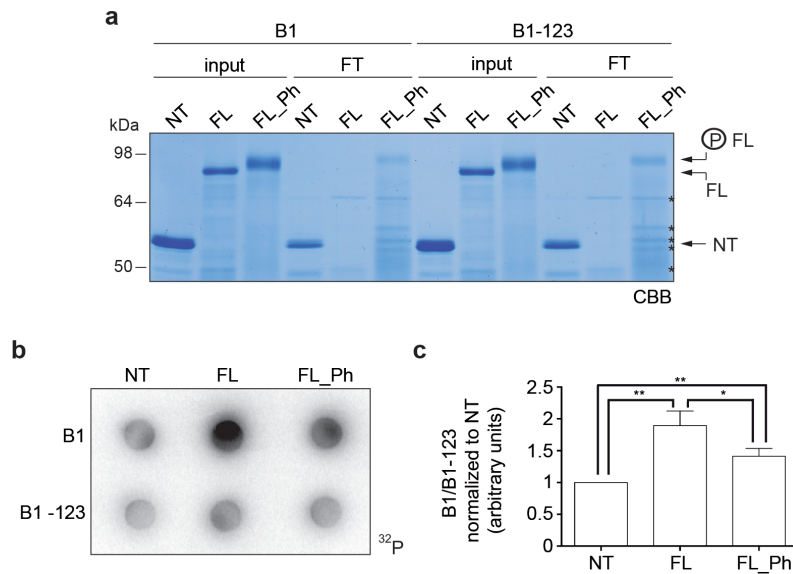


Figure 47. xCPEB4 aggregates specifically bind CPE-containing RNAs. (a) Coomassie stained SDS-PAGE gel of the input (4%) and the flow through (FT, 20%) after filtration through cellulose acetate 0.22 μ m filters. NTD, xCPEB4 N-terminal domain; FL, xCPEB4 full-length; FL_Ph, FL phosphorylated with p42MAPK and Cdc2/cyclin B. Samples from the incubation with cyclin B1 or B1-123 3' UTR are shown. Asterisks (*) show degradation products. **(b)** Cyclin B1 and B1-123 3' UTR radioactive probe retention in cellulose acetate 0.22 μ m filters. **(c)** Quantification of the cyclin B1 and B1-123 3' UTR radioactive probe retention from three independent experiments. Significance was addressed with a t test, (*) $p < 0.05$, (**) $p < 0.005$.

DISCUSSION

1. CPEB1 and CPEB4 RNA-binding domain structures reveal similitudes and differences between CPEB paralogs

All four CPEB paralogs recognize and bind CPE elements in the 3' UTR of target mRNAs and assemble mRNPs that repress or activate translation. In order to gain further insights into how CPEBs nucleate the assembly of mRNP complexes in CPE-containing mRNAs, we have solved the structures of the RNA-binding domain of hCPEB1 and hCPEB4.

Despite the sequence identity between CPEB1 and CPEB4 RBDs is 46%, we have shown that both of them bind to CPE elements using a very similar RNA-binding mode.

CPEB1 and CPEB4 tandem RRM adopt a novel conformation when compared to other tandem RRMs. Generally, tandem RRMs are separated by a flexible inter-domain linker and therefore do not interact in their free state, although there are a few cases in which the tandem RRMs make inter-RRM interactions. The solved structures of CPEB1 and CPEB4 tandem RRMs reveal an unprecedented arrangement of the two RRMs, in which they adopt a fixed V-shaped structure. This positioning of both RRMs is not due to inter-RRM interactions but due to interactions established mainly by the inter-domain linker, which fixes the RRMs in a precise conformation already in the free state. Upon RNA binding, RRMs undergo a closing motion that positions RRM2 almost perpendicular to RRM1, in a manner that the RNA 5' end is bound by RRM1 and the 3' end by RRM2. Thus, RRM1 binds the first four uracils of the CPE and constitutes the major RNA-binding region, while RRM2 is responsible for binding the fifth nucleotide of the CPE, which is usually an adenine but can be a cytosine in non-consensus CPEs. Taking into account this directionality in the binding of the RNA, we propose a two-step mechanism for RNA binding. First, CPEB RRM1 would specifically recognize and bind poly(U) stretches in 3' UTRs. Second, CPEBs would scan the 3' UTR until the recognition of an adenine (or a cytosine in non-consensus CPEs) after a stretch of four uracils. Finally, once CPEBs recognize the CPE sequence, the RRMs would rotate and trap the CPE in between.

Even though the overall structures of CPEB1 and CPEB4 tandem RRMs appear to be very similar, there are some differences with potential functional implications. First, in the case of CPEB1, the region of the N-terminal domain upstream of RRM1 forms an additional β -strand that extends RRM2 and helps to position both RRMs. This region is not conserved among CPEB paralogs and in the case of CPEB4 appears to be unstructured. This feature may differentially affect the spatial orientation of CPEBs N-terminal domains. Thus, in CPEB1, this N-terminal region that extends RRM2 forces the N-terminal domain to position near RRM2 and the ZZ domain. Since the NTD of the CPEBs is the major interaction platform for CPEB cofactors, this positioning of CPEB1 NTD would favour the assembly of mRNPs in those mRNAs that have CPEs located upstream of the PAS (Figure 48). On the contrary, since this region, and the whole NTD, in CPEB4 is unstructured, it could adopt different orientations and probably would allow the assembly of CPEB4 mRNPs regardless the CPE is upstream or downstream of the PAS, although most of the CPEs have been described upstream of the PAS.

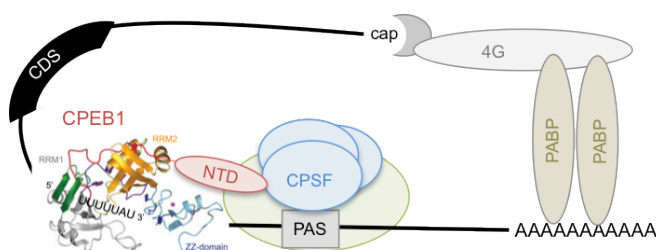


Figure 48. Assembly of CPEB1 activation complexes. A model of CPEB1 full-length is shown in ribbon representation. CPEB1 RRM1 (grey and green), RRM2 (yellow), the ZZ domain (cyan) and the N-terminal (red) are shown. Note that the interaction of CPEB1 NTD with RRM2 positions the NTD towards the 3' end of the mRNA, where a downstream poly(A) signal (PAS) is located. CPEB1 recruits CPSF (blue) to the PAS and an activation complex is assembled (simplified in a green oval) to drive the cytoplasmic polyadenylation of the mRNA and translation initiation.

In agreement with this hypothesis, the 3' UTR of cyclin B2 mRNA, which contains a CPE downstream the PAS, is worst translated in the presence of the downstream CPE in early meiotic stages, indicating that CPEB1 positioned there negatively affects the cytoplasmic polyadenylation and translational activation of that particular mRNA. Most probably, this negative effect is due to the inability of CPEB1 positioned in the downstream CPE to assemble an activating mRNP. On the contrary, in late meiotic stages, when CPEB4 is present, this negative effect of the downstream CPE is not appreciated (Piqué et al., 2008), probably because the flexibility of CPEB4 NTD allows the assembly of the mRNP even if the CPE is downstream the PAS.

In addition, it has been proposed that this N-terminal region upstream of CPEB1 RRM1 contains a non-canonical nuclear localization signal (Lin et al., 2010). The structure of CPEB1 RBD clearly shows that this region is absolutely required for the correct folding of CPEB1 tandem RRMs. Thus, we suggest that the failure to translocate to the nucleus of a CPEB1 mutant lacking this N-terminal region is due to the misfolding of the protein.

Another difference between CPEB1 and CPEB4 RBDs is the binding pocket for the fifth nucleotide of CPE elements, which in consensus CPEs is an adenine (5'-UUUUUAU-3' or 5'-UUUUAAU-3'), but in non-consensus CPEs can be a cytosine (5'-UUUUCAU-3'). Whereas in CPEB1, this pocket is less hydrophobic and can accommodate an adenine and a cytosine, in CPEB4 this position is restricted to an adenine. This difference implies that CPEB1 can more easily bind to non-consensus CPEs containing cytosines in the fifth position, while CPEB4 may only bind to consensus CPEs or non-consensus CPEs with adenines at the fifth position (5'-UUUUACU-3', 5'-UUUUAAAU-3', 5'-UUUUAAAGU-3'). The role of CPE nucleotides from position sixth onward has not been addressed in this study, since the structures in complex with RNA were done with the pentanucleotides 5'-UUUUUA-3' and 5'-CUUUUA-3'. Nevertheless, the chemical shift perturbations observed with these pentanucleotides and the consensus CPE 5'-UUUUUAU-3' were very similar if not identical, suggesting that the first five nucleotides of the CPE are the critical ones for tandem RRMs binding.

The solved structures of CPEB1 and CPEB4 tandem RRMs were functionally validated in *Xenopus* oocytes by *in vivo* competition experiments. Hence, we

conclude that the key residues for RRM positioning and folding, as well as for RNA binding, identified *in vitro* are indeed essential in physiological conditions. Furthermore, the *in vivo* competition experiments, beyond ratifying the structures solved by NMR, allowed us to evaluate the requirement of the ZZ domain for RNA binding and, interestingly, unveiled a different competition behaviour between CPEB1 and CPEB4.

To start with, the ZZ domain has been proposed to function as a protein-protein interaction domain (Merkel et al., 2013), although previous studies have shown that this domain is important for RNA binding (Hake et al., 1998). The structure of the ZZ domain solved in this study revealed a hydrophobic helical surface ideal for protein-protein interactions, as well as two β strands that expose positively charged residues that could provide a binding surface for nucleic acids. In agreement with its role in RNA binding, competition experiments showed that the ZZ domain is absolutely required for the ability of CPEB1 to compete endogenous cytoplasmic polyadenylation, indicating that the ZZ domain is needed for RNA binding *in vivo*. According to the model of CPEB1 RRM followed by the ZZ domain (Figure 22a), the ZZ domain is positioned in close proximity to RRM2. Hence, we propose that, although the ZZ domain by its own is not able to bind CPE elements, it may interact with nucleotides downstream the CPE and enhance the binding affinity of the CPEBs. We do not exclude the possibility that apart from binding RNA, the ZZ domain may also interact with CPEB cofactors.

Second, competition experiments clearly show a difference in the competition effect exerted by CPEB1 and CPEB4. CPEB1 RRM12ZZ generates a complete deadenylated fraction of *emi2* 3' UTR probe, whereas CPEB4 RRM12ZZ mainly affects the length of the poly(A) tail (Figure 19). Despite *in vitro* RNA gel shift assays show similar dissociation constants between CPEB1 and CPEB4 (86 nM \pm 28 nM for CPEB1 and 102 nM \pm 4nM for CPEB4) (Novoa et al., 2010), competition experiments suggest that CPEB1 has more affinity for *emi2* 3' UTR than CPEB4 *in vivo* and, consequently, competes polyadenylation completely. We suggest that CPEB4 RRM12ZZ binds the probe with less affinity, allowing some endogenous CPEB molecules to extend the poly(A) tail to some degree. If this difference in RNA-binding affinity applies for other CPEB target mRNAs, it will definitely influence the translational control of CPE-containing mRNAs in cells co-expressing both CPEBs.

CPEBs are highly conserved across vertebrates, especially in their RNA-binding domain that presents 99% identity among vertebrate orthologs (Figure 16). For this reason, the structures and the RNA-binding mode described for hCPEB1 and hCPEB4 in this study can be applied to CPEBs in other species. Furthermore, considering that CPEB2, CPEB3 and CPEB4 RBDs share 96% identity between them, while only 46% with CPEB1, we can assume that CPEB2-4 tandem RRM fold and bind CPEs in a preserved manner.

In conclusion, there are some structural differences in the RBDs from CPEB1 and the other CPEBs. These differences may have potential functional implications in particular scenarios of coexistence, where the differences in RNA-binding affinity and in the recognition of non-consensus CPEs may influence the targeting of CPE-containing mRNAs by specific CPEBs. However, all CPEB family members bind CPEs in the 3'UTR of target mRNAs in a similar fashion. Hence, the major difference between the CPEBs still relies on their divergent N-terminal domain.

2. CPEB4 activity is regulated by Cdc2- and p42MAPK-mediated hyperphosphorylation

xCPEB4 synthesis is activated at the PI-MI meiotic transition by CPEB1-mediated cytoplasmic polyadenylation of its maternal mRNA (Igea and Méndez, 2010). However, xCPEB4 synthesis is not sufficient to drive cytoplasmic polyadenylation of mRNAs during the second meiotic division. Instead, CPEB4 requires to be post-translationally activated to sustain polyadenylation (Novoa et al., 2010). Our results show that xCPEB4 activation is driven by Cdc2- and p42MAPK-mediated hyperphosphorylation of at least twelve residues, all of them localized in xCPEB4 N-terminal disordered domain.

The specific phosphorylation sites that we have mapped are S18, S38, S40, S97, S250, S253, T324, S328, S330, S351, S357 and S362. Specifically, we have identified seven of the sites as p42MAPK-mediated phosphorylation sites (S18, S38,

S40, S97, S250, S253 and S351) and five of the sites as Cdc2-mediated phosphorylation sites (T324, S328, S330, S357 and S362). Importantly, these twelve phosphosites additively activate xCPEB4. Therefore, the function of xCPEB4 in cytoplasmic polyadenylation and meiotic progression requires phosphorylation in these twelve identified sites and, consequently, both Cdc2 and p42MAPK are necessary for the full activation of xCPEB4.

Cdc2 and p42MAPK are proline-directed kinases that preferentially phosphorylate the minimal consensus sequence S/TP. However, two out of the seven p42MAPK sites (S18 and S351) and three out of the five Cdc2 sites (S328, S357 and S362) in xCPEB4 NTD are not proline-directed. Nevertheless, Cdc2 and p42MAPK can phosphorylate non-consensus motifs under some conditions. Cdc2 has been shown to phosphorylate non-consensus sites in Emi2 and Swe1, the yeast homolog of Wee1 (Harvey et al., 2005; Isoda et al., 2011), and p42MAPK can phosphorylate non-consensus sites in the TNF α receptor (Van Linden et al., 2005). In the majority of these cases, phosphorylation at non-consensus sites is facilitated by kinase recruitment at previously phosphorylated consensus sites. Thus, Cdc2 and p42MAPK can generate self-priming events to phosphorylate non-consensus sites. At the moment, we cannot rule out the possibility that this is also the case for xCPEB4 phosphorylation and that Cdc2 and p42MAPK perform self-priming events to phosphorylate xCPEB4 in non-consensus motifs. However, we know that Cdc2 and p42MAPK do not require priming events from each other in order to phosphorylate xCPEB4, since neither the Cdc2-specific mutant nor the p42MAPK-specific mutant behave as the 12A mutant in competition experiments.

Our results show that the functional xCPEB4 phosphorylation sites have been mapped, since the mutation of the twelve identified phosphosites produce a xCPEB4 variant unable to mediate cytoplasmic polyadenylation and drive meiotic progression. Notwithstanding, we know that xCPEB4 is phosphorylated in at least three more sites (pp 1, pp 2 and pp 7 have not been mapped). While pp 1 and pp 2 are most probably phosphorylated by p42MAPK, pp 7 is not phosphorylated by Cdc2 or p42MAPK (Figure 27). We speculate that pp 7 could be phosphorylated by Plk1 since it is localized in xCPEB4 fragment 3, which harbours Plk1 consensus sites and its phosphorylation is partially affected by Plk1 inhibition. Whether Plk1

phosphorylates xCPEB4 or not is not clear. Nonetheless, our results show that the two major and essential players in xCPEB4 activation are p42MAPK and Cdc2.

3. xCPEB4 hyperphosphorylation as a mechanism to generate ultrasensitivity and switch-like responses

The meiotic cell cycle is driven by irreversible discrete phase-transitions that are sustained by feedback loops and ultrasensitive responses. Hence, the intrinsic ultrasensitivity of specific components in signalling networks helps to generate switch-like responses and bistability, which is the nature of cell cycle.

Protein hyperphosphorylation is a mechanism to generate ultrasensitive responses. In this case, the highest ultrasensitivity is accomplished when half of the phosphorylation sites are not essential for substrate activation (Ferrell and Ha, 2014c). Considering that xCPEB4 is activated by hyperphosphorylation and that it is phosphorylated in more than the twelve essential phosphorylation sites, we propose that xCPEB4 hyperphosphorylation can generate an ultrasensitive response. This ultrasensitivity, together with the positive feedback loop generated by CPEB4 targeting its own mRNA (Igea and Méndez, 2010), can generate a switch-like transition from interphase to metaphase II, contributing to the unidirectionality of the meiotic cell cycle.

4. xCPEB4 hyperphosphorylation regulates the assembly of membraneless organelles through bulk electrostatics

This work shows that non-phosphorylated xCPEB4 has the ability to aggregate through its N-terminal disordered domain, and, importantly, this property is regulated by phosphorylation on the twelve identified phosphorylation sites.

The aggregates formed by xCPEB4 NTD resemble what has been described as liquid-like droplets, membraneless organelles or hydrogels, which are spherical dynamic aggregates assembled through an extensive network of weak, multivalent protein-protein interactions (Weber and Brangwynne, 2012). These aggregates exhibit liquid-like behaviours, like fusion and fission events (Brangwynne et al., 2009). Live cell imaging of U2OS cells over-expressing eGFP-xCPEB4 shows that xCPEB4 aggregates behave as liquid-like droplets (Appendix 2), indicating that xCPEB4 aggregates are dynamic and present properties of membraneless organelles.

The dynamic interaction networks that build up this kind of aggregates are established between multivalent molecules, as proteins and mRNAs, as well as between IDRs (Kato et al., 2012; Li et al., 2012). McKnight and colleagues have revealed that low-complexity sequences, such as repetitions of the [G/S]Y[G/S] motif, are necessary and sufficient for the transition to a hydrogel state (Kato et al., 2012). Considering that the NTD of xCPEB4 contains two major regions of disorder, although such motif repetitions are not evident, it is plausible to assume that the molecular basis for the formation of xCPEB4 aggregates rely on interactions between these IDRs. Thus, we propose a model in which xCPEB4 IDRs establish multiple weak intermolecular interactions that mediate xCPEB4 phase transition into membraneless organelles, while the RBD specifically binds CPE-containing mRNAs.

Our results clearly show that xCPEB4 aggregates bind CPE-containing mRNAs. Moreover, a non-phosphorylatable xCPEB4 variant not only is not active in cytoplasmic polyadenylation but also actively represses translation of a CPE-containing mRNA probe, as shown by the major competition effect exerted by

xCPEB4 12A when compared to xCPEB4 RBD (Figure 35). Hence, we conclude that xCPEB4 sequesters target mRNAs into membraneless organelles and represses their translation. Since we have not detected major differences in cofactor recruitment between the phospho-mimetic and the phospho-null mutants of xCPEB4, we think that the repressing function of CPEB4 aggregates might rely on the conformation of the assembled complexes. Thus, although the phospho-null mutant of CPEB4 is able to recruit the poly(A) polymerase Gld-2, the intermolecular interactions established between xCPEB4 NTDs within the aggregates might impede the correct disposition of the factors and, as a consequence, cytoplasmic polyadenylation cannot take place. Moreover, we have detected Ddx1 and Ddx20 RNA-helicases specifically interacting with the 12A mutant of xCPEB4. It is possible that Ddx1 and Ddx20 are contributing to CPEB4-mediated repression, resembling the role of the RNA helicase p54 in CPEB1 repressing mRNPs (Minshall et al., 2007).

Importantly, the assembly of xCPEB4 aggregates is regulated by hyperphosphorylation of xCPEB4 NTD. Hence, upon Cdc2- and p42MAPK-mediated phosphorylation, the sum of the negative charges distributed along xCPEB4 NTD disrupts the intermolecular interactions within the aggregates, and, as a consequence, aggregates disassemble and cytoplasmic polyadenylation takes place. It is the phosphorylation of the twelve identified sites what regulates aggregate assembly, since the xCPEB4 12A mutant still forms aggregates upon phosphorylation, although it is phosphorylated to some extent. When considering the positions of the identified phosphosites in xCPEB4, they are distributed along the NTD flanking two major disordered regions. In other system where bulk electrostatics regulate intermolecular interactions, like Ste5, it is the number of phosphorylations and not their exact position what has an effect (Strickfaden et al., 2007). Although not having directly tested this hypothesis for xCPEB4, we suspect that bulk electrostatics distributed along xCPEB4 NTD and not the exact position of the phosphosites is what regulates xCPEB4 aggregation and activity. One interesting observation in that direction comes from DLS experiments of xCPEB4 NTD upon phosphorylation with p42MAPK and Cdc2. According to our model in which the twelve phosphorylation sites are essential for xCPEB4 activation, *in vitro* phosphorylation with individual kinases should not be enough for aggregate disassembly. As expected, p42MAPK alone was not able to revert xCPEB4

aggregation. However, surprisingly, Cdc2 was able to disassemble xCPEB4 NTD aggregates (data not shown). The reason why Cdc2 is able to revert aggregation might be that it phosphorylates xCPEB4 fragments 1 and 2 *in vitro*, two fragments that are not Cdc2 targets *in vivo*. Thus, the unspecific phosphorylation of Cdc2 on the first half of xCPEB4 NTD, which is really targeted by p42MAPK, might add the negative charges required for the disruption of the intermolecular interactions that build the aggregates. Note that Cdc2 phosphorylates fragments 1 and 2 on different sites than p42MAPK (Figure 27), which would be in line with the hypothesis of bulk electrostatics being more important than the exact position of the phosphorylation sites.

In conclusion, our results support a model in which non-phosphorylated xCPEB4 represses CPE-containing mRNAs translation through the formation of membraneless organelles. Upon xCPEB4 hyperphosphorylation, the aggregates disassemble and xCPEB4 mRNPs can adopt the right conformation for cytoplasmic polyadenylation of target mRNAs.

Despite the conclusive experiments to define the molecular mechanism for xCPEB4 activity regulation were made in U2OS cells and with recombinant protein, we strongly believe that the same mechanism makes CPEB4 hyperphosphorylation required for meiotic progression. In agreement with this hypothesis, the sucrose gradient experiments performed with oocyte extracts show that the phospho-null mutant also has a stronger tendency to oligomerize than the phospho-mimetic mutant in *Xenopus* oocytes (Figure 39).

5. CPEBs are differentially regulated at a post-translational level

Our working model is that the divergent NTDs of the CPEBs specify a different post-translational regulation for every CPEB and widen the number of situations in which CPEBs fine-tune the translation of specific mRNAs subpopulations. Accordingly, the

molecular mechanism that we have described for xCPEB4 activity regulation is specific for CPEB4 and has not been previously described for other CPEBs.

On the one hand, CPEB1 activity is known to be also regulated by phosphorylation. However, in the case of CPEB1, a single phosphorylation event mediated by Aurora A kinase causes a differential recruitment of cofactors and a switch from a repressing to an activating CPEB1 mRNP (Mendez et al., 2000a, 2000b). Furthermore, CPEB1 phosphorylation by Cdc2 and PIK1 target the protein for ubiquitin-mediated degradation (Mendez et al., 2002). These effects of CPEB1 phosphorylation are clearly different from what we have described for xCPEB4, in which phosphorylation regulates the assembly of hydrogel-like aggregates. More recently it has been shown that CPEB1 dimerizes through its RBD, generating a pool of CPEB1 inactive for RNA-binding (Lin et al., 2012). CPEB4 RBD has also been shown to dimerize, although in low proportion and with no effect in RNA-binding capacity (Schelhorn et al., 2014). Nevertheless, our results show that CPEB4 oligomerization capacity relies on its N-terminal disordered domain and not in the RBD.

On the other hand, CPEB3 activity is regulated by the assembly of stable and inheritable amyloid-like aggregates (Drisaldi et al., 2015; Fioriti et al., 2015; Stephan et al., 2015). Although both CPEB3 and CPEB4 assemble aggregates, those are structurally and functionally distinct. First, the nature of the aggregates is different. CPEB3 aggregates are stable, amyloid-like and resistant to SDS treatment, as prions, whereas CPEB4 aggregates are dynamic and not resistant to SDS or 2 M urea conditions. In fact, the prion-like properties of CPEB3 rely on its Q-rich domain, which is not conserved in CPEB4 or in the other CPEBs. Moreover, in the case of CPEB3 the aggregates are active in cytoplasmic polyadenylation, which is the contrary of what we have found for CPEB4 liquid-like droplet aggregates, which repress cytoplasmic polyadenylation. Finally, while CPEB3 aggregates are regulated through SUMOylation, CPEB4 aggregates are disassembled by hyperphosphorylation.

These results support the fact that the post-translational regulation of the CPEBs is specific and, consequently, CPEBs will differentially respond in a given cellular environment. It is easy to imagine a situation in which the signalling cascades active in that moment will determine which CPEBs are active and which are inactive or

even degraded. This fact, in addition to the dual role in translational control of the CPEBs, their capacity to regulate overlapping mRNA subpopulations (Novoa et al., 2010) and their different RNA-binding affinities, generates a complex scenario in cells expressing different CPEBs.

6. CPEB1 and CPEB4 activities are coordinated in meiosis

The regulation of xCPEB4 by Cdc2 and p42MAPK is consistent with the sequential functions of xCPEB1 and xCPEB4 in meiotic progression. xCPEB1 is activated by Aurora A kinase upon meiotic resumption from the PI arrest (Mendez et al., 2000a). As a consequence of this activation, the early wave of cytoplasmic polyadenylation takes place and Mos, Cyclin B1 and xCPEB4 are synthesized, although the presence of AREs in *xCPEB4* 3'UTR delays the accumulation of xCPEB4 protein until interkinesis (Igea and Méndez, 2010; Piqué et al., 2008). Mos and Cyclin B1 synthesis result in the activation of p42MAPK and Cdc2, which would then activate xCPEB4 to sustain the cytoplasmic polyadenylation of mRNAs after MI. In interkinesis, Aurora A kinase is inactivated (Ma et al., 2003; Pascreau et al., 2008) and the levels of the phosphatase PP1 that dephosphorylates xCPEB1 increase (Belloc and Méndez, 2008; Tay et al., 2003). Thus, in order to avoid xCPEB1 reassembling repression complexes, Cdc2 triggers the degradation of xCPEB1 in MI (Mendez et al., 2002), reinforcing the substitution of xCPEB1 by xCPEB4 in the second meiotic division. Hence, xCPEB1 and xCPEB4 activities are coordinated at two levels. First, xCPEB1 controls the synthesis of xCPEB4 and, second, the same kinase that activates xCPEB4 triggers the degradation of xCPEB1 (Figure 49). This coordination of xCPEB1 and xCPEB4 activities in meiosis assures that the late waves of cytoplasmic polyadenylation take place in order to proceed to the MII arrest.

In meiosis, the function of xCPEB4 is to drive the cytoplasmic polyadenylation of those mRNAs that encode proteins required for MII entry and arrest (Igea and

Méndez, 2010). Thence, xCPEB4 does not repress translation in this biological context. Consistently, as soon as xCPEB4 is synthesized, it is phosphorylated by Cdc2 and p42MAPK, which are already active in interkinesis and remain active at MII. Therefore, xCPEB4 repressing hydrogel-like aggregates are not present during meiosis. However, CPEB4 has been shown to repress mRNA translation in terminal erythroid differentiation (Hu et al., 2014) and in mitosis (Novoa et al., 2010), where the same mechanism that we have described for xCPEB4 regulation may apply.

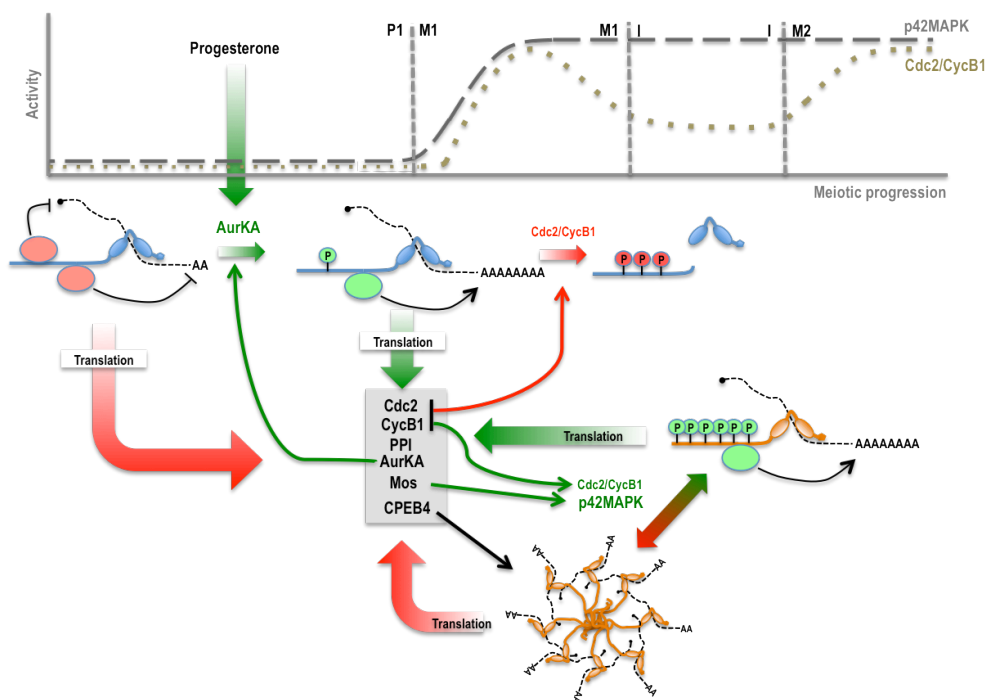


Figure 49. xCPEB1 and xCPEB4 functions in meiosis are coordinated. Model to illustrate the sequential and coordinated functions of xCPEB1 and xCPEB4 in the meiotic cell cycle. On the top, the different meiotic phases (P1, prophase I; M1, metaphase I; M2, metaphase II) are shown, as well as the activity profiles of p42MAPK (grey) and Cdc2/cyclin B (brown). Bellow, the sequential functions of xCPEB1 (blue) and xCPEB4 (orange) are shown. Red arrows and red phosphorylation events (P) show inhibitory effects, as well as red ovals represent CPEB repression complexes. On the contrary, green arrows and green phosphorylation events (P) show activating effects, as well as green ovals represent CPEB activation complexes. mRNAs activated in the early wave of cytoplasmic polyadenylation mediated by xCPEB1 are shown in the grey box.

7. CPEB4 regulation beyond meiosis

We strongly believe that the molecular mechanism for CPEB4 regulation that we have identified can be extrapolated to other organisms and other biological scenarios. All the identified phosphorylation sites in xCPEB4, except S40, are evolutionarily conserved among vertebrates and, importantly, S97, S250, S253, T324, S328 and S330 have been identified as phosphorylated residues in high-throughput mass spectrometry studies in human, mouse and rat (www.phosphosite.org) (Dephoure et al., 2008; Huttlin et al., 2010; Olsen et al., 2010). This fact suggests that the activation of CPEB4 by hyperphosphorylation most probably can be extrapolated to other vertebrates. Supporting this hypothesis, when U2OS cellular extracts are solved in sucrose gradients, hCPEB4 is found in very dense fractions, indicating that hCPEB4 is not in a monomeric state in basal conditions. Despite we can not exclude the possibility that hCPEB4 dense mRNPs are a consequence of its assembly with other proteins or organelles, this result lets us consider that hCPEB4 may form repressing aggregates in unsynchronized and unstimulated cells.

Adding the post-translational regulation of CPEB4 in the general picture of the CPEBs may help us understand some intriguing observations. For example, CPEB4 overexpression has the same effect as knocking down CPEB4 in terminal erythropoiesis (Hu et al., 2014). We believe that CPEB4 misexpression can result in CPEB4 misregulation at a post-translational level. For example, if CPEB4 is overexpressed but the activating kinases, Cdc2 and p42MAPK, remain limiting, CPEB4 overexpression can cause a switch in CPEB4 function from activation to repression. This may explain the effect of overexpressed WT xCPEB4 in competition experiments, which shows some level of competition of polyadenylation that are not present in the phospho-mimetic mutant (Figure 34), and might also explain why overexpressing CPEB4 causes the same effect as knocking it down in terminal erythropoiesis. Furthermore, CPEB4 protein level needs to be finely tuned since its misexpression can lead to pathological conditions such as cancer. In pancreatic ductal adenocarcinoma, CPEB4 is overexpressed and promotes the cytoplasmic polyadenylation and translational activation of mRNAs that are silenced in normal

tissue, including the mRNA of tissue plasminogen activator (tPA) (Ortiz-Zapater et al., 2012). Most probably, in this context of high proliferation, Cdc2 and p42MAPK kinases are not limiting and are even overactivated, generating a situation in which overexpressed CPEB4 is active in cytoplasmic polyadenylation.

Studying CPEB4 phosphorylation and aggregation dynamics in other contexts would be of great interest in order to understand whether CPEB4 is acting as a repressor or an activator of translation in every particular moment. Developing CPEB4 phosphospecific antibodies would help to address this kind of questions in the future.

In conclusion, our study provides new insights into the RNA-binding mode of the CPEBs and their differential post-translational regulation, contributing to the understanding of the complex mRNA translational control exerted by the CPEBs.

CONCLUSIONS

The present study provides new insights into the differential post-translational regulation of the CPEBs, identifying the molecular mechanism governing CPEB4 activity. Moreover, we have solved the structures of the RNA-binding domain of two representative members of the CPEB family of RNA-binding proteins, uncovering their RNA-binding mode and how it influences CPEB mRNP assembly. The main conclusions of the work are the following:

1. CPEBs tandem RRM adopt a novel V-shaped structure to bind CPE elements. The overall structure is conserved among paralogs, although some differences in the N-terminal region upstream of RRM1 and the specificity of the fifth CPE nucleotide may have important functional implications.
2. xCPEB4 is activated by Cdc2 and p42MAPK-mediated hyperphosphorylation of its N-terminal disordered domain. Specifically, p42MAPK phosphorylates xCPEB4 at S18, S38, S40, S97, S250, S253 and S351, while Cdc2 phosphorylates xCPEB4 at T324, S328, S330, S357 and S362.
3. xCPEB4 hyperphosphorylation in the twelve identified sites is essential for xCPEB4-mediated cytoplasmic polyadenylation of target mRNAs as well as for proper meiotic progression to metaphase II.
4. xCPEB4 hyperphosphorylation retains the protein in a monomeric state able to mediate the cytoplasmic polyadenylation of target mRNAs.
5. Non-phosphorylated xCPEB4 assembles hydrogel-like dynamic aggregates through its N-terminal domain and represses CPE-containing mRNAs.
6. xCPEB4 aggregates are reversible upon CPEB4 phosphorylation on the twelve identified sites, most probably due to the effect of bulk electrostatics.
7. xCPEB1 and xCPEB4 activities in meiosis are coordinated by Cdc2-mediated phosphorylation, which targets xCPEB1 for degradation while activates xCPEB4.

MATERIALS AND METHODS

***Xenopus laevis* oocyte preparation**

Xenopus laevis ovaries were extracted by surgery from *X. laevis* females and kept in Modified Bath's Saline media (1X MBS; 88 mM NaCl, 1 mM KCl, 1 mM MgSO₄, 2.5 mM NaHCO₃, adjusted to pH 7.8 and supplemented with fresh 0.7 mM CaCl₂). Ovary lobes were digested with a mixture of 0.8 mg/ml collagenase and 0.48 mg/ml dispase II (Sigma-Aldrich) in 1X MBS for 3h at 23°C. Then, oocytes were thoroughly washed with 1X MBS and cultured in 1X MBS. Stage VI oocytes were manually selected under a dissecting microscope. Oocyte microinjection was performed using the Nanoject II Drummond microinjector and 3.5" Drummond 3-000-203-G/X replacement glass capillaries. Oocyte maturation was induced with 10 µM of progesterone (Sigma-Aldrich) in 1X MBS at RT.

Plasmid constructions and mutagenesis

For CPEB4 tandem RRM structure validation, xCPEB4 (GQ338835) RRM12ZZ sequence was amplified (sense: 5'-CGGGATCCTTGGGATCGCCACACTG-3' / antisense: 5'-GCGATATCTCAGTTCCAGCGGAATG-3') and cloned into pBSK_HIS_HA vector (from E. Belloc) using BamHI and EcoRV restriction sites. The mutants tested for RNA binding were generated with the QuickChange Lightning Multi Site-Directed Mutagenesis Kit (Agilent Technologies), using the following mutagenic primers (mutated codons are highlighted in bold letters. Note that the residues follow xCPEB4 numbering. Their corresponding *H. sapiens* residue number is specified in parenthesis):

F448A (F68A): 5'-GTTATTCTCGCAAAGTG**GCT**GTGGGAGGTCTGCCTCC-3'

D459A (D79A): 5'-CAGATATAGATGAAG**CT**GAGATCACAGCTAG-3'

K488A (K108A): 5'-GTCTTACTTTCCTCCG**GC**AGGTTATGCGTTCTTGC-3'

Y490A (Y110A): 5'-CTTTCCTCCGAAAGGT**GCT**GCGTTCTTGCTGTTCC-3'

F492A (F112A): 5'-CCGAAAGGTTATGCG**GC**CTTGCTGTTCCAAGATG-3'

Y516A (Y136A): 5'-GAGGATGGCAAGCTT**GCC**CTGTGTGTGTCAAG-3'

K527A (K147A): 5'-CCTACAATCAAAGAC**GCG**CCTGTTGAGATCCG-3'

Q530A (Q150A): 5'-CAAAGACAAGCCTGTT**GCA**ATCCGTCCTGGAAC-3'

R532A (R152A): 5'-AAGCCTGTTGAGATC**GCT**CCCTGGAACCTCAG-3'

W534A (W154A): 5'-GTTCAAATCCGTCCC**GCG**AACCTCAGTGACAG-3'

F541A (F161A): 5'-CTCAGTGACAGTGAC**GCT**GTGATGGACGGCTC-3'
F556A (F176A): 5'-CCTCGGAAAACCAT**TGCT**GTTGGAGGTGTTCC-3'
K595A (K215A): 5'-GAGCTAAAGTACCCC**GC**AGGAGCTGGGCGTG-3'
Q606A (Q249A): 5'-GCCTTTTCAAATCAG**GCG**AGTTACATAGCTGC-3'
Y608F (Y251A): 5'-CAAATCAGCAGAGT**TTT**CATAGCTGCTATCAG-3'
Y633A (Y253A): 5'-GTGGAAGTGAAGCCAG**GCT**GTCTTGGATGATC-3'

As control, pet30_MS2_HA plasmid was generated. An HA-tag was inserted using KpnI and XhoI restriction sites downstream the MS2 in pet30_MS2 vector (from I. Novoa): two primers encoding for the HA-tag and harbouring a KpnI restriction site at the 5'-end and a XhoI at the 3'-end were phosphorylated with T4 Polynucleotide Kinase, hybridized and ligated to the already digested plasmid (sense: 5'-GTACCTACCCATACGACGTACCAGATTACGCTC-3' / antisense: 5'-TCGAGAGCGTAATCTGGTACGTCGTATGGGTAG-3').

For CPEB1 tandem RRM structure validation, pBSK HA-RRM12ZZ and pBSK HA-RRM12 were cloned by E. Belloc. The mutants tested for RNA binding were generated by E. Belloc following the same strategy as for CPEB4.

For protein purification, xCPEB4 CDS, full length or fragments, were amplified and cloned into pet30a vector. The pet30a_xCPEB4 full-length plasmid was cloned by A. Igea (Igea and Méndez, 2010). For the cloning of the fragments, the sequences were amplified by PCR, digested and ligated to the vector using BamHI and NotI restriction sites. The following primers were used for the amplification:

| | Sense primer | Antisense primer |
|---|--|---|
| xCEB4 fragment 1 (1-202 aa) | 5'-CGGGATCCATGGGG GATTACGGGTTTGGAG- 3' | 5'-ATAGTTTAGCGGCCGC AGCACCATTATTAGCTGAA GCAGCAGG-3' |
| xCEB4 fragment 2 (203-290 aa) | 5'-CCCGGATCCCTGCT TTTCCAGAATTTCCT-3' | 5'-GCAGCGGCCGCGCA TGGACTTTGGTAGCT-3' |
| xCEB4 fragment 3 (291-409 aa) | 5'-GCAGGATCCCCTACA CCCTCATCTTCATGG-3' | 5'-ATGGCGGCCGCTTCCA TTGGAAAGAGAGAGGACT G-3' |
| xCEB4 fragment NTD (1-409 aa) | 5'-CGGGATCCATGGGG GATTACGGGTTTGGAG- 3' | 5'-GCAGCGGCCGCTCATT CCATTGGAAAGAGAGAGG -3' |
| xCEB4 fragment RBD (402-702 aa, from <i>A. Igea</i>) | 5'-CGGGATCCCAGTCC TCTCTCTTCCAATGG-3' | 5'-ATAGTTTAGCGGCCGC TCAGTTCCAGCGGAATGA AATATGCCTCG-3' |

Table 1. Primers used for xCEB4 fragments cloning into pet30 vector

For competition and rescue experiments, pBSK HA-xCEB4+3'UTR plasmid was generated from pBSK_myc-CEB4 (Igea and Méndez, 2010). The following modifications were introduced: a HA-tag was added substituting the myc-tag and the xCEB4 3' UTR was cloned after xCEB4 CDS. The HA-tag was added at the N-terminus with SacI and BamHI restriction sites following the strategy described previously (sense: 5'-CATGGAGTACCCATACGACGTACCAGATTACGCTG-3' / antisense: 5'-GATCCAGCGTAATCTGGTACGTCGTATGGGTACTCCATGAGCT-3'). The 3' UTR was cloned downstream xCEB4 CDS with Sall and XhoI restriction sites (sense: 5'-ACGCGTCGACTTGGCTCACTTTGCAAGC-3' / antisense: 5'-CCGCTCGAGTGCTTAATGCTTTTAATAGG-3'). In the case of the 3' UTR amplification, those nucleotides that are targeted by the 20AS used for xCEB4 depletion in oocytes were not included. Moreover, a mutagenesis reaction using the QuickChange Lightning Multi Site-Directed Mutagenesis Kit (Agilent Technologies) was carried out to make conservative mutations at the end of xCEB4 CDS to avoid any annealing with the 20AS (mutagenic primer: 5'-TTCATTCCGCTGGAATTAGCC CGGGTCGACTTGGC-3').

For the generation of the RNA-binding defective mutant, Y490 and K595 were mutated into alanine using the QuickChange Lightning Multi Site-Directed

Mutagenesis Kit (Agilent Technologies) and the following mutagenic primers (Afroz et al., 2014):

Y490A: 5'-CTTTCCTCCGAAAGGT**GCT**GCGTTCTTGCTGTTCC-3'

K595A: 5'-GAGCTAAAGTACCC**CGC**AGGAGCTGGGCGTG-3'

pBSK-emi2 3' UTR used in competition experiments was obtained from E. Belloc (Belloc and Méndez, 2008).

For cell transfection, xCPEB4 sequences (full length or fragments) were cloned into pPEU16, which contains an N-terminal OneStrep-eGFP tag, by In-Fusion™ (BD Clontech trademark) cloning reaction (Berrow et al., 2007). xCPEB4 full length CDS or fragments were amplified by PCR using the following primers:

| | Sense primer | Antisense primer |
|---------------------------------------|--|--|
| pPEU16 xCPEB4 full-length | 5'- AAGTTCTGTTTCAGG GCCCCGGGGGATTACGG GTTTGGAGTGC-3' | 5'- ATGGTCTAGAAAGCTT TAGTTCAGCGGAATGAA ATATGC-3' |
| pPEU16 xCPEB4 NTD (1-409 aa) | 5- AAGTTCTGTTTCAGG GCCCCGGGGGATTACGG GTTTGGAGTGC-3' | 5'- ATGGTCTAGAAAGCTTT ATTCCATTGAAAGAGAG AGG-3' |
| pPEU16 xCPEB4 RBD (426-702 aa) | 5'- AAGTTCTGTTTCAGG GCCCCGTTGGGATCGCC ACACTGTTTCC-3' | 5'- ATGGTCTAGAAAGCTT TAGTTCAGCGGAATGAA ATATGC-3' |

Table 2. Primers used for xCPEB4 cloning into pPEU16 vector

For MS2 tethering experiments, xCPEB4 CDS was cloned into pet30_MS2 vector (Novoa et al., 2010), downstream the MS2. xCPEB4 CDS was amplified by PCR, digested and ligated to the vector using KpnI and XhoI restriction sites. An HA-tag was added between the MS2 and the xCPEB4 CDS with KpnI restriction site: two primers encoding for the HA-tag and harbouring a KpnI restriction site at both sites were phosphorylated with T4 Polynucleotide Kinase, hybridized and ligated to the already digested plasmid (sense: 5'-CTACCCATACGACGTACCAGATTACGCTGGTAC-3' / antisense: 5'-CAGCGTAATCTGGTACGTCGTATGGGTAGGTAC-3'). Pet30_MS2-EGFP, pet30_MS2-xCPEB1, pLuc_MS2x3_B1 and pLUC_MS2x3_B1-123 were obtained from I. Novoa (Novoa et al., 2010). pBSK_renilla was obtained from M. Piqué (Piqué et al., 2008).

Mutagenesis of xCPEB4 phosphorylation sites was performed with the QuickChange Lightning Multi Site-Directed Mutagenesis Kit (Agilent Technologies) following manufacturer's instructions and using the following mutagenic primers (mutated codons are highlighted in bold letters):

| | ALANINE MUTAGENIC PRIMER | ASPARTIC ACID MUTAGENIC PRIMER |
|---------------------|---|--|
| S18 | 5'-CACTGGGAACAAG GCA GCTTTTCCAGTC-3' | 5'-CACTGGGAACAAG GAC GCTTTTCCAGTC-3' |
| S38 | 5'-CATCATCAGAATACAG GCC CCCAGCCCCGCTGC-3' | 5'-CATCATCAGAATACA GACCCC AGCCCCGCTGC- 3' |
| S38/40 | 5'-CATCATCAGAATACAG GCC CCC GCCCC CGCTGCTTTTA TA-3' | 5'-CAGAATACAG ACCCC GACCCC CGCTGCTTTTAT-3' |
| S97 | 5'-CCTTAGACAAACAGCTC GCTCCT AGCCAAAGC-3' | 5'-CCTTAGACAAACAGCTC GATCCT AGCCAAAGC-3' |
| S250/253 | 5'-CCAACAGCAAAGGAGA GCTCCTGCCC GCT CCCCATC TGCCTCC-3' | 5'-CCAACAGCAAAGGAGA GATCCTGCCC GAT CCCCAT CTGCCTCC-3' |
| S324/330 | 5'-CTTAATGGAGGAATAG CA CCCTTGAATTCCATAG CACA TTAAAGAAG-3' | - |
| S324/328/330 | - | 5'-CTTAATGGAGGAATA GATCCCTTGAAT GACATA GACCCATTAAGA AAGAAT- 3' |
| S328/330 | 5'-CACCCCTTGAAT GCCATA GCACCATTAAG -3' | - |
| S351 | 5'-GGCAGGCCCAAT GCTGC CTTTGCAC-3' | 5'-GGCAGGCCCAAT GAT GCCTTTGCAC-3' |
| S357/362 | 5'-CTTTGCACCAAAAG GCTTG GATGGATGAC GCCTTGAAC AGAGC-3' | 5'-CTTTGCACCAAAAG GATT GGATGGATGAC GC GACTTGA ACAGAGC-3' |

Table 3. Primers for xCPEB4 phosphosites mutation

RNA *in vitro* transcription

RNAs used for HA-xCPEB4 overexpression in oocytes, as well as Firefly luciferase and Renilla luciferase reporter RNAs, were synthesized with T3 mMESSAGE mMACHINE kit (Ambion) following manufacturer's indications. RNAs encoding MS2 fusion proteins for tethering experiments were synthesized with T7 mMESSAGE mMACHINE kit (Ambion) following manufacturer's indications. B1, B1-23 and B1-

123 3' UTR RNA probes were synthesized with the MEGAscript T7 Transcription Kit (Ambion) following manufacturer's indications (templates were obtained from M. Piqué (Piqué et al., 2008)). When indicated, the resulting RNA was *in vitro* polyadenylated with Poly(A) Tailing kit (Ambion) following manufacturer's indications. RNAs were recovered with lithium chloride precipitation. Exceptionally, RNAs used for rescue experiments were purified with phenol:chloroform (Ambion) and precipitated with isopropanol.

Emi2 3' UTR radioactive probe was synthesized with T3 RNA polymerase (Fermentas). 100 ng of EcoRI linearized DNA template (pBSK-emi2 3' UTR from E. Belloc (Belloc and Méndez, 2008)) were mixed with rNTPs (0.5 mM ATP, 0.5 mM CTP, 0.1 mM UTP and 0.05 mM GTP), 30 µCi of [α -³²P]-UTP, 0.5 mM of cap analogue (Ambion), 20 U of RNase inhibitor (Fermentas), 10 U of T3 RNA polymerase and Transcription Buffer 1X (40 mM Tris-HCl pH 7.9, 6 mM MgCl₂, 10 mM dithiothreitol, 10 mM NaCl and 2 mM spermidine, Fermentas) in a final reaction volume of 10 µl. The reaction was incubated at 37°C for 2 h. Then, DNA template was digested with 2 U of TURBO DNase (Ambion) for 15 min at 37°C. RNA probe was purified by filtration through MicroSpin G-25 columns (GE Healthcare).

Western blot analysis

For western blot, unless specified, oocytes were homogenized in 10 µl per oocyte of cold 1X H1 kinase buffer (80 mM sodium β -glycerolphosphate pH 7.4, 20 mM EGTA, 15 mM MgCl₂, 0.5 mM Na₂VaO₄) supplemented with 0.5% NP-40 and EDTA-free protease inhibitors (Roche). Lysates were centrifuged at 12000 g for 10 min at 4°C and the clarified extract was recovered. 10-20 µl of oocyte extract were resolved in 8-10% SDS-PAGE.

Antibodies

Anti-HA (clone 3F10, Roche), anti- α -Tubulin (clone DM1A, Sigma-Aldrich), anti-xCPEB1 (raised in rabbits against HIS-xCPEB1), anti-Gld-2 (raised in rabbits against KRRSDEGNSPYDVKC peptide), anti-GFP-HRP (Miltényi Biotec), anti-4E-T

(2297, Cell Signaling), anti-DDX6 (ab40684, Abcam), anti-CPEB4 (ab83009, Abcam).

Competition experiment for tandem RRM structure validation

Stage VI oocytes were injected with 0.036 pmols of *in vitro* transcribed and polyadenylated RNA encoding for HA-CPEB1 or HA-CPEB4 RRM12ZZ (wild type or mutants) and incubated O/N at 18°C in 1X MBS. After 16 h, 4.6 fmols of radiolabelled *emi2* 3'-UTR RNA probe were injected into the oocytes. Oocytes were then incubated 1 h at RT, induced to mature and collected 2 h after germinal vesicle breakdown (GVBD). Total RNA was extracted from oocytes collected at stage VI and 2 h after GVBD with Ultraspec RNA Isolation System (Biotecx) following manufacturer's indications. The RNA from 1.5 oocytes was loaded in 4% acryl-urea gel and run for 3h 30 min at 20 W. Then, the gel was dried and visualized by autoradiography. The results were analysed using Fiji. In order to assign a percentage of competition, for CPEB1 assays, we calculated the percentage of deadenylated probe, while for CPEB4, the distance of the median polyadenylation was taken into account. In both cases, 0% competition was assigned to MS2 control and 100% competition to the wild type variant. The percentage of competition shown by the mutants was normalized according to these values.

Lambda Protein Phosphatase assay (λ -PPase)

Stage VI oocytes were injected with 2.43 fmols of *in vitro* transcribed and polyadenylated RNA encoding for HA-xCPEB4. Oocytes were incubated O/N at 18°C, induced to mature and collected at indicated times. Oocytes were homogenized with 1X λ -PPase reaction buffer (50 mM Tris-HCl pH 7.5, 100 mM NaCl, 0.1 mM EGTA, 2 mM dithiothreitol and 0.01% Brij 35, New England BioLabs) supplemented with 0.4% NP-40 and EDTA-free protease inhibitors (Roche) (10 μ l buffer / oocyte). Lysates were centrifuged at 12000 g for 10 min at 4°C and the clarified extract was recovered. 10 μ l of oocyte extract were incubated with 2 mM MnCl_2 and 400 U of λ -PPase (New England BioLabs) for 1 h at 30°C. The reaction was stopped by the addition of 3X Laemmli sample buffer (180 mM Tris-HCl pH 6.8, 30% glycerol, 6% SDS, 0.03% bromophenol blue) to a final concentration of 1X and

boiling 10 min at 95°C. Finally, samples were resolved in 8% SDS-PAGE and analysed by western blot.

Protein purification

BL-21 competent *Escherichia coli* transformed with pet30 HIS-xCPEB4 (full length or fragments) were grown in 100 ml of Luria broth (LB) O/N at 37°C and 200 rpm. The culture was diluted in LB to a final volume of 1 L and grown at 37°C and 200 rpm until $OD_{600} \approx 0.5$. Bacteria were induced with 0.5 mM Isopropyl β -D-1-thiogalactopyranoside (IPTG) during 1 h at 30°C. The culture was then centrifuged at 6000 rpm during 10 min at 4°C and the pellet was frozen at -20°C. The pellet was lysed with 40 ml of 1X J buffer (25 mM Tris-HCl pH 8, 1 M NaCl, 5 mM $MgCl_2$, 1% NP-40, 5% glycerol and 6 M urea) supplemented with 10 mM imidazole pH 8, 1 complete EDTA-free protease inhibitor cocktail (Roche) and 1 mM phenylmethanesulfonyl fluoride (PMSF). The lysate was sonicated at 30% efficiency 1 sec ON – 2 sec OFF during 1 min and centrifuged at 16000 g for 10 min at 4°C. The supernatant was recovered and incubated with 4 ml of Ni^{2+} -NTA agarose (Qiagen), washed and re-suspended 50:50 with 1X J buffer, during 1 h at 4°C. After the incubation, the protein-resin complex was packed in a 5 ml polypropylene column (Qiagen) and washed with 3 column volumes of washing buffer (25 mM Tris-HCl pH 8, 500 mM NaCl, 5 mM $MgCl_2$, 5% glycerol, 6 M urea and 20 mM imidazole). Seven consecutive elutions with 600 μ l of elution buffer [25 mM Tris-HCl pH 8, 300 mM NaCl, 5 mM $MgCl_2$, 5% Glycerol, 6 M Urea, 300 mM imidazole and EDTA-free protease inhibitors (Roche)] were done. Next, imidazole and urea concentration were reduced by a two-step dialysis: first, eluted fractions were dialyzed against buffer 1 (25 mM Tris-HCl pH 8, 150 mM NaCl, 5 mM $MgCl_2$, 5% glycerol and 4 M urea) and then against buffer 2 (25 mM Tris-HCl pH 8, 100 mM NaCl, 5 mM $MgCl_2$, 5% glycerol and 2 M urea). For *in vitro* kinase assays a third dialysis step in buffer 3 (25 mM Tris-HCl pH 8, 100 mM NaCl, 5 mM $MgCl_2$ and 5% glycerol) was added to remove urea. All the purification process was carried out at 4°C.

***In vitro* kinase assays with oocyte extracts**

Oocytes from different maturation stages were collected and homogenized in 10 μ l per oocyte of cold 1X H1 kinase buffer (80 mM sodium β -glycerolphosphate pH 7.4, 20 mM EGTA, 15 mM $MgCl_2$, 0.5 mM Na_2VO_4) supplemented with 0.5% NP-40 and EDTA-free protease inhibitors (Roche). Lysates were centrifuged at 12000 g for 10 min at 4°C and the clarified extract was recovered. 1-4 μ g of purified recombinant protein (HIS-xCPEB4 full length or fragments; H1 protein from Sigma) were incubated with 8 μ l of oocyte extract, 50 μ M ATP, 1 μ Ci of [Y - ^{32}P] ATP and 1X H1 kinase buffer in a final volume of 12 μ l. The kinase reaction was carried out at RT for 15 min. The reaction was stopped by adding 3X Laemmli sample buffer (180 mM Tris-HCl pH 6.8, 30% glycerol, 6% SDS, 0.03% bromophenol blue) to a final concentration of 1X and boiling for 10 minutes at 95°C. The samples were analysed by 12% or 15% SDS-PAGE followed by autoradiography.

For kinase inhibitor assays, 2 μ l of metaphase II oocyte extract pre-incubated with specific kinase inhibitors for 30 minutes at 4°C were used: FR180204 33 μ M (Calbiochem), Roscovitine 80 μ M (Calbiochem), SL0101 0.66 mM (Tocris Bioscience), BI-2536 66 nM (BioVision), U0126 130 μ M (Promega).

For two-dimensional phosphopeptide maps some modifications were introduced in the protocol to enhance radiolabeled phosphorylations: oocyte extracts were prepared the double concentrated (each oocyte was homogenized with 5 μ l of H1 kinase buffer) and the kinase reaction was carried out in a final volume of 24 μ l, with 16 μ l of oocyte extract and without cold ATP. The reaction was stopped in ice and HIS-xCPEB4 fragments were re-purified from the reaction. 100 μ l of 50:50 Ni^{2+} -NTA agarose (Qiagen) and 400 μ l of HIS Purification Buffer (25 mM Tris-HCl pH 8, 500 mM NaCl, 5% glycerol and 5 mM $MgCl_2$) supplemented with 10 mM imidazole and EDTA-free protease inhibitors (Roche) were added to the reaction and incubated for 1h at 19°C. Six washes with HIS Purification Buffer, supplemented with 30 mM imidazole and EDTA-free protease inhibitors (Roche) were performed in batch. Finally the protein was eluted with 15 μ l of 1X Laemmli sample buffer (60 mM Tris-HCl pH 6.8, 10% glycerol, 2% SDS, 0.01% bromophenol blue) and boiled for 10 minutes at 95°C.

***In vitro* kinase assays with p42MAPK and Cdc2/cyclin B**

p42MAPK: 400ng of purified HIS-xCPEB4 fragments were *in vitro* phosphorylated with 50 units of p42MAPK (New England BioLabs) in 1X NEBuffer for PK (50 mM Tris-HCl pH 7.5, 10 mM MgCl₂, 1 mM EGTA, 2 mM DTT, 0.01% Brij 35), with 100 μM ATP and 1 μCi of [Y-³²P] ATP, for 30 minutes at 30°C.

Cdc2/cyclin B: 400ng of purified HIS-xCPEB4 fragments were *in vitro* phosphorylated with 100 ng of Cdc2/Cyclin B (Invitrogen). The reaction was performed in a buffer containing 20 mM Tris-HCl pH 7.5 and 5 mM MgCl₂, with 100 μM ATP and 1 μCi of [Y-³²P] ATP, for 30 minutes at 30°C.

The kinase reaction was stopped by adding 3X Laemmli sample buffer (180 mM Tris-HCl pH 6.8, 30% glycerol, 6% SDS, 0.03% bromophenol blue) to a final concentration of 1X and boiling for 10 minutes at 95°C. The samples were analysed by 12% or 15% SDS-PAGE followed by autoradiography.

Phosphorylation conditions used for xCPEB4 aggregation experiments are specified in the following sections.

Two-dimensional phosphopeptide maps

In vitro phosphorylated xCPEB4 protein fragments were loaded in 15% SDS-PAGE gel and stained with colloidal blue (Invitrogen). Phosphorylation was checked by autoradiography. The band corresponding to the phosphorylated protein was excised from the gel and washed with 500 μl of 100 mM NH₄HCO₃ for 1 h at RT. Washing solution was discarded and replaced by 150 μl of 100 mM NH₄HCO₃ and 10 μl of 45 mM DL-dithiothreitol (DTT) freshly prepared. It was incubated at 60°C for 30 min and cooled down to RT. After, 10 μl of fresh 100 mM iodoacetamide were added and the sample was incubated at RT for 30 min in the dark. The solvent was discarded and the gel slice was washed with 500 μl of 100 mM NH₄HCO₃ / 50% acetonitrile for 1 h. Washing solution was discarded and the gel slice was cut into four pieces, transferred to an eppendorf and shrank with 50 μl of acetonitrile. After 15 min at RT, the acetonitrile was removed and the gel pieces dried in a vacuum concentrator for 5 min at 30°C. Next, gel pieces were covered with 100 μl of 25 mM NH₄HCO₃ containing either sequencing grade modified trypsin (Promega) at 100

ng/μl (for xCPEB4 fragment 3) or a combination of sequencing grade modified trypsin and chymotrypsin (Promega) at 100 ng/μl each one (for xCPEB4 fragments 1 and 2). For fragment 3, digestion was carried out at 37°C O/N, whereas for fragments 1 and 2 was done at 25°C for 16 h followed by a 4 h incubation at 37°C. Following digestion, the supernatant was taken and acidified by the addition of 10% trifluoroacetic acid (TFA) to a final concentration of 1% TFA. Peptides were extracted from the gel pieces with a 20 min incubation with 50 μl of 60% acetonitrile / 0.1% TFA at RT. This extraction was performed four times. All supernatants were combined in an eppendorf and nearly dried in a vacuum concentrator at 30°C. Extracted peptides were dissolved with 6 μl of pH 1.9 buffer (2.2% formic acid / 7.8% glacial acetic acid in deionized water), vortexed and spun down. The sample was loaded in glass-backed TLC plates (Sigma-Aldrich or C.B.S. Scientific) drop by drop (0.5 μl) in the sample origin (bottom-left side of the TLC plate). 0.5 μl of green marker dye [5 mg/ml ε-dinitrophenyl-lysine and 1 mg/ml xylene cyanol FF dissolved in 50% pH 4.72 buffer (5% 1-butanol / 2.5% pyridine / 2.5% glacial acetic acid in deionized water)] was spotted in the dye origin (upper-left side of the TLC plate). The first dimension thin-layer electrophoresis was carried out in a Hunter Thin Layer Peptide Mapping Electrophoresis System (C.B.S. Scientific) with pH 1.9 buffer at 1000V for 45 min (Sigma-Aldrich TLC plates) or 35 min (C.B.S. Scientific TLC plates). Next, plates were dried, 0.5 μl of green marker dye were placed 2 cm left of the sample origin and the second dimension thin-layer chromatography was run in Phospho-chromatography buffer (37.5% 1-butanol / 25% pyridine / 7.5% glacial acetic acid in deionized water) until the front reached 2 cm from the top of the plates. Finally, the plates were dried, exposed and developed with phosphorimager.

Mass spectrometry analysis of phosphorylated xCPEB4

xCPEB4 phosphorylated with metaphase II oocyte extract: the experiment was performed in the “CRG/UPF Proteomics Unit, Centre de Regulació Genòmica (CRG), Universitat Pompeu Fabra (UPF), 08003 Barcelona”.

Gel bands were destained with 40% ACN / 100mM ABC. Samples were reduced with dithiothreitol (2 μM, 30 min, 56°C) and alkylated in the dark with iodoacetamide (10 mM, 30 min, 25 °C). Gel bands were then dehydrate with ACN and digested with

0.3 mg of trypsin (Promega) (fragment 3) or trypsin followed by chymotrypsin (Roche) (full length, fragments 1 and 2) overnight at 37°C. After digestion, peptides were extracted and cleaned up on a homemade Empore C18 column (3M, St. Paul, MN, USA).

Samples were analysed using an LTQ-Orbitrap Velos mass spectrometer (Thermo Fisher Scientific) coupled to an EasyLC (Thermo Fisher Scientific). Peptides were loaded directly onto the analytical column at 1.5-2 µl / min using a wash-volume of 4 to 5 times injection volume and were separated by reversed-phase chromatography using a 12-cm column with an inner diameter of 75 µm, packed with 5 µm C18 particles (Nikkoy Technos Co.). Chromatographic gradients started at 97% buffer A and 3% buffer B with a flow rate of 300 nl/min, and gradually increased to 93% buffer A and 7% buffer B in 1 min, and to 65% buffer A / 35% buffer B in 60 min. After each analysis, the column was washed for 10 min with 10% buffer A / 90% buffer B. Buffer A: 0.1% formic acid in water. Buffer B: 0.1% formic acid in acetonitrile. The mass spectrometer was operated in positive ionization mode with nanospray voltage set at 2.2 kV and source temperature at 250 °C. Ultramark 1621 for the FT mass analyser was used for external calibration prior the analyses. Moreover, an internal calibration was also performed using the background polysiloxane ion signal at m/z 445.1200. The instrument was operated in DDA mode and full MS scans with 1 micro scans at resolution of 60,000 were used over a mass range of m/z 250-2000 with detection in the Orbitrap. Auto gain control (AGC) was set to 1E6, dynamic exclusion (60 seconds) and charge state filtering disqualifying singly charged peptides was activated. In each cycle of DDA analysis, following each survey scan the top twenty most intense ions with multiple charged ions above a threshold ion count of 5000 were selected for fragmentation at normalized collision energy of 35%. Each sample was injected twice, fragment ion spectra produced via collision-induced dissociation (CID) and via high-energy collision dissociation (HCD). Isolation window of 2.0 m/z , activation time of 0.1ms and maximum injection time of 100 ms was used. All data were acquired with Xcalibur software v2.2.

For data analysis, Mascot search engine (v2.3, Matrix Science) was used for peptide identification. The data was searched against NCBI nr (*Xenopus laevis* (African clawed frog)). A precursor ion mass tolerance of 10 ppm at the MS1 level was used. Up to three miscleavages for trypsin were allowed. The fragment ion mass tolerance

was set to 0.5 Da. Oxidation of methionine, protein acetylation at the N-terminal, phosphorylation at serine, threonine and tyrosine were defined as variable modification; whereas carbamidomethylation on cysteines was set as a fix modification. Peptides were filtered using an expectation value [EXPECT] cut-off of 0.1.

xCPEB4 phosphorylated with p42MAPK and Cdc2/cyclin B: the experiment was performed at the Mass Spectrometry Core Facility from the Institute for Research in Biomedicine (IRB).

Samples were in-gel digested with trypsin at the Parc Científic Proteomic's Platform. After the digestion, samples were dried in the speed-vac and resuspended in 20 μ l of 1% formic acid for LC-MS/MS analysis. The nano-LC-MS/MS set up was as follows. Digested peptides were diluted in 1% FA. Samples were loaded to a 180 μ m x 2 cm C18 Symmetry trap column (Waters Corp.) at a flow rate of 15 μ l/min using a nanoAcquity Ultra Performance LCTM chromatographic system (Waters Corp.). Peptides were separated using a C18 analytical column with a 60 min run, comprising three consecutive steps with linear gradients from 1 to 35% B in 60 min, from 35 to 50% B in 5 min, and from 50 % to 85 % B in 3 min, followed by isocratic elution at 85 % B in 10 min and stabilization to initial conditions (A= 0.1% FA in water, B= 0.1% FA in CH₃CN). The column outlet was directly connected to an Advion TriVersa NanoMate (Advion) fitted on an LTQ-FT Ultra mass spectrometer (Thermo). The mass spectrometer was operated in a data-dependent acquisition (DDA) mode. Up to six of the most intense ions per scan were fragmented and detected in the linear ion trap. Target ions already selected for MS/MS were dynamically excluded for 30 s. Spray voltage in the NanoMate source was set to 1.70 kV. The spectrometer was working in positive polarity mode and singly charge state precursors were rejected for fragmentation.

For data analysis, a database search was performed with Proteome Discoverer software v1.3 (Thermo) using Sequest search engine and SwissProt database (Xenopodinae, release 2013_06 and the common Repository of Adventitious Proteins, cRAP database). Searches were run against targeted and decoy databases to determine the false discovery rate (FDR). Search parameters included trypsin enzyme specificity, allowing for two missed cleavage sites, carbamidomethyl in cysteine as static modification and methionine oxidation and phosphorylation at

serine, threonine and tyrosine as dynamic modifications. Peptide mass tolerance was 10 ppm and the MS/MS tolerance was 0.8 Da. Peptides with a q-value lower than 0.1 and a FDR < 1% were considered as positive identifications with a high confidence level.

MS2 tethering experiments

Stage VI oocytes were injected with 0.14 – 7 fmols of *in vitro* transcribed and polyadenylated RNA encoding MS2-EGFP, MS2-CPEB1 or MS2-HA-xCPEB4. Oocytes were incubated O/N at 18°C in 1X MBS. After, 0.02 fmols of Firefly luciferase reporter RNA with three MS2-binding sites together with 0.02 fmols of Renilla luciferase as normalizing RNA were injected. After 1 h incubation at RT, oocytes were induced to mature and collected 4 h after GVBD. Oocytes were homogenized in 1X Passive Lysis Buffer (Promega) (10 µl buffer / oocyte). Lysates were centrifuged at 12000 g for 10 min at 4°C and the clarified extract was recovered. 10 µl of extract were used to measure luciferase activity with the Dual-Luciferase Reporter Assay System (Promega), according to the manufacturer's instructions. 10 µl of oocyte extract were loaded in 8–10% SDS-PAGE and analysed by western blot to assess MS2 fusion proteins overexpression.

Competition experiments for xCPEB4 phosphorylation sites functional analysis

Stage VI oocytes were injected with 0.146 pmols of *in vitro* transcribed and polyadenylated RNA encoding for HA-CPEB4 (wild type or mutants) and incubated O/N at 18°C in 1X MBS. After 16 h, 4.6 fmols of radiolabelled *emi2* 3'-UTR RNA probe were injected into the oocytes. Oocytes were then incubated 1 h at RT, induced to mature and collected 2 h after GVBD. Total RNA was extracted from oocytes collected at stage VI and 2 h after GVBD with Ultraspec RNA Isolation System (Biotechx) following manufacturer's indications. The RNA from 1.5 oocytes was loaded in 4% acryl-urea gel and run for 3h 30 min at 20 W. Then, the gel was dried and visualized by autoradiography. The results were analysed using Fiji. For the 2 h after GVBD time points, we calculated the distance from the top to the

median polyadenylation. 0% competition was assigned to HA-xCPEB4 WT, while 100% competition was assigned to the HA-CPEB4-12A mutant. Then, the percentage of competition of the other conditions was normalized according to these values.

Rescue experiments and chromosomes observation

In order to ablate xCPEB4, 116 ng of 20AS oligonucleotide (5'-GCAATGGGTTGCTCAGTTCCA-3') targeting xCPEB4 3' UTR were injected into stage VI oocytes. As a control, the same amount of 23S oligonucleotide was injected (5'-CTTTGCAAGCATCCAAATAAG-3') (Igea and Méndez, 2010). After O/N incubation at 18°C, 2.43 fmols of *in vitro* transcribed HA-xCPEB4+3'UTR (wild type or phospho-mutants) were injected. Oocytes were incubated 1 h at RT and maturation was induced. 2.5 h after GVBD, oocytes were collected and fixed with 100% methanol O/N at 4°C. Chromosomes and polar body were stained with Hoechst (20 µg/l) in 1X MBS O/N at RT. Images were obtained with a Nikon TE200 microscope (x 100 magnification, Olympus DP72 camera).

Immunoprecipitation and mass spectrometry analysis of xCPEB4 interacting proteins

Anti-HA antibody was covalently cross-linked to Dynabeads protein G (Invitrogen): 5 µg of Anti-HA antibody were incubated with 50 µl of Dynabeads protein G on wheel for 2 h at RT. After one wash with 1X PBS and 2 washes with 0.2 M triethanolamine pH 8 (Sigma-Aldrich), the beads were incubated during 30 min at RT with 1 ml of 20 mM dimethyl pimelimidate·2HCl (DMP, Thermo Scientific) freshly prepared in 0.2 M triethanolamine pH 8. The reaction was stopped with two 5 min washes with 1 ml of 50 mM Tris-HCl pH 8 at RT followed by 3 washes with 1X PBS. After, the beads were incubated for 2 min at RT with 100 µl of 0.1 M citric acid pH 3 and washed with 1X IP lysis buffer (20 mM Tris-HCl pH 8, 1 mM EDTA, 0.5% NP-40, 1 mM MgCl₂ and 100 mM NaCl).

Stage VI oocytes were injected with 4.9 fmols of *in vitro* transcribed HA-xCPEB4+3'UTR (wild type or phospho-mutants), incubated O/N at 18°C, induced to

mature and collected at indicated times. Oocytes were homogenized (10 µl of buffer per oocyte) in 1X IP lysis buffer supplemented with 1X H1K buffer (80 mM sodium β-glycerolphosphate pH 7.4, 20 mM EGTA, 15 mM MgCl₂, 0.5 mM Na₂VaO₄) and EDTA-free protease inhibitors (Roche). Lysates were centrifuged at 12000 g for 10 min at 4°C and the clarified extract was recovered.

280 µl of oocyte extract were pre-cleared with 25 µl of Dynabeads protein G during 1 h at 4°C on wheel. Then, the pre-cleared extract was added to the antibody cross-linked beads and incubated 2 h at 4°C on wheel. When specified, RNase A (Fermentas) was added to the oocyte extract (10 µg RNase A / 100 µl oocyte extract) during the pre-clear and the immunoprecipitation. Immunoprecipitates were washed six times with IP lysis buffer and eluted with 30 µl of 1X Laemmli sample buffer (60 mM Tris-HCl pH 6.8, 10% glycerol, 2% SDS, 0.01% bromophenol blue) at 65°C for 20 min. Finally, eluates were recovered, supplemented with 30 mM DTT and boiled at 95°C. Samples were resolved in SDS-PAGE and analysed by western blot, silver staining (Pierce® Silver Stain for Mass Spectrometry, Thermo Scientific) or colloidal blue (Invitrogen).

For the identification of xCPEB4 interacting proteins, specific bands stained with silver staining or colloidal blue were subjected to mass spectrometry analysis at the Mass Spectrometry Core Facility from the Institute for Research in Biomedicine (IRB), as described previously.

Sucrose gradients with oocyte extracts

Stage VI oocytes were injected with 0.146 pmols of *in vitro* transcribed and polyadenylated RNA encoding for HA-CPEB4 (wild type or mutants) and incubated O/N at 18°C in 1X MBS. Oocytes were homogenized in SG buffer (20 mM Tris-HCl pH 8, 1 mM MgCl₂ and 100 mM NaCl) supplemented with EDTA-free protease inhibitors (Roche) and 40U/ml of RiboLock RNase inhibitor (Thermo Scientific) (4 µl buffer / oocyte). Lysates were centrifuged at 12000 g for 10 min at 4°C and the clarified extract was recovered. 135 µl of oocyte extract were loaded in 5-40% sucrose gradient (manually prepared in polypropylene Beckman Coulter tubes 13x51 mm. Sucrose solutions were prepared in SG buffer) and centrifuged at 50000 rpm with MLS-50 rotor (Beckman Coulter) for 6 h at 4°C. Fractions of 200 µl were

manually obtained from the top to the bottom of the tube. 12 µl of the indicated fractions were loaded in 10% SDS-PAGE and analysed by western blot. When specified, oocyte extracts were incubated with 20 µg of B1 3' UTR RNA (wild type or CPE mutated) during 10 min at 20°C before loading the extract into the sucrose gradient.

Cell culture and transfection

U2OS cells were grown in Dulbecco's Modified Eagle Medium (DMEM) with 10% fetal bovine serum (FBS) and 1% penicillin/streptomycin. 24 h before transfection, cells were seeded to be 70% confluent at transfection. Transfection was performed with Lipofectamine LTX and PLUS Reagent (Life Technologies) following manufacturer's instructions. For 6-well plate transfections, 5 µl of Lipofectamine and 2.5 µg of DNA were used. For p100 transfections, 30 µl of Lipofectamine and 15 µg of DNA were used.

GFP-xCPEB4 distribution in U2OS cells

Cells were plated on glass coverslips and transfected as described. 24 h after transfection, cells were fixed with 4% formaldehyde (Electron Microscopy Sciences) freshly prepared in 1X PBS for 10 min at RT. Then, cells were permeabilized with 1X PBS / 0.2 % Triton X-100 for 5 min at RT and mounted with VECTASHIELD Mounting Medium with DAPI (Vector Laboratories). Image acquisition was performed with a High Throughput Automated Wide-field Olympus IX81 Microscope (Olympus Life science Europe) and a 20x objective. ScanR Acquisition software was used to automatically take 64 images per condition. Between 100-300 cells were analysed with Fiji software and classified according to GFP distribution (diffuse vs. aggregated). Three independent experiments were performed. Significance was addressed with a Sidak's multiple comparisons test, $p < 0.05$.

Live cell imaging of GFP-xCPEB4 transfected U2OS cells

Automated Wide-field Olympus IX81 Microscope (Olympus Life science Europe) equipped with temperature and CO₂ incubation chamber was used to acquire time-lapse imaging of cell cultures with a 20X / 0.45 objective. Images were acquired every 5 min with the CellR software (Olympus Life Science). Software autofocus was used to adjust the z-focus.

Immunofluorescence

Cells were plated, transfected, fixed and permeabilized as described. Blocking was performed with 1X PBS / 10% FBS / 0.03% Triton X-100 for 1h at RT. Incubation with primary antibodies (1/100) was done O/N at 4°C, followed by three 5 min washes with 1X PBS. Finally, samples were incubated with the corresponding secondary antibodies for 1h at RT, washed three times with 1X PBS and mounted with VECTASHIELD Mounting Medium with DAPI (Vector Laboratories). Images were obtained on an inverted Leica TCS SP5 confocal microscope with a 63x/1.40-0.60 Oil objective.

Size exclusion chromatography (SEC)

Purified xCPEB4 N-terminal domain, contained in 25 mM Tris-HCl pH 8, 100 mM NaCl, 5% glycerol, 5 mM MgCl₂ and 2 M urea buffer, was diluted to a final protein concentration of 0.5 mg/ml and 2 M or 0.2 M urea. Samples were centrifuged at 12000 g and 4°C for 5 min. 0.5 ml of sample were loaded in a Superdex 200 SEC column (GE Healthcare). Elution fractions were collected and 30 µl of the selected fractions were resolved by 10% SDS-PAGE. For SEC upon xCPEB4 phosphorylation, samples were prepared as described for dynamic light scattering and 100 µl were loaded in a Superdex 200 SEC column.

Dynamic light scattering (DLS)

Purified xCPEB4 N-terminal domain, in 25 mM Tris-HCl pH 8, 100 mM NaCl, 5% glycerol, 5 mM MgCl₂ and 2 M urea buffer, was diluted in a non-containing urea

buffer to a final protein concentration of 0.5 mg/ml and 0.2 M urea (other buffer components were kept at the same concentration). Samples were incubated at 4°C for 30 min before DLS analysis. For phosphorylation assays, proteins were diluted in NEBuffer for PK (New England Biolabs) containing 200 µM ATP, incubated on ice for 30 min and immediately phosphorylated with Cdc2/cyclin B (20 ng / µg xCPEB4 N-terminal domain) and p42MAPK (10 U / µg xCPEB4 N-terminal domain) at 30°C for 30 min. Kinase reactions were stopped with 20 mM EDTA and kept at 4°C. 100 µl of sample were analysed by DLS with a Zetasizer Nano-S instrument (Malvern) at 25°C. Three measurements were obtained for each condition. Three independent experiments were performed.

Transmission Electron microscopy (TEM)

Sample preparation was performed as described for DLS. 6 µl of sample were deposited on carbon film only grids (CF200-CU, Electron Microscopy Sciences) and stained with uranyl formate for 1 min. EM was performed with a Tecnai Spirit microscope (EM) (FEI, Eindhoven, The Netherlands), equipped with a LaB6 cathode. Images were acquired at 120 kV and RT with a 1376 x 1024 pixel CCD camera (FEI, Eindhoven, The Netherlands).

RNA immunoprecipitation (RIP) of aggregated GFP-xCPEB4

U2OS cells were plated and transfected in p100 plates as described before. Cells were washed with 1X PBS and crosslinked with 0.5% formaldehyde in DMEM for 10 min at RT. Crosslinking was stopped with 0.25 M glycine during 5 min. After, cells were washed twice with cold 1X PBS and lysed in 300 µl of RIPA buffer (50 mM Tris-HCl pH 8, 150 mM NaCl, 1 mM MgCl₂, 1 % NP-40, 0.5 % sodium deoxicholate, 0.1 % SDS, 1 mM EDTA) supplemented with 1 mM PMSF, EDTA-free protease inhibitor cocktail (Roche) and 50 U of RiboLock RNase inhibitor (Life Technologies). Cell lysate was sonicated 4 min at low intensity and centrifuged 10 min at 12000 g and 4°C. The supernatant was recovered. 175 µl of cellular extract were loaded in 5-40 % sucrose gradient and centrifuged at 50000 rpm with MLS-50 rotor (Beckman Coulter) for 4 h at 4°C. Fractions of 200 µl were manually obtained from the top to the bottom of the tube. 20 µl of the selected fractions were analysed by western blot.

150 µl of fraction 24 were used for RIP with GFP-Trap beads (ChromoTek) following manufacture's instructions. Beads were resuspended in proteinase K buffer (200 mM Tris-HCl pH 7.5, 100 mM NaCl, 10 mM EDTA and 1% SDS) containing 70 µg of proteinase K and incubated 1 h at 65°C. RNA was then extracted by phenol-chloroform followed by isopropanol precipitation and used for retro-transcription with SuperScript III Reverse Transcriptase (Invitrogen). cDNA was used for qPCR.

***In vitro* xCPEB4 aggregates RNA-binding assay**

4 µl of purified xCPEB4 (full-length or N-terminal domain) at 2 mg/ml and 6 M urea were diluted with a non-containing urea buffer to a final volume of 12 µl, in the presence of 3 µg of radiolabelled B1 or B1-123 RNA probe and 20 µg of tRNA. Samples were incubated 15 min at RT. After, proteins were diluted with NEBuffer for PK (New England Biolabs) containing 200 µM ATP to a final volume of 100 µl and incubated 30 min at 4°C. When specified, proteins were phosphorylated with 500 U of p42MAPK and 1 µg of Cdc2/cyclin B for 30 min at 30°C. Following phosphorylation, samples were loaded in Corning® Costar® Spin-X® cellulose acetate 0.22 µm tube filters and centrifuged at 12000 g for 1 min. Flow through was recovered and the filter column was washed with NEBuffer for PK. 4% of input and 20% of flow through were resolved in SDS-PAGE. Filters were exposed and developed with Phosphorimager.

REFERENCES

A

Abaza, I., Coll, O., Patalano, S., and Gebauer, F. (2006). *Drosophila* UNR is required for translational repression of male-specific lethal 2 mRNA during regulation of X-chromosome dosage compensation. *Genes Dev.* 20, 380–389.

Afroz, T., Skrisovska, L., Belloc, E., and Guillén-Boixet, J. (2014). A fly trap mechanism provides sequence-specific RNA recognition by CPEB proteins. *Genes Dev.* 1498–1514.

Aguilera, A. (2005). Cotranscriptional mRNP assembly: From the DNA to the nuclear pore. *Curr. Opin. Cell Biol.* 17, 242–250.

Alarcon, J.M., Hodgman, R., Theis, M., Huang, Y.-S., Kandel, E.R., and Richter, J.D. (2004). Selective Modulation of Some Forms of Schaffer Collateral-CA1 Synaptic Plasticity in Mice With a Disruption of the CPEB-1 Gene. *Learn. Mem.* 11, 318–327.

Alexandrov, I.M., Ivshina, M., Jung, D.Y., Friedline, R., Ko, H.J., Xu, M., O'Sullivan-Murphy, B., Bortell, R., Huang, Y.-T., Urano, F., et al. (2012). Cytoplasmic polyadenylation element binding protein deficiency stimulates PTEN and Stat3 mRNA translation and induces hepatic insulin resistance. *PLoS Genet.* 8, e1002457.

Amrani, N., Ghosh, S., Mangus, D. a, and Jacobson, A. (2008). Translation factors promote the formation of two states of the closed-loop mRNP. *Nature* 453, 1276–1280.

Andrésson, T., and Ruderman, J. V (1998). The kinase Eg2 is a component of the *Xenopus* oocyte progesterone-activated signaling pathway. *EMBO J.* 17, 5627–5637.

Arumugam, K., Wang, Y., Hardy, L.L., MacNicol, M.C., and MacNicol, A.M. (2010). Enforcing temporal control of maternal mRNA translation during oocyte cell-cycle progression. *EMBO J.* 29, 387–397.

Atkins, C.M., Nozaki, N., Shigeri, Y., and Soderling, T.R. (2004). Cytoplasmic polyadenylation element binding protein-dependent protein synthesis is regulated by calcium/calmodulin-dependent protein kinase II. *J. Neurosci.* 24, 5193–5201.

B

Bah, A., Vernon, R.M., Siddiqui, Z., Krzeminski, M., Muhandiram, R., Zhao, C., Sonenberg, N., Kay, L.E., and Forman-Kay, J.D. (2015). Folding of an intrinsically disordered protein by phosphorylation as a regulatory switch. *Nature* 519, 106–109.

Baltz, A.G., Munschauer, M., Schwanhäusser, B., Vasilé, A., Murakawa, Y., Schueler, M., Youngs, N., Penfold-Brown, D., Drew, K., Milek, M., et al. (2012). The mRNA-bound proteome and its global occupancy profile on protein-coding transcripts. *Mol. Cell* 46, 674–690.

Banjade, S., and Rosen, M.K. (2014). Phase Transitions of Multivalent Proteins Can Promote Clustering of Membrane Receptors. *Elife* 3, e04123.

Barkoff, a F., Dickson, K.S., Gray, N.K., and Wickens, M. (2000). Translational control of cyclin B1 mRNA during meiotic maturation: coordinated repression and cytoplasmic polyadenylation. *Dev. Biol.* 220, 97–109.

Barnard, D.C., Ryan, K., Manley, J.L., and Richter, J.D. (2004). Symplekin and xGLD-2 are required for CPEB-mediated cytoplasmic polyadenylation. *Cell* 119, 641–651.

Bava, F.-A., Eliscovich, C., Ferreira, P.G., Miñana, B., Ben-Dov, C., Guigó, R., Valcárcel, J., and Méndez, R. (2013). CPEB1 coordinates alternative 3'-UTR formation with translational regulation. *Nature* 495, 121–125.

Bayaa, M., Booth, R. a, Sheng, Y., and Liu, X.J. (2000). The classical progesterone receptor mediates *Xenopus* oocyte maturation through a nongenomic mechanism. *Proc. Natl. Acad. Sci. U. S. A.* 97, 12607–12612.

Beckmann, K., Grskovic, M., Gebauer, F., and Hentze, M.W. (2005). A dual inhibitory mechanism restricts msl-2 mRNA translation for dosage compensation in *Drosophila*. *Cell* 122, 529–540.

Belloc, E., and Méndez, R. (2008). A deadenylation negative feedback mechanism governs meiotic metaphase arrest. *Nature* 452, 1017–1021.

Belloc, E., Piqué, M., and Méndez, R. (2008). Sequential waves of polyadenylation and deadenylation define a translation circuit that drives meiotic progression. *Biochem. Soc. Trans.* 36, 665–670.

Berger-Sweeney, J., Zearfoss, N.R., and Richter, J.D. (2006). Reduced extinction of hippocampal-dependent memories in CPEB knockout mice. *Learn. Mem.* 13, 4–7.

Berrow, N.S., Alderton, D., Sainsbury, S., Nettleship, J., Assenberg, R., Rahman, N., Stuart, D.I., and Owens, R.J. (2007). A versatile ligation-independent cloning method suitable for high-throughput expression screening applications. *Nucleic Acids Res.* 35, e45.

Borg, M., Mittag, T., Pawson, T., Tyers, M., Forman-Kay, J.D., and Chan, H.S. (2007). Polyelectrostatic interactions of disordered ligands suggest a physical basis for ultrasensitivity. *Proc. Natl. Acad. Sci. U. S. A.* 104, 9650–9655.

Brangwynne, C.P., Eckmann, C.R., Courson, D.S., Rybarska, A., Hoege, C., Gharakhani, J., Jülicher, F., and Hyman, A.A. (2009). Germline P granules are liquid droplets that localize by controlled dissolution / condensation. *Science* 324, 1729–1732.

Bregues, M., Teixeira, D., and Parker, R. (2005). Movement of eukaryotic mRNAs between polysomes and cytoplasmic processing bodies. *Science* 310, 486–489.

Buchan, J.R. (2014). mRNP granules. *RNA Biol.* 11, 1019–1030.

Buchan, J.R., and Parker, R. (2009). Eukaryotic Stress Granules: The Ins and Outs of Translation. *Mol. Cell* 36, 932–941.

Burns, D.M., and Richter, J.D. (2008). CPEB regulation of human cellular senescence, energy metabolism, and p53 mRNA translation. *Genes Dev.* 22, 3449–3460.

Burns, D.M., D'Ambrogio, A., Nottrott, S., and Richter, J.D. (2011). CPEB and two poly(A) polymerases control miR-122 stability and p53 mRNA translation. *Nature* 473, 105–108.

C

Cao, Q., and Richter, J.D. (2002). Dissolution of the maskin-eIF4E complex by cytoplasmic polyadenylation and poly(A)-binding protein controls cyclin B1 mRNA translation and oocyte maturation. *EMBO J.* 21, 3852–3862.

Cao, Q., Kim, J.H., and Richter, J.D. (2006). CDK1 and calcineurin regulate Maskin association with eIF4E and translational control of cell cycle progression. *Nat. Struct. Mol. Biol.* 13, 1128–1134.

Castello, A., Fischer, B., Eichelbaum, K., Horos, R., Beckmann, B.M., Strein, C., Davey, N.E., Humphreys, D.T., Preiss, T., Steinmetz, L.M., et al. (2012). Insights into RNA biology from an atlas of mammalian mRNA-binding proteins. *Cell* **149**, 1393–1406.

Chang, Y.-W., and Huang, Y.-S. (2014). Arsenite-activated JNK signaling enhances CPEB4-Vinexin interaction to facilitate stress granule assembly and cell survival. *PLoS One* **9**, e107961.

Charlesworth, A., Wilczynska, A., Thampi, P., Cox, L.L., and MacNicol, A.M. (2006). Musashi regulates the temporal order of mRNA translation during *Xenopus* oocyte maturation. *EMBO J.* **25**, 2792–2801.

Chen, P.-J., and Huang, Y.-S. (2012). CPEB2-eEF2 interaction impedes HIF-1 α RNA translation. *EMBO J.* **31**, 959–971.

Cohen, P. (2000). The regulation of protein function by multisite phosphorylation--a 25 year update. *Trends Biochem. Sci.* **25**, 596–601.

Coll, O., Villalba, A., Bussotti, G., Notredame, C., and Gebauer, F. (2010). A novel, noncanonical mechanism of cytoplasmic polyadenylation operates in *Drosophila* embryogenesis. *Genes Dev.* **24**, 129–134.

Cougot, N., Babajko, S., and Séraphin, B. (2004). Cytoplasmic foci are sites of mRNA decay in human cells. *J. Cell Biol.* **165**, 31–40.

Cragle, C., and MacNicol, A.M. (2014). Musashi protein-directed translational activation of target mRNAs is mediated by the poly(A) polymerase, germ line development defective-2. *J. Biol. Chem.* **289**, 14239–14251.

D

D'Ambrogio, A., Nagaoka, K., and Richter, J.D. (2013). Translational control of cell growth and malignancy by the CPEBs. *Nat. Rev. Cancer* **13**, 283–290.

Decker, C.J., and Parker, R. (2012). P-bodies and stress granules: possible roles in the control of translation and mRNA degradation. *Cold Spring Harb. Perspect. Biol.* **4**, a012286.

Dephoure, N., Zhou, C., Villén, J., Beausoleil, S. a, Bakalarski, C.E., Elledge, S.J., and Gygi, S.P. (2008). A quantitative atlas of mitotic phosphorylation. *Proc. Natl. Acad. Sci. U. S. A.* **105**, 10762–10767.

Derti, A., Garrett-Engele, P., MacIsaac, K.D., Stevens, R.C., Sriram, S., Chen, R., Rohl, C. a., Johnson, J.M., and Babak, T. (2012). A quantitative atlas of polyadenylation in five mammals. *Genome Res.* **22**, 1173–1183.

Dever, T.E., and Green, R. (2012). Phases of Translation in Eukaryotes. *Cold Spring Harb. Perspect. Biol.* **4**, a013706.

Drisaldi, B., Colnaghi, L., Fioriti, L., Rao, N., Myers, C., Snyder, A.M., Metzger, D.J., Tarasoff, J., Konstantinov, E., Fraser, P.E., et al. (2015). SUMOylation Is an Inhibitory Constraint that Regulates the Prion-like Aggregation and Activity of CPEB3. *Cell Rep.* **11**, 1694–1702.

E

Erickson, S.L., and Lykke-Andersen, J. (2011). Cytoplasmic mRNP granules at a glance. *J. Cell Sci.* **124**, 293–297.

F

Fabian, M.R., Sonenberg, N., and Filipowicz, W. (2010). Regulation of mRNA translation and stability by microRNAs. *Annu. Rev. Biochem.* 79, 351–379.

Fernández-Miranda, G., and Méndez, R. (2012). The CPEB-family of proteins, translational control in senescence and cancer. *Ageing Res. Rev.* 11, 460–472.

Ferrell, J.E. (1999). Building a cellular switch: More lessons from a good egg. *BioEssays* 21, 866–870.

Ferrell, J.E. (2002). Self-perpetuating states in signal transduction: Positive feedback, double-negative feedback and bistability. *Curr. Opin. Cell Biol.* 14, 140–148.

Ferrell, J.E., and Ha, S.H. (2014a). Ultrasensitivity part I: Michaelian responses and zero-order ultrasensitivity. *Trends Biochem. Sci.* 39, 496–503.

Ferrell, J.E., and Ha, S.H. (2014b). Ultrasensitivity part III : cascades , bistable switches , and oscillators. *Trends Biochem. Sci.* 39, 612–618.

Ferrell, J.E., and Ha, S.H. (2014c). Ultrasensitivity part II: multisite phosphorylation, stoichiometric inhibitors, and positive feedback. *Trends Biochem. Sci.* 39, 556–569.

Fioriti, L., Myers, C., Huang, Y.-Y., Li, X., Stephan, J.S., Trifilieff, P., Colnaghi, L., Kosmidis, S., Drisaldi, B., Pavlopoulos, E., et al. (2015). The Persistence of Hippocampal-Based Memory Requires Protein Synthesis Mediated by the Prion-like Protein CPEB3. *Neuron* 86, 1433–1448.

Fowler, D.M., Koulov, A. V., Balch, W.E., and Kelly, J.W. (2007). Functional amyloid - from bacteria to humans. *Trends Biochem. Sci.* 32, 217–224.

Frank-Vaillant, M., Haccard, O., Thibier, C., Ozon, R., Arlot-Bonnemains, Y., Prigent, C., and Jessus, C. (2000). Progesterone regulates the accumulation and the activation of Eg2 kinase in *Xenopus* oocytes. *J. Cell Sci.* 113, 1127–1138.

Frey, S., and Görlich, D. (2007). A Saturated FG-Repeat Hydrogel Can Reproduce the Permeability Properties of Nuclear Pore Complexes. *Cell* 130, 512–523.

Frey, U., and Morris, R.G. (1997). Synaptic tagging and long-term potentiation. *Nature* 385, 533–536.

Frey, S., Richter, R.P., and Görlich, D. (2006). FG-rich repeats of nuclear pore proteins form a three-dimensional meshwork with hydrogel-like properties. *Science* (80-.). 314, 815–817.

G

Gao, M., Fritz, D.T., Ford, L.P., and Wilusz, J. (2000). Interaction between a poly(A)-specific ribonuclease and the 5' cap influences mRNA deadenylation rates in vitro. *Mol. Cell* 5, 479–488.

Garneau, N.L., Wilusz, J., and Wilusz, C.J. (2007). The highways and byways of mRNA decay. *Nat. Rev. Mol. Cell Biol.* 8, 113–126.

Gebauer, F., and Hentze, M.W. (2004). Molecular mechanisms of translational control. *Nat. Rev. Mol. Cell Biol.* 5, 827–835.

Gebauer, F., Preiss, T., and Hentze, M.W. (2012). From cis-regulatory elements to complex RNPs and back. *Cold Spring Harb. Perspect. Biol.*

Di Giammartino, D.C., Nishida, K., and Manley, J.L. (2011). Mechanisms and Consequences of Alternative Polyadenylation. *Mol. Cell* **43**, 853–866.

Graindorge, A., Le Tonquèze, O., Thuret, R., Pollet, N., Osborne, H.B., and Audic, Y. (2008). Identification of CUG-BP1/EDEN-BP target mRNAs in *Xenopus tropicalis*. *Nucleic Acids Res.* **36**, 1861–1870.

Gray, D. a., and Woulfe, J. (2013). Structural disorder and the loss of rna homeostasis in aging and neurodegenerative disease. *Front. Genet.* **4**, 1–10.

Gray, N.K., and Wickens, M. (1998). Control of translation initiation in animals. *Annu. Rev. Cell Dev. Biol.* **14**, 399–458.

Groisman, I., Jung, M.-Y., Sarkissian, M., Cao, Q., and Richter, J.D. (2002). Translational control of the embryonic cell cycle. *Cell* **109**, 473–483.

Groisman, I., Ivshina, M., Marin, V., Kennedy, N.J., Davis, R.J., and Richter, J.D. (2006). Control of cellular senescence by CPEB. *Genes Dev.* **20**, 2701–2712.

Groppo, R., and Richter, J.D. (2011). CPEB control of NF-kappaB nuclear localization and interleukin-6 production mediates cellular senescence. *Mol. Cell. Biol.* **31**, 2707–2714.

Gsponer, J., Futschik, M.E., Teichmann, S. a, and Babu, M.M. (2008). Tight regulation of unstructured proteins: from transcript synthesis to protein degradation. *Science* (80-.). **322**, 1365–1368.

H

Hägele, S., Kühn, U., Böning, M., and Katschinski, D.M. (2009). Cytoplasmic polyadenylation-element-binding protein (CPEB)1 and 2 bind to the HIF-1alpha mRNA 3'-UTR and modulate HIF-1alpha protein expression. *Biochem. J.* **417**, 235–246.

Hake, L.E., Mendez, R., and Richter, J.D. (1998). Specificity of RNA binding by CPEB: requirement for RNA recognition motifs and a novel zinc finger. *Mol. Cell. Biol.* **18**, 685–693.

Han, T.W., Kato, M., Xie, S., Wu, L.C., Mirzaei, H., Pei, J., Chen, M., Xie, Y., Allen, J., Xiao, G., et al. (2012). Cell-free formation of RNA granules: Bound RNAs identify features and components of cellular assemblies. *Cell* **149**, 768–779.

Hansen, D. V, Tung, J.J., and Jackson, P.K. (2006). CaMKII and polo-like kinase 1 sequentially phosphorylate the cytosolic factor Emi2/XErp1 to trigger its destruction and meiotic exit. *Proc. Natl. Acad. Sci. U. S. A.* **103**, 608–613.

Harvey, S.L., Charlet, A., Haas, W., Gygi, S.P., and Kellogg, D.R. (2005). Cdk1-dependent regulation of the mitotic inhibitor Wee1. *Cell* **122**, 407–420.

Hinnebusch, A.G., and Lorsch, J.R. (2012). The mechanism of eukaryotic translation initiation - new insights and challenges. *Cold Spring Harb. Perspect. Biol.* **4**, a011544.

Hochegger, H., Klotzbücher, A., Kirk, J., Howell, M., le Guellec, K., Fletcher, K., Duncan, T., Sohail, M., and Hunt, T. (2001). New B-type cyclin synthesis is required between meiosis I and II during *Xenopus* oocyte maturation. *Development* **128**, 3795–3807.

Hocine, S., Singer, R.H., and Grünwald, D. (2010). RNA processing and export. *Cold Spring Harb. Perspect. Biol.* 2, a000752.

Hosoda, N., Funakoshi, Y., Hirasawa, M., Yamagishi, R., Asano, Y., Miyagawa, R., Ogami, K., Tsujimoto, M., and Hoshino, S. (2011). Anti-proliferative protein Tob negatively regulates CPEB3 target by recruiting Caf1 deadenylase. *EMBO J.* 30, 1311–1323.

Hu, W., Yuan, B., and Lodish, H.F. (2014). Cpeb4-mediated translational regulatory circuitry controls terminal erythroid differentiation. *Dev. Cell* 30, 660–672.

Huang, Y.-S., Kan, M.-C., Lin, C.-L., and Richter, J.D. (2006). CPEB3 and CPEB4 in neurons: analysis of RNA-binding specificity and translational control of AMPA receptor GluR2 mRNA. *EMBO J.* 25, 4865–4876.

Huang, Y.S., Jung, M.Y., Sarkissian, M., and Richter, J.D. (2002). N-methyl-D-aspartate receptor signaling results in Aurora kinase-catalyzed CPEB phosphorylation and α CaMKII mRNA polyadenylation at synapses. *EMBO J.* 21, 2139–2148.

Huang, Y.S., Carson, J.H., Barbarese, E., and Richter, J.D. (2003). Facilitation of dendritic mRNA transport by CPEB. *Genes Dev.* 17, 638–653.

Huttlin, E.L., Jedrychowski, M.P., Elias, J.E., Goswami, T., Rad, R., Beausoleil, S. a, Villén, J., Haas, W., Sowa, M.E., and Gygi, S.P. (2010). A tissue-specific atlas of mouse protein phosphorylation and expression. *Cell* 143, 1174–1189.

I

Igea, A., and Méndez, R. (2010). Meiosis requires a translational positive loop where CPEB1 ensues its replacement by CPEB4. *EMBO J.* 29, 2182–2193.

Imataka, H., Gradi, A., and Sonenberg, N. (1998). A newly identified N-terminal amino acid sequence of human eIF4G binds poly(A)-binding protein and functions in poly(A)-dependent translation. *EMBO J.* 17, 7480–7489.

Inoue, D., Ohe, M., Kanemori, Y., Nobui, T., and Sagata, N. (2007). A direct link of the Mos-MAPK pathway to Erp1/Emi2 in meiotic arrest of *Xenopus laevis* eggs. *Nature* 446, 1100–1104.

Isoda, M., Sako, K., Suzuki, K., Nishino, K., Nakajo, N., Ohe, M., Ezaki, T., Kanemori, Y., Inoue, D., Ueno, H., et al. (2011). Dynamic regulation of Emi2 by Emi2-bound Cdk1/PIK1/CK1 and PP2A-B56 in meiotic arrest of *Xenopus* eggs. *Dev. Cell* 21, 506–519.

Ivshina, M., Lasko, P., and Richter, J.D. (2014). Cytoplasmic Polyadenylation Element Binding Proteins in Development, Health, and Disease. *Annu. Rev. Cell Dev. Biol.* 30, 393–415.

Iwabuchi, M., Ohsumi, K., Yamamoto, T.M., Sawada, W., and Kishimoto, T. (2000). Residual Cdc2 activity remaining at meiosis I exit is essential for meiotic M-M transition in *Xenopus* oocyte extracts. *EMBO J.* 19, 4513–4523.

J

Jenal, M., Elkon, R., Loayza-Puch, F., Van Haaften, G., Kühn, U., Menzies, F.M., Vrielink, J. a F.O., Bos, A.J., Drost, J., Rooijers, K., et al. (2012). The poly(A)-binding protein nuclear 1 suppresses alternative cleavage and polyadenylation sites. *Cell* 149, 538–553.

Jiang, H., Wang, S., Huang, Y., He, X., Cui, H., Zhu, X., and Zheng, Y. (2015). Phase Transition of Spindle-Associated Protein Regulate Spindle Apparatus Assembly. *Cell* **163**, 1–15.

Jonas, S., and Izaurralde, E. (2013). The role of disordered protein regions in the assembly of decapping complexes and RNP granules. *Genes Dev.* **27**, 2628–2641.

Jung, H., Gkogkas, C.G., Sonenberg, N., and Holt, C.E. (2014). Remote control of gene function by local translation. *Cell* **157**, 26–40.

Jung, M.-Y., Lorenz, L., and Richter, J.D. (2006). Translational control by neuroguidin, a eukaryotic initiation factor 4E and CPEB binding protein. *Mol. Cell. Biol.* **26**, 4277–4287.

Jurado, A.R., Tan, D., Jiao, X., Kiledjian, M., and Tong, L. (2014). Structure and function of pre-mRNA 5'-end capping quality control and 3'-end processing. *Biochemistry* **53**, 1882–1898.

K

Kan, M.-C., Oruganty-Das, A., Cooper-Morgan, A., Jin, G., Swanger, S. a, Bassell, G.J., Florman, H., van Leyen, K., and Richter, J.D. (2010). CPEB4 is a cell survival protein retained in the nucleus upon ischemia or endoplasmic reticulum calcium depletion. *Mol. Cell. Biol.* **30**, 5658–5671.

Kapp, L.D., and Lorsch, J.R. (2004). The molecular mechanics of eukaryotic translation. *Annu. Rev. Biochem.* **73**, 657–704.

Kato, M., Han, T.W., Xie, S., Shi, K., Du, X., Wu, L.C., Mirzaei, H., Goldsmith, E.J., Longgood, J., Pei, J., et al. (2012). Cell-free formation of RNA granules: Low complexity sequence domains form dynamic fibers within hydrogels. *Cell* **149**, 753–767.

Kedersha, N., Cho, M.R., Li, W., Yacono, P.W., Chen, S., Gilks, N., Golan, D.E., and Anderson, P. (2000). Dynamic shuttling of TIA-1 accompanies the recruitment of mRNA to mammalian stress granules. *J. Cell Biol.* **151**, 1257–1268.

Kedersha, N., Stoecklin, G., Ayodele, M., Yacono, P., Lykke-Andersen, J., Fitzler, M.J., Scheuner, D., Kaufman, R.J., Golan, D.E., and Anderson, P. (2005). Stress granules and processing bodies are dynamically linked sites of mRNP remodeling. *J. Cell Biol.* **169**, 871–884.

Keleman, K., Krüttner, S., Alenius, M., and Dickson, B.J. (2007). Function of the Drosophila CPEB protein Orb2 in long-term courtship memory. *Nat. Neurosci.* **10**, 1587–1593.

Keryer-Bibens, C., Barreau, C., and Osborne, H.B. (2008). Tethering of proteins to RNAs by bacteriophage proteins. *Biol. Cell* **100**, 125–138.

Kim, J.H., and Richter, J.D. (2006). Opposing polymerase-deadenylase activities regulate cytoplasmic polyadenylation. *Mol. Cell* **24**, 173–183.

Kim, J.H., and Richter, J.D. (2007). RINGO/cdk1 and CPEB mediate poly(A) tail stabilization and translational regulation by ePAB. *Genes Dev.* **21**, 2571–2579.

Kim, S.Y., and Ferrell, J.E. (2007). Substrate competition as a source of ultrasensitivity in the inactivation of Wee1. *Cell* **128**, 1133–1145.

Kozak, M. (2002). Pushing the limits of the scanning mechanism for initiation of translation. *Gene* **299**, 1–34.

Krupp, M., Marquardt, J.U., Sahin, U., Galle, P.R., Castle, J., and Teufel, A. (2012). RNA-Seq Atlas-a reference database for gene expression profiling in normal tissue by next-generation sequencing. *Bioinformatics* 28, 1184–1185.

Krüttner, S., Stepien, B., Noordermeer, J.N., Mommaas, M. a, Mechtler, K., Dickson, B.J., and Keleman, K. (2012). *Drosophila* CPEB Orb2A mediates memory independent of its RNA-binding domain. *Neuron* 76, 383–395.

L

Lécuyer, E., Yoshida, H., Parthasarathy, N., Alm, C., Babak, T., Cerovina, T., Hughes, T.R., Tomancak, P., and Krause, H.M. (2007). Global Analysis of mRNA Localization Reveals a Prominent Role in Organizing Cellular Architecture and Function. *Cell* 131, 174–187.

Lee, R. Van Der, Buljan, M., Lang, B., Weatheritt, R.J., Daughdrill, G.W., Dunker, a K., Fuxreiter, M., Gough, J., Gsponer, J., Jones, D.T., et al. (2014). Classification of Intrinsically Disordered Regions and Proteins. *Chem. Rev.* 114, 6589–6631.

Li, P., Banjade, S., Cheng, H.-C., Kim, S., Chen, B., Guo, L., Llaguno, M., Hollingsworth, J. V., King, D.S., Banani, S.F., et al. (2012). Phase transitions in the assembly of multivalent signalling proteins. *Nature* 483, 336–340.

Lin, C.-L., Evans, V., Shen, S., Xing, Y., and Richter, J.D. (2010). The nuclear experience of CPEB: implications for RNA processing and translational control. *RNA* 16, 338–348.

Lin, C.-L., Huang, Y.-T., and Richter, J.D. (2012). Transient CPEB dimerization and translational control. *RNA* 18, 1050–1061.

Van Linden, A. a., Cottin, V., Frankel, S.K., and Riches, D.W.H. (2005). Hierarchical phosphorylation of the TNF- α receptor, TNF-R1, by p42mapk/erk at basic pro-directed kinase sites. *Biochemistry* 44, 6980–6989.

Liu, J., and Maller, J.L. (2005). Calcium elevation at fertilization coordinates phosphorylation of XErp1/Emi2 by Plx1 and CaMK II to release metaphase arrest by cytostatic factor. *Curr. Biol.* 15, 1458–1468.

M

Ma, C., Cummings, C., and Liu, X.J. (2003). Biphasic activation of Aurora-A kinase during the meiosis I-meiosis II transition in *Xenopus* oocytes. *Mol. Cell. Biol.* 23, 1703–1716.

Majumdar, A., Cesario, W.C., White-Grindley, E., Jiang, H., Ren, F., Khan, M.R., Li, L., Choi, E.M.-L., Kannan, K., Guo, F., et al. (2012). Critical role of amyloid-like oligomers of *Drosophila* Orb2 in the persistence of memory. *Cell* 148, 515–529.

Mayr, C., and Bartel, D.P. (2009). Widespread Shortening of 3'UTRs by Alternative Cleavage and Polyadenylation Activates Oncogenes in Cancer Cells. *Cell* 138, 673–684.

Mendez, R., and Richter, J.D. (2001). Translational control by CPEB: a means to the end. *Nat. Rev. Mol. Cell Biol.* 2, 521–529.

Mendez, R., Hake, L.E., Andresson, T., Littlepage, L.E., Ruderman, J. V, and Richter, J.D. (2000a). Phosphorylation of CPE binding factor by Eg2 regulates translation of c-mos mRNA. *Nature* 404, 302–307.

Mendez, R., Murthy, K.G., Ryan, K., Manley, J.L., and Richter, J.D. (2000b). Phosphorylation of CPEB by Eg2 mediates the recruitment of CPSF into an active cytoplasmic polyadenylation complex. *Mol. Cell* **6**, 1253–1259.

Mendez, R., Barnard, D., and Richter, J.D. (2002). Differential mRNA translation and meiotic progression require Cdc2-mediated CPEB destruction. *EMBO J.* **21**, 1833–1844.

Merkel, D.J., Wells, S.B., Hilburn, B.C., Elazzouzi, F., Pérez-Alvarado, G.C., and Lee, B.M. (2013). The C-terminal region of cytoplasmic polyadenylation element binding protein is a ZZ domain with potential for protein-protein interactions. *J. Mol. Biol.* **425**, 2015–2026.

Minshall, N., Reiter, M.H., Weil, D., and Standart, N. (2007). CPEB interacts with an ovary-specific eIF4E and 4E-T in early *Xenopus* oocytes. *J. Biol. Chem.* **282**, 37389–37401.

Molliex, A., Temirov, J., Lee, J., Coughlin, M., Kanagaraj, A.P., Kim, H.J., Mittag, T., and Taylor, J.P. (2015). Phase Separation by Low Complexity Domains Promotes Stress Granule Assembly and Drives Pathological Fibrillization. *Cell* **163**, 123–133.

De Moor, C.H., and Richter, J.D. (1999). Cytoplasmic polyadenylation elements mediate masking and unmasking of cyclin B1 mRNA. *EMBO J.* **18**, 2294–2303.

N

Nagaoka, K., Udagawa, T., and Richter, J.D. (2012). CPEB-mediated ZO-1 mRNA localization is required for epithelial tight-junction assembly and cell polarity. *Nat. Commun.* **3**, doi: 10.1038/ncomms1678.

Nebreda, a R., and Ferby, I. (2000). Regulation of the meiotic cell cycle in oocytes. *Curr. Opin. Cell Biol.* **12**, 666–675.

Newby, G. a., and Lindquist, S. (2013). Blessings in disguise: Biological benefits of prion-like mechanisms. *Trends Cell Biol.* **23**, 251–259.

Nishiyama, T., Ohsumi, K., and Kishimoto, T. (2007). Phosphorylation of Erp1 by p90rsk is required for cyostatic factor arrest in *Xenopus laevis* eggs. *Nature* **446**, 1096–1099.

Nott, T.J.J., Petsalaki, E., Farber, P., Jervis, D., Fussner, E., Plochowietz, A., Craggs, T.D., Bazett-Jones, D.P.P., Pawson, T., Forman-Kay, J.D.D., et al. (2015). Phase Transition of a Disordered Nuage Protein Generates Environmentally Responsive Membraneless Organelles. *Mol. Cell* **57**, 936–947.

Novoa, I., Gallego, J., Ferreira, P.G., and Mendez, R. (2010). Mitotic cell-cycle progression is regulated by CPEB1 and CPEB4-dependent translational control. *Nat. Cell Biol.* **12**, 447–456.

O

Olsen, J. V., Vermeulen, M., Santamaria, A., Kumar, C., Miller, M.L., Jensen, L.J., Gnad, F., Cox, J., Jensen, T.S., Nigg, E. a, et al. (2010). Quantitative phosphoproteomics reveals widespread full phosphorylation site occupancy during mitosis. *Sci. Signal.* **3**, ra3.

Ortiz-Zapater, E., Pineda, D., Martínez-Bosch, N., Fernández-Miranda, G., Iglesias, M., Alameda, F., Moreno, M., Eliscovich, C., Eyra, E., Real, F.X., et al. (2012). Key contribution of CPEB4-mediated translational control to cancer progression. *Nat. Med.* **18**, 83–90.

Oruganty-Das, A., Ng, T., Udagawa, T., Goh, E.L.K., and Richter, J.D. (2012). Translational control of mitochondrial energy production mediates neuron morphogenesis. *Cell Metab.* 16, 789–800.

P

Parker, R., and Sheth, U. (2007). P bodies and the control of mRNA translation and degradation. *Mol. Cell* 25, 635–646.

Parker, R., and Song, H. (2004). The enzymes and control of eukaryotic mRNA turnover. *Nat. Struct. Mol. Biol.* 11, 121–127.

Pascreau, G., Delcros, J.-G., Morin, N., Prigent, C., and Arlot-Bonnemains, Y. (2008). Aurora-A kinase Ser349 phosphorylation is required during *Xenopus laevis* oocyte maturation. *Dev. Biol.* 317, 523–530.

Pavlopoulos, E., Trifilieff, P., Chevalleyre, V., Fioriti, L., Zairis, S., Pagano, A., Malleret, G., and Kandel, E.R. (2011). Neuralized1 activates CPEB3: a function for nonproteolytic ubiquitin in synaptic plasticity and memory storage. *Cell* 147, 1369–1383.

Perdiguero, E., and Nebreda, A.R. (2004). Regulation of Cdc25C activity during the meiotic G2/M transition. *Cell Cycle* 3, 733–737.

Peters, J.-M. (2006). The anaphase promoting complex/cyclosome: a machine designed to destroy. *Nat. Rev. Mol. Cell Biol.* 7, 644–656.

Piqué, M., López, J.M., Foissac, S., Guigó, R., and Méndez, R. (2008). A combinatorial code for CPE-mediated translational control. *Cell* 132, 434–448.

Proudfoot, N.J. (2011). Ending the message: poly (A) signals then and now. *Genes Dev.* 25, 1770–1782.

R

Raveendra, B.L., Siemer, A.B., Puthanveetil, S. V., Hendrickson, W. a, Kandel, E.R., and McDermott, A.E. (2013). Characterization of prion-like conformational changes of the neuronal isoform of Aplysia CPEB. *Nat. Struct. Mol. Biol.* 20, 495–501.

Richter, J.D. (2007). CPEB: a life in translation. *Trends Biochem. Sci.* 32, 279–285.

Richter, J.D., and Sonenberg, N. (2005). Regulation of cap-dependent translation by eIF4E inhibitory proteins. *Nature* 433, 477–480.

S

Sachs, a B., Sarnow, P., and Hentze, M.W. (1997). Starting at the beginning, middle, and end: translation initiation in eukaryotes. *Cell* 89, 831–838.

Sandberg, R., Neilson, J.R., Sarma, A., Sharp, P.A., and Burge, C.B. (2008). Proliferating cells express mRNAs with shortened 3' untranslated regions and fewer microRNA target sites. *Science* 320, 1643–1647.

Schelhorn, C., Gordon, J.M.B., Ruiz, L., Alguacil, J., Pedroso, E., and Macias, M.J. (2014). RNA recognition and self-association of CPEB4 is mediated by its tandem RRM domains. *Nucleic Acids Res.* **42**, 10185–10195.

Schmid, M., and Jensen, T.H. (2008). Quality control of mRNP in the nucleus. *Chromosoma* **117**, 419–429.

Schmidt, H.B., and Görlich, D. (2015). Nup98 FG domains from diverse species spontaneously phase-separate into particles with nuclear pore-like permselectivity. *Elife* **4**, e04251.

Schmitt, A., and Nebreda, A.R. (2002). Signalling pathways in oocyte meiotic maturation. *J. Cell Sci.* **115**, 2457–2459.

Serber, Z., and Ferrell, J.E. (2007). Tuning bulk electrostatics to regulate protein function. *Cell* **128**, 441–444.

Shatkin, a J., and Manley, J.L. (2000). The ends of the affair: capping and polyadenylation. *Nat. Struct. Biol.* **7**, 838–842.

Shukla, S., and Oberdoerffer, S. (2012). Co-transcriptional regulation of alternative pre-mRNA splicing. *Biochim. Biophys. Acta* **1819**, 673–683.

Si, K., Giustetto, M., Etkin, A., Hsu, R., Janisiewicz, A.M., Miniaci, M.C., Kim, J.H., Zhu, H., and Kandel, E.R. (2003a). A Neuronal Isoform of CPEB Regulates Local Protein Synthesis and Stabilizes Synapse-Specific Long-Term Facilitation in Aplysia. *Cell* **115**, 893–904.

Si, K., Lindquist, S., and Kandel, E.R. (2003b). A Neuronal Isoform of the Aplysia CPEB Has Prion-Like Properties. *Cell* **115**, 879–891.

Si, K., Choi, Y.-B., White-Grindley, E., Majumdar, A., and Kandel, E.R. (2010). Aplysia CPEB can form prion-like multimers in sensory neurons that contribute to long-term facilitation. *Cell* **140**, 421–435.

Somers, J., Pöry, T., and Willis, A.E. (2013). A perspective on mammalian upstream open reading frame function. *Int. J. Biochem. Cell Biol.* **45**, 1690–1700.

Sonenberg, N., and Hinnebusch, A.G. (2007). New Modes of Translational Control in Development, Behavior, and Disease. *Mol. Cell* **28**, 721–729.

Stebbins-Boaz, B., Cao, Q., de Moor, C.H., Mendez, R., and Richter, J.D. (1999). Maskin is a CPEB-associated factor that transiently interacts with eIF-4E. *Mol. Cell* **4**, 1017–1027.

Stephan, J.S., Fioriti, L., Lamba, N., Colnaghi, L., Karl, K., Derkatch, I.L., and Kandel, E.R. (2015). The CPEB3 Protein Is a Functional Prion that Interacts with the Actin Cytoskeleton. *Cell Rep.* **1**–14.

Strickfaden, S.C., Winters, M.J., Ben-Ari, G., Lamson, R.E., Tyers, M., and Pryciak, P.M. (2007). A Mechanism for Cell-Cycle Regulation of MAP Kinase Signaling in a Yeast Differentiation Pathway. *Cell* **128**, 519–531.

T

Tarun, S., and Sachs, A.B. (1995). A common function for mRNA 5' and 3' ends in translation initiation in yeast. *Genes Dev.* **9**, 2997–3007.

Tay, J., Hodgman, R., Sarkissian, M., and Richter, J.D. (2003). Regulated CPEB phosphorylation during meiotic progression suggests a mechanism for temporal control of maternal mRNA translation. *Genes Dev.* 17, 1457–1462.

Theis, M., Si, K., and Kandel, E.R. (2003). Two previously undescribed members of the mouse CPEB family of genes and their inducible expression in the principal cell layers of the hippocampus. *Proc. Natl. Acad. Sci. U. S. A.* 100, 9602–9607.

Tian, J., Kim, S., Heilig, E., and Ruderman, J. V (2000). Identification of XPR-1, a progesterone receptor required for *Xenopus* oocyte activation. *Proc. Natl. Acad. Sci. U. S. A.* 97, 14358–14363.

Trunnell, N.B., Poon, A.C., Kim, S.Y., and Ferrell, J.E. (2011). Ultrasensitivity in the Regulation of Cdc25C by Cdk1. *Mol. Cell* 41, 263–274.

Tunquist, B.J., and Maller, J.L. (2003). Under arrest: cytostatic factor (CSF)-mediated metaphase arrest in vertebrate eggs. *Genes Dev.* 17, 683–710.

Tunquist, B.J., Schwab, M.S., Chen, L.G., and Maller, J.L. (2002). The spindle checkpoint kinase Bub1 and cyclin E/Cdk2 both contribute to the establishment of meiotic metaphase arrest by cytostatic factor. *Curr. Biol.* 12, 1027–1033.

U

Ubersax, J. a, and Ferrell, J.E. (2007). Mechanisms of specificity in protein phosphorylation. *Nat. Rev. Mol. Cell Biol.* 8, 530–541.

Uchida, N., Hoshino, S.I., Imataka, H., Sonenberg, N., and Katada, T. (2002). A novel role of the mammalian GSPT/eRF3 associating with poly(A)-binding protein in cap/poly(A)-dependent translation. *J. Biol. Chem.* 277, 50286–50292.

Udagawa, T., Swanger, S. a., Takeuchi, K., Kim, J.H., Nalavadi, V., Shin, J., Lorenz, L.J., Zukin, R.S., Bassell, G.J., and Richter, J.D. (2012). Bidirectional Control of mRNA Translation and Synaptic Plasticity by the Cytoplasmic Polyadenylation Complex. *Mol. Cell* 47, 253–266.

Ulitsky, I., Shkumatava, A., Jan, C.H., Subtelny, A.O., Koppstein, D., Bell, G.W., Sive, H., and Bartel, D.P. (2012). Extensive alternative polyadenylation during zebrafish development. *Genome Res.* 22, 2054–2066.

Uversky, V.N., Oldfield, C.J., and Dunker, a K. (2008). Intrinsically disordered proteins in human diseases: introducing the D2 concept. *Annu. Rev. Biophys.* 37, 215–246.

W

Wang, C.-F., and Huang, Y.-S. (2012). Calpain 2 activated through N-methyl-D-aspartic acid receptor signaling cleaves CPEB3 and abrogates CPEB3-repressed translation in neurons. *Mol. Cell. Biol.* 32, 3321–3332.

Wang, X., and Cooper, N.G.F. (2010). Bioinformatics and Biology Insights Comparative in Silico Analyses of Cpeb1 – 4 with Functional Predictions. *Bioinform. Biol. Insights* 4, 61–83.

Weber, S.C., and Brangwynne, C.P. (2012). Getting RNA and protein in phase. *Cell* 149, 1188–1191.

Weill, L., Belloc, E., Bava, F.-A., and Méndez, R. (2012). Translational control by changes in poly(A) tail length: recycling mRNAs. *Nat. Struct. Mol. Biol.* **19**, 577–585.

Wells, S.E., Hillner, P.E., Vale, R.D., and Sachs, A.B. (1998). Circularization of mRNA by Eukaryotic Translation Initiation Factors. *Mol. Cell* **2**, 135–140.

White-Grindley, E., Li, L., Mohammad Khan, R., Ren, F., Saraf, A., Florens, L., and Si, K. (2014). Contribution of Orb2A Stability in Regulated Amyloid-Like Oligomerization of *Drosophila* Orb2. *PLoS Biol.* **12**, e1001786.

Wilczynska, a, Aigueperse, C., Kress, M., Dautry, F., and Weil, D. (2005). The translational regulator CPEB1 provides a link between dcp1 bodies and stress granules. *J. Cell Sci.* **118**, 981–992.

Wright, P.E., and Dyson, H.J. (2014). Intrinsically disordered proteins in cellular signalling and regulation. *Nat. Rev. Mol. Cell Biol.* **16**, 18–29.

Wu, J.Q., and Kornbluth, S. (2008). Across the meiotic divide - CSF activity in the post-Emi2/XErp1 era. *J. Cell Sci.* **121**, 3509–3514.

Z

Zhang, X., Virtanen, A., and Kleiman, F.E. (2010). To polyadenylate or to deadenylate: That is the question. *Cell Cycle* **9**, 4437–4449.

APPENDIX

Appendix 1. xCPEB4 12A- and 12D-interacting proteins

HA-xCPEB4 12A and 12D phospho-mutants were immunoprecipitated and the interacting proteins were analysed by mass spectrometry. Only proteins with fold enrichment >1.5 with respect to the control IP in two independent experiments are shown.

| | Accession number | Description |
|---|------------------|--|
| ENRICHED PROTEINS IN xCPEB4 12A IP (1.5 fold enrichment respect control IP) | Q7ZTK0 | MGC53106 protein OS=Xenopus laevis PE=2 SV=1 (chaperone) |
| | Q7ZTR6 | Hspd1 protein (Fragment) OS=Xenopus laevis GN=Hspd1 PE=2 SV=1 |
| | A0AUT4 | LOC100036778 protein OS=Xenopus laevis GN=LOC100036778 PE=2 SV=1 |
| | Q6NRZ4 | Collagen type IV alpha-3-binding protein OS=Xenopus laevis GN=col4a3bp PE=2 SV=1 |
| | Q5XGK8 | LOC495278 protein OS=Xenopus laevis GN=LOC495278 PE=2 SV=1 |
| | Q801N3 | Camk2g-prov protein OS=Xenopus laevis PE=2 SV=1 |
| | F6QW20 | Uncharacterized protein OS=Xenopus tropicalis GN=mthfd1l PE=3 SV=1 |
| | A9ULY4 | Uncharacterized protein (Fragment) OS=Xenopus laevis PE=2 SV=1 |
| | Q6GP08 | MGC80755 protein dhrr7 OS=Xenopus laevis GN=MGC80755 PE=2 SV=1 |
| | Q801P9 | MGC53795 protein OS=Xenopus laevis PE=2 SV=1 |
| | F6ZI40 | Uncharacterized protein OS=Xenopus tropicalis GN=sf3b3 PE=4 SV=1 |
| | Q5XH91 | ATP-dependent RNA helicase DDX1 OS=Xenopus tropicalis GN=ddx1 PE=2 SV=1 |
| | I6L8K5 | DBIRD complex subunit ZNF326 OS=Xenopus tropicalis GN=znf326 PE=4 SV=1 |
| | F7BAE6 | Uncharacterized protein (Fragment) OS=Xenopus tropicalis PE=3 SV=1 |
| | F6ZDW4 | Uncharacterized protein (Fragment) OS=Xenopus tropicalis GN=ddx20 PE=3 SV=1 |
| | F7E2N6 | Uncharacterized protein OS=Xenopus tropicalis GN=tsc1 PE=4 SV=1 |
| | Q5I083 | Hypothetical LOC496959 OS=Xenopus tropicalis GN=rpn2 PE=2 SV=1 |
| | Q3KPN4 | MGC132198 protein fgfr1op OS=Xenopus laevis GN=MGC132198 PE=2 SV=1 |
| | F7E721 | Uncharacterized protein OS=Xenopus tropicalis GN=ap4e1 PE=4 SV=1 |
| | B5DED5 | Uncharacterized protein OS=Xenopus tropicalis GN=ogdh PE=2 SV=1 |

Table 4. xCPEB4 12A mutant specific interacting proteins

| | Accession number | Description |
|---|------------------|---|
| ENRICHED PROTEINS IN xCEB4 12D IP (1.5 fold enrichment respect control IP) | Q7SYU9 | Ldhba protein OS=Xenopus laevis GN=ldhba PE=2 SV=1 |
| | B0BM40 | Triosephosphate isomerase OS=Xenopus tropicalis GN=tpi1 PE=2 SV=1 |
| | Q7ZWN5 | Triosephosphate isomerase OS=Xenopus laevis GN=tpi1 PE=2 SV=1 |
| | Q641I6 | LOC494638 protein periplin OS=Xenopus laevis GN=LOC494638 PE=2 SV=1 |
| | Q7SZ23 | Gstm2-prov protein OS=Xenopus laevis PE=2 SV=1 |
| | Q498I1 | LOC398508 protein grhpr.2 OS=Xenopus laevis GN=LOC398508 PE=2 SV=1 |
| | P30759 | Arginase-1 OS=Xenopus laevis GN=arg1 PE=2 SV=1 |

Table 5. xCEB4 12D mutant specific interacting proteins

| | Accession number | Description |
|--|------------------|---|
| PROTEINS EQUALLY ENRICHED IN xCEB4 12A and 12D IPs (1.5 fold enrichment respect control IP) | B3DLK7 | LOC100037071 protein (Fragment) OS=Xenopus laevis GN=LOC100037071 PE=2 SV=1 |
| | P30883 | Tubulin beta-4 chain OS=Xenopus laevis GN=tubb4 PE=2 SV=1 |
| | Q7ZY50 | MGC53997 protein OS=Xenopus laevis PE=2 SV=1 |
| | Q9PSN9 | Lipovitellin 1, PCDZN=ZN(2+)- and CD(2+)-binding protein (Fragments) OS=Xenopus laevis PE=1 SV=1 |
| | Q5U4V6 | LOC397931 protein OS=Xenopus laevis GN=LOC397931 PE=2 SV=1 |
| | Q6NRV3 | MGC81323 protein tuba1a OS=Xenopus laevis GN=MGC81323 PE=2 SV=1 |
| | Q6P367 | Tubulin, beta 2B OS=Xenopus tropicalis GN=tubb2b PE=2 SV=1 |
| | P19011 | Vitellogenin-B2 (Fragment) OS=Xenopus laevis PE=1 SV=1 |
| | P18709 | Vitellogenin-A2 OS=Xenopus laevis PE=1 SV=1 |
| | Q5EB23 | MGC97820 protein tuba3e OS=Xenopus tropicalis GN=MGC97820 PE=2 SV=1 |
| | Q5BL39 | Tubulin, beta 2 OS=Xenopus tropicalis GN=tubb4a PE=2 SV=1 |
| | Q28CH9 | Novel protein similar to tubulin, alpha 1 (Tuba1) OS=Xenopus tropicalis GN=TGas122d03.1-001 PE=2 SV=1 |
| | Q7SZF6 | Vitellogenin B1 OS=Xenopus laevis GN=vtg b1 PE=2 SV=1 |
| | Q63ZG6 | Phosphorylase OS=Xenopus laevis GN=pygl PE=2 SV=1 |
| | Q6P2W6 | Elongation factor Tu (Fragment) OS=Xenopus tropicalis GN=tubb4 PE=2 SV=1 |
| | Q6PCI8 | Pyruvate carboxylase OS=Xenopus laevis GN=MGC68971 PE=2 SV=1 |
| | F7E1Q0 | Phosphorylase OS=Xenopus tropicalis GN=pygl PE=3 SV=1 |

**PROTEINS EQUALLY
ENRICHED IN xCPEB4 12A
and 12D IPs
(1.5 fold enrichment respect
control IP)**

| | |
|---------------|--|
| Q2VPL8 | MGC131189 protein aldh6a1 OS=Xenopus laevis GN=MGC131189 PE=2 SV=1 |
| Q7SYA0 | MGC64276 protein c9 OS=Xenopus laevis PE=2 SV=1 |
| Q68EY5 | ATP synthase subunit alpha OS=Xenopus laevis GN=LOC397732 PE=2 SV=1 |
| F7DHH5 | Pyruvate carboxylase OS=Xenopus tropicalis GN=pc.1 PE=3 SV=1 |
| Q6PAX2 | ATPase family AAA domain-containing protein 3-B OS=Xenopus laevis GN=atad3-b PE=2 SV=1 |
| Q6GMF0 | MGC81784 protein aldh18a1 OS=Xenopus laevis GN=MGC81784 PE=2 SV=1 |
| P55862 | DNA replication licensing factor mcm5-A OS=Xenopus laevis GN=mcm5-a PE=1 SV=2 |
| Q7ZXN9 | T-complex protein 1 subunit alpha OS=Xenopus laevis PE=2 SV=1 |
| Q6NTQ5 | T-complex protein 1 subunit alpha OS=Xenopus laevis GN=tcpl1-A-prov PE=2 SV=1 - |
| Q58E76 | ATPase family AAA domain-containing protein 3-A OS=Xenopus laevis GN=atad3-a PE=2 SV=1 |
| D8V196 | Cytoplasmic polyadenylation element binding protein 4 OS=Xenopus laevis PE=2 SV=1 |
| Q6INS0 | MGC81156 protein gstd1 OS=Xenopus laevis GN=MGC81156 PE=2 SV=1 |
| Q4QR22 | MGC114925 protein OS=Xenopus laevis GN=MGC114925 PE=2 SV=1 |
| L7N325 | Uncharacterized protein OS=Xenopus tropicalis PE=4 SV=1 |
| Q6GNR4 | MGC80936 protein cltc OS=Xenopus laevis GN=MGC80936 PE=2 SV=1 |
| Q5XHB7 | Hypothetical LOC496448 cltc OS=Xenopus tropicalis GN=LOC496448 PE=2 SV=1 |
| F7A9C1 | Uncharacterized protein (Fragment) OS=Xenopus tropicalis PE=4 SV=1 |
| Q5M7D5 | LOC496233 protein ndufs3 OS=Xenopus laevis GN=LOC496233 PE=2 SV=1 |
| F6Q5T7 | Uncharacterized protein OS=Xenopus tropicalis GN=ruvbl1 PE=4 SV=1 |
| Q6GR29 | Ruvbl1 protein OS=Xenopus laevis GN=Ruvbl1 PE=2 SV=1 |
| Q6GQ98 | MGC80234 protein crat.2 OS=Xenopus laevis GN=MGC80234 PE=2 SV=1 |
| Q0IH65 | LOC733268 protein OS=Xenopus laevis GN=LOC733268 PE=2 SV=1 |
| A4QN94 | LOC100125119 protein (Fragment) OS=Xenopus tropicalis GN=LOC100125119 PE=2 SV=1 |
| Q0IH85 | LOC398205 protein ruvbl2 OS=Xenopus laevis GN=LOC398205 PE=2 SV=1 |
| F6W4K0 | Uncharacterized protein OS=Xenopus tropicalis GN=vtga2 PE=4 SV=1 |
| Q6GMA6 | MGC81949 protein OS=Xenopus laevis GN=cct6a PE=2 SV=1 |
| Q7ZTL5 | Cct8-prov protein OS=Xenopus laevis PE=2 SV=1 |
| A9UMK9 | Uncharacterized protein OS=Xenopus tropicalis GN=actr1a PE=2 SV=1 |
| P50143 | T-complex protein 1 subunit gamma OS=Xenopus laevis GN=cct3 PE=2 SV=2 |
| Q6NTQ9 | Ndufa10b protein OS=Xenopus laevis GN=ndufa10b PE=2 SV=1 |
| Q5XGR6 | Ndufa10a protein OS=Xenopus laevis GN=ndufa10a PE=2 SV=1 |

| | | |
|---|--------|---|
| PROTEINS EQUALLY ENRICHED IN xCPEB4 12A and 12D IPs (1.5 fold enrichment respect control IP) | B7ZSB2 | Pcm-1 protein OS=Xenopus laevis GN=pcm-1 PE=2 SV=1 |
| | Q6IND5 | MGC83495 protein vwa5a.2 OS=Xenopus laevis GN=MGC83495 PE=2 SV=1 |
| | Q6GM62 | MGC83400 protein isocitrate dehydrogenase OS=Xenopus laevis GN=MGC83400 PE=2 SV=1 |
| | Q4QR45 | Importin subunit alpha OS=Xenopus laevis GN=LOC398026 PE=2 SV=1 |
| | Q8AVB7 | Cct2-prov protein OS=Xenopus laevis PE=2 SV=1 |
| | Q32NR8 | MGC130896 protein ndufs2 OS=Xenopus laevis GN=MGC130896 PE=2 SV=1 |
| | Q0IH35 | MGC154791 protein slc25a11 OS=Xenopus laevis GN=MGC154791 PE=2 SV=1 |
| | F7B7N1 | Uncharacterized protein OS=Xenopus tropicalis GN=snmp200 PE=4 SV=1 |
| | F6T034 | Uncharacterized protein (Fragment) OS=Xenopus tropicalis GN=decr1 PE=4 SV=1 |
| | Q68F13 | MGC82958 protein succinyl-CoA ligase subunit beta OS=Xenopus laevis GN=MGC82958 PE=2 SV=1 |
| | Q6P8B9 | Hydroxyacyl-Coenzyme A dehydrogenase/3-ketoacyl-Coenzyme A thiolase/enoyl-Coenzyme A hydratase (Trifunctional protein), beta subunit OS=Xenopus tropicalis GN=hadhb PE=2 SV=1 |
| | Q08BT7 | LOC100145662 protein cul9 OS=Xenopus tropicalis GN=LOC100145662 PE=2 SV=1 |
| | F6PZY0 | Dolichyl-diphosphooligosaccharide--protein glycosyltransferase 48 kDa subunit (Fragment) OS=Xenopus tropicalis GN=ddost PE=4 SV=1 |
| | Q4QQX3 | MGC115711 protein coq6 OS=Xenopus laevis GN=MGC115711 PE=2 SV=1 |

Table 6. xCPEB4 12A and 12D mutants interacting proteins

Appendix 2. GFP-xCPEB4 live cell imaging

Supplemental Movie 1 that shows GFP-xCPEB4 granule dynamics in U2OS cells by live cell imaging. Granule fusion and fission events can be appreciated.

Appendix 3. Publications

Jordina Guillén-Boixet, Víctor Buzon, Xavier Salvatella and Raúl Méndez. CPEB4 is regulated by ERK/Cdk1 phosphorylation and liquid-like-droplet aggregation. Under review in *Molecular Cell*.

Tariq Afroz, Lenka Skrisovska, Eulàlia Belloc, **Jordina Guillén-Boixet**, Raúl Méndez and Frédéric H.T-Allain. A fly-trap mechanism provides sequence-specific RNA recognition by CPEB proteins. *Genes and Development*, 2014. 28(13):1498-514.

ACKNOWLEDGEMENTS

Han estat moltes les negatives frustrades abans d'arribar aquí. Als 16 anys volia estudiar qualsevol cosa menys Biologia, quina mandra classificar plantes, pensava (perdona TT). I als 17 entrava per iniciativa pròpia a estudiar Biologia, humana sí, però Biologia. Dels 18 als 21 la recerca biomèdica no encaixava amb les meves idees de futur. I als 22 entrava al laboratori directa a aventurar-me en un doctorat. I ara? El post-doctorat ha passat de ser de les meves últimes opcions a una de les primeres... això sí, que sigui curt, si us plau. Hauré de començar a acceptar que per molt dur que sigui, fins i tot frustrant en alguns moments, la ciència te alguna cosa que enganxa, i m'encanta...

Sou moltes les persones que d'una o altra manera heu contribuït en aquesta tesi. Aquestes línies són per vosaltres.

Recuerdo llegar a quinto de carrera y leer todo de posibles proyectos para hacer las prácticas. Finalmente escogí uno que hablaba de CPEB, C3H-4, *cytoplasmic polyadenylation*... ¡qué lío! No entendía mucho la verdad, pero ¡sonaba tan bien eso de microinyectar *RNA reporters* en oocitos de rana! ¡MICROINYECTAR! ¡UAAA! Pensaba... Después de microinyectar unas decenas de miles de oocitos quizás el ¡UAAA! ha cambiado un poquito de entonación, pero sin duda fue una muy buena elección. Raúl, ante todo agradecerte permitirme hacer la tesis en tu laboratorio, ha sido una experiencia muy positiva en muchos aspectos. Gracias por ofrecerme y dirigir este proyecto, lo he disfrutado mucho. Gracias por tu apoyo, tus consejos, tus ideas siempre tan acertadas, por la confianza que me has dado y por todos los conocimientos que he adquirido. Me considero muy afortunada de haber descubierto lo que significa hacer ciencia en tu laboratorio.

Y aquí llegáis vosotros, ¡compañeros y amigos del laboratorio! Los presentes: Eulàlia, Carlos, Vero, Judit, Chiara, Clara, Rosa, Annarita, Gonzalo, Oriol, Irene, Nere, Alba, Héctor, Manuel y Berta. Y los pasados: Laure, Carolina S, Vitto, Valeria, Alessio, Ivan, Ana, Maria, Isabel y Carolina E. Sin vosotros este doctorado no hubiera sido lo mismo. Habéis sido cruciales para superar los *negative feedback loops* de las CPEBs, con vuestros SUPERPODERES, consejos, ánimos y ayuda. Y ha sido genial ver como los pequeños logros se traducían en explosiones de alegría y en riquísimos pasteles (que sí, que os debo uno... o dos!). Especial mención a:

¿Cómo ha dicho que se llama? ¿LO? Debe ser china... ¡Ah! ¡No! es francesa... creo que es LOG... por si acaso no la llamaré por su nombre... ¡Ei! ¡Tu! Claro que está *in frame*... Pasaron unos días y entonces llegó esa placa de bacterias que me iluminó... ¡LAURE! ¡qué fácil era! (no como el *cloning* que al final lo que se dice *in frame* no estaba...). Laure Weill, gracias infinitas por enseñarme tantas cosas y por estar siempre dispuesta a ayudarme y escucharme. Has sido un gran apoyo durante estos años, tanto a nivel científico como a nivel personal. Es reconfortante poder compartir nuestras pequeñas locuras y reírnos de ellas. *Ne me quitte pas*.

Eulàlia Bellooooooooooc! Mil gràcies per tot! Per creure en els oòcits, pel teu suport, els consells, els ànims i els riures. He après molt treballant al teu costat i ha estat un plaer compartir cervell amb tu! Un mundo ideaaal...

Vero, gràcies per cuidar tan bé de les granotes, els oòcits no són iguals quan no hi ets. Juditinyi! M'encantes tu, les teves abraçades i la teva paella! I com no, els nostres mini-bailoteos que són tan terapèutics. Mil gràcies a totes dues per fer-nos el dia a dia al laboratori més fàcil. No podríem avançar igual sense la vostra ajuda.

Seguint amb la línia científica, gràcies Xavier Salvatella i membres del teu laboratori per guiar-me en el desordre de les CPEBs. Especialment al Víctor! La teva contribució ha estat clau per a resoldre l'enigma dels agregats. He après molt, m'ha entusiasmat i ha estat, fins i tot, divertit. Gràcies!

Thanks to Frédéric H.T-Allain and Tariq Afroz for solving the structures of the CPEBs and get us involved in that exciting project.

Ángel Nebreda, Manuel Palacín y Cristina Fillat, gracias por seguir este proyecto año tras año.

Gracias Fátima Gebauer y miembros de tu laboratorio por vuestras contribuciones en los JLM.

I gràcies també a les facilities de Mass Spectrometry i Advanced Digital Microscopy de l'IRB i al servei de Crio-microscopia electrònica del CCiTUB per la seva col·laboració.

Més enllà del laboratori tinc la sort d'estar envoltada de grans persones que fan que tot plegat tingui sentit. Caminar al vostre costat em fa feliç i ha estat essencial per arribar fins aquí.

Superhullahops!! Sense cap mena de dubte la millor conseqüència d'haver triat Biologia a la UPF ha estat haver-vos trobat. M'aporteu tants bons moments, tants! Riures, rumbes, aire fresc, viatges inoblidables, vídeos de primera fent esquí de fons... sou increïbles i m'encanta compartir la vida amb vosaltres!

““Espléndidas”” (entre muchas comillas para que se entienda la ironía del nombre), si hemos superado una adolescencia confusa entre gomina, borregos y plataformas en el Consell de Cent, ¡podemos con todo! Gracias por los buenos momentos.

Porto tota la vida esperant els estius amb entusiasme, per arribar a Estopanyà! el poble de la llibertat, de les pujades, de la piscina, del bosc màgic, dels paso dobles i sobre tot, el poble on esteu vosaltres, la Penya la Huevada! Ha estat un plaer créixer amb vosaltres i m'encanta seguir reservant aquells quatre dies sagrats per retrobar-nos, com si el temps no hagués passat. Gràcies per tants i tants moments!

Heleia, pisin-mate... què dir-te? Gràcies per estar sempre disposada a venir corrents. Ets un sol i em reconforta saber que estàs aquí. Núria, tu em vas donar forces per embarcar-me en una aventura que em semblava impossible, mai t'estaré prou agraïda per portar-m'hi i cuidar-me tant. Lucía, juntes vam viure una d'aquelles experiències que et canvien, gracies per totes les vivències compartides. I Sònia, és divertit pensar com de malament vam començar i com de bé hem acabat. Gràcies per les forces que em vas donar quan no en tenia. M'agrada veure't feliç.

Mar i Brisa, Brisa i Mar, la Brisa del Mar, es podria fer poesia amb els vostres noms! No m'imagino la vida sense vosaltres, així de simple. Sou els meus pilars. Gràcies per tots aquests anys d'amistat amb majúscules.

Gràcies a la meva família per ser tan fantàstica! Tietes, tiets, cosins, avis... Gràcies per la vostra estima. Una menció especial a les meves tates. Joy, mil gràcies per il·luminar una època de foscor. Carme, gràcies per les confidències a la cuina d'Estopanyà, són molt reveladores. Gracies també a la família Buirra Garcia per fer-me sentir una més.

I com no... TT, gràcies per protegir-me i estimar-me, a vegades no calen les paraules. Iaia, eres mi persona preferida! Tu cariño me llena. Gracias por regalarme momentos tan dulces. Papes, assembleu-me a vosaltres és tot un orgull. Us estimo i admiro. Vosaltres m'heu ensenyat que la vida és una i s'ha d'expressar, m'heu animat a superar les pors, a vèncer l'adversitat i a viure amb un somriure. Gràcies pel vostre suport incondicional i per tots els vostres consells que m'han guiat fins aquí.

Finalment, gràcies a TU, el noi dels mil noms. Malgrat que t'esforcis per semblar un home serio, compartir la vida amb tu és ben divertit! Marc, gràcies per la teua pau i tranquil·litat, són reconfortants, i gràcies per confiar tant en mi. Tu em planteiges reptes i em recordes cada dia que puc. Ets tot un exemple de com es persegueixen els somnis i es construeix el propi destí.

Amb vosaltres, res és ni tan alt ni tan difícil.